POLITECNICO DI MILANO

Facoltá di Ingegneria Industriale e dell'Informazione
Dipartimento di Energia

Corso di Laurea Magistrale in Ingegneria Energetica

CFD Modeling of a Beta-type Stirling Engine

Relatore: Prof. Gianluca MONTENEGRO

Co Relatore Ing. Augusto DELLA TORRE

Tesi di Laurea di:

Andrea GUZZETTI Matr. 783502

Anno Accademico 2012-2013

Abstract

In the present work CFD is applied to the simulation of a Stirling device. As preliminary step, in order to model the specific features of the machine, ad-hoc sub-models were implemented on the basis of the open-source software OpenFOAM. Then, simulation were run for the case of a small 300 cc Beta Stirling configuration, installed at the laboratory TEMPO (University of Valenciennes, France) and instrumented with thermocouples and pressure transducers. The computational model of this engine was validated both on global quantities, such as the power and heat transferred to the cold sink in a cycle, and on local measurement of temperature in the machine.
Once validated, the model was applied in order to perform a parametric study involving different aspects related to the machine: mean cycle operating pressure, amount of heat introduced in the machine, regenerator properties and working fluid. Finally, by means of a comparison with an ideal case, the losses related to the real behavior of the engine components were investigated, in particular: fluid-dynamics losses in the regenerator, non-isothermal heat exchangers and non-ideal law for the variation of the volumes of the cold and hot spaces.

Key words: Stirling engine, CFD modeling, Regenerator, Heat transfer, Ideal motion, OpenFOAM

Sommario

Nel presente lavoro l'analisi CFD è stata applicata ad un motore Stirling. Al fine di modellare le caratteristiche specifiche della macchina, appositi sotto-modelli sono stati implementati sulla base del codice open-source OpenFOAM. Numerose simulazioni sono state svolte su di un piccolo motore Stirling di 300*cc* in configurazione Beta, installato presso il laboratorio TEMPO (Università di Valenciennes, Francia) e strumentato con termocoppie e trasduttori di pressione. Il modello computazionale è stato validato su questo motore sia in termini di quantità globali, quali la potenza prodotta e calore rimosso dal sistema di raffreddamento, sia su misure locali di temperatura nel dispositivo.
Una volta validato, il modello CFD è stato utilizzato per effettuare uno studio parametrico dei vari fattori che influenzano il comportamento della macchina, tra cui la pressione media di esercizio ciclo, la quantità di calore introdotto, le proprietà termofisiche del rigeneratore e le caratteristiche del fluido di lavoro. Infine, attraverso il confronto con un caso ideale, è stato possibile analizzare le perdite relative al comportamento reale dei componenti del motore, come le perdite fluidodinamiche nel rigeneratore, le perdite connesse a scambiatori non isotermi, e l'effetto di una legge di variazione dei volumi di lavoro non ideale.

Parole chiave: Motore Stirling, Modellazione CFD, Rigeneratore, Scambio termico, Movimento ideale, OpenFOAM

Riassunto

Introduzione

Negli ultimi decenni la tecnologia Stirling ha registrato un rinnovato interesse nel mondo industriale e accademico grazie ad una vasta gamma di sue possibili applicazioni per la generazione di energia da fonti rinnovabili e il recupero di calore. Rispetto alle altre tecnologie disponibili, un motore Stirling è caratterizzato da diversi aspetti interessanti e punti di forza, tra cui: la possibilità di operare con diverse fonti di calore, un funzionamento silenzioso con vibrazioni ridotte, bassi livelli di emissioni inquinanti e possibilità di operare in assenza di ossigeno. I principali svantaggi sono invece legati alle ancora basse potenze specifiche, la lentezza della fase avviamento ed a problemi di affidabilità meccanica.

Il ciclo Stirling ideale, su cui si basa il funzionamento dell'omonima macchina, è un ciclo chiuso rigenerativo, in cui il fluido di lavoro subisce compressione ciclica ed espansione a diversi livelli di temperatura. Tale ciclo si compone di quattro trasformazioni: a) compressione isoterma, b) riscaldamento isocoro rigenerativo, c) espansione isoterma, d) raffreddamento isocoro rigenerativo. Il ciclo ideale è caratterizzato non solo dalla stessa efficienza del ciclo di Carnot (che rappresenta la massima efficienza teoricamente raggiungibile) ma presenta anche un lavoro specifico maggiore, grazie alla sostituzione delle trasformazioni isoentropiche con quelle isocore. Tuttavia, se realizzato in una macchina reale, le prestazioni del ciclo Stirling risultano notevolmente penalizzate a causa di diversi motivi: a) irreversibilità delle trasformazioni termodinamiche reali, b) non idealità degli scambi termici (negli scambiatori di calore e nel rigeneratore), che idealmente dovrebbero avvenire con gradiente di temperatura nullo e c) non idealità degli aspetti meccanici/fluidodinamici della macchina reale, in particolare dovuti all'impossibilità nelle applicazioni pratiche, di imporre un movimento discontinuo a pistoni e rigeneratore [1, 2]. In particolare, mentre la prima categoria di problematiche è comune a tutte le macchine termiche, la seconda e la terza sono tipiche dei dispositivi funzionanti sulla base di un ciclo Stirling.

Il rigeneratore è sicuramente il componente più innovativo e più complesso del motore e recentemente, diversi studi teorici e sperimentali si so-

no concentrati sulla sua ottimizzazione, al fine di minimizzarne le perdite fluidodinamiche e di migliorare lo scambio termico col fluido di lavoro [3, 4, 5].

La progettazione di una macchina Stirling è particolarmente impegnativa, dal momento che coinvolge diversi e complessi fenomeni fisici. I modelli teorici proposti in letteratura, anche se utili per la descrizione e la comprensione dei principali comportamenti della macchina, risultano troppo semplificati per poter essere applicati al disegno dettagliato del dispositivo. Per questo motivo, la ricerca e l'ottimizzazione del layout della macchina sono di solito eseguite su prototipi reali. In questo contesto, l'utilizzo di strumenti CFD può dare un contributo sostanziale nelle fasi di progettazione di una nuova macchina, in quanto consente di migliorare la comprensione dei fenomeni fisici fornendo pratiche indicazioni per lo sviluppo. Inoltre, le simulazioni CFD permettono di testare diversi layout e soluzioni, al fine di individuare la configurazione più promettente da costruire prima dei test sperimentali.

Revisione dei modelli esistenti

Per l'analisi del ciclo Stirling sono stati proposti in letteratura diversi approcci, che possono essere classificati sulla base della loro complessità in cinque categorie: ordine zero, primo ordine, secondo ordine, terzo ordine e quarto ordine. [2, 6, 7].

L'analisi di ordine zero, proposta da Beale nel 1971, è il metodo più semplice ed è stato formulato nel tentativo di stabilire una similitudine tra tutte le macchine Stirling. Si basa sul presupposto che la maggior parte dei motori operino in condizioni di similitudine e tenta di stabilire una correlazione generale tra la potenza prodotta e le principali condizioni operative (pressione e frequenza di sistema) e parametri di progetto (cilindrata). A causa delle semplificazioni introdotte nell'approccio, questa analisi può essere adottata solo per una stima preliminare delle prestazioni della macchina.

L'analisi del primo ordine è stata pubblicata nel 1871 da Gustav Schmidt e, per molti anni (fino al 1960), ha rappresentato il modello di riferimento per gli sviluppatori della tecnologia Stirling; ancora oggi, grazie alla sua semplicità, questo modello è ampiamente utilizzato per il dimensionamento iniziale dei motori. Questa analisi ha il vantaggio di produrre un'informazione sulle prestazioni del motore in forma chiusa, non richiedendo quindi l'utilizzo di metodi numerici per la soluzione delle equazioni di governo. L'assunzione principale di questo modello è che sia lo spazio caldo che il corrispettivo scambiatore di calore hanno una temperatura costante T_h, mentre lo spazio freddo e lo scambiatore freddo hanno una temperatura costante pari a T_k. Questa assunzione implica che gli scambiatori di calore, rigeneratore incluso, si comportano in maniera ideale. Nel modello il motore è configurato come

serie di cinque componenti rappresentanti rispettivamente lo spazio di compressione, il dispositivo di raffreddamento, il rigeneratore, il riscaldatore e lo spazio caldo. Ogni componente viene considerato omogeneo e le proprietà termofisiche del gas al suo interno sono modellate mediante l'equazione di stato dei gas perfetti. Inoltre si assume che le perdite di attrito, le perdite meccaniche e i trafilamenti siano trascurabili sull'intero motore. Queste ipotesi ideali mirano a semplificare il problema, fornendo un modo rapido per valutare il rapporto tra la dimensione complessiva del motore e la sua potenza. D'altra parte, non includendo la maggior parte delle irreversibilità della macchina, tale analisi non può essere applicata come strumento utile alla progettazione.

L' analisi di secondo ordine, come quella del primo, ha lo scopo principale di determinare la potenza e l'efficienza della macchina risolvendo equazioni di bilancio su un sistema semplificato. Il miglioramento più importante dei metodi del secondo ordine rispetto al primo, è che individuano e quantificano alcune irreversibilità, risultando quindi in un'informazione più precisa sulle prestazioni della macchina. Alcuni di questi modelli, tra cui le analisi proposte da Finkelstein (1960), Walker e Kahan (1965) e Lee e Berchowitz (1978), sono classificati sotto il nome di *modelli adiabatici*, e rimuovono l'assunzione che gli spazi di espansione e compressione siano isotermi. A partire da questi modelli, vari miglioramenti sono stati introdotti da analisi successive, al fine di includere e studiare un numero sempre maggiore di perdite. Questi metodi, classificati come *analisi quasi-stazionarie*, sono stati introdotti inizialmente da Urieli e Berchowitz nel 1984 [2] e poi ampiamente utilizzati negli anni successivi.

I metodi del terzo ordine, noti anche come analisi nodali, raggruppano tutte le simulazioni 1D dei motori Stirling e sono normalmente costituiti da tre fasi: (1) dividere il motore in una rete di nodi o volumi di controllo; (2) impostare le equazioni differenziali per la conservazione della massa, quantità di moto ed energia, oltre all'equazione di stato per il gas di lavoro; (3) risolvere il sistema di equazioni differenziali con un metodo numerico adeguato. Questi metodi sono stati introdotti con lo scopo di considerare contemporaneamente i molteplici processi coesistenti in un motore Stirling, ritenuti disaccoppiati dalle analisi precedenti; tuttavia necessitano anch essi di correlazioni empiriche per modellare i coefficienti di scambio termico e i fattori di attrito. I metodi del terzo ordine sono sicuramente più sofisticati dei precedenti, ma implicano la risoluzione di equazioni su di un dominio composto da numerosi elementi; richiedono quindi un onere computazionale molto maggiore, tempi di risoluzione più lunghi, e possono portare a problemi di instabilità numerica. Il sistema di equazioni differenziali alle derivate parziali può essere risolto sia con metodi alle differenze finite che con il me-

todo delle caratteristiche (organ (1981) [1] e Larson (1981)). Questo tipo di analisi può essere applicato per simulare il comportamento della macchina e prevedere le sue prestazioni, tuttavia presenta ancora alcuni limiti. In particolare non considera gli effetti che la geometria della macchina ha sui flussi interni e sulle distribuzioni delle proprietà del fluido su assi longitudinali, risultando così in informazioni incomplete per essere utilizzate nelle fasi di progettazione ed ottimizzazione.

L'ultima classe di metodi (quarto ordine) è rappresentata dall'analisi CFD. Nonostante la CFD sia oggi ampiamente applicata in diversi campi (motori a combustione interna, aerodinamica, acustica, ecc), il suo utilizzo per la modellazione dei motori Stirling è solo recente e soffre ancora molte problematiche. Infatti la macchina Stirling è di per sé un sistema che coinvolge diversi fenomeni fisici (fluidodinamica, trasferimento di calore) che si verificano in diverse fasi (liquido e solido), su diverse scale di lunghezza (dalla scala della macchina alla micro scala dei pori della matrice solida del rigeneratore) e con diversi tempi caratteristici (convezione e conduzione). Inoltre la simulazione deve tener conto delle parti mobili della macchina, che richiedono strategie di movimentazione della griglia computazionale. Un aspetto che rende particolarmente difficile l'applicazione della CFD all'ottimizzazione della macchina Stirling è legato alla natura oscillatoria instazionaria del flusso all'interno del sistema. Questa peculiarità rende difficile affrontare la simulazione di un singolo componente come un sistema isolato, poichè spesso non sono disponibili le informazioni necessarie per imporre condizioni al contorno realistiche. La simulazione di tutta la macchina d'altra parte, richiede lunghi tempi di calcolo per raggiungere la convergenza, poichè influenzata dal tempo caratteristico della conduzione nei componenti solidi. In letteratura sono presenti pochi esempi di applicazione dell'analisi CFD ai singoli componeneti del motore Stirling [8, 9], mentre nella maggior parte delle pubblicazioni recenti si preferice modellare l'intero motore in un'unica simulazione, utilizzando sia modelli 2D che 3D [10, 11, 12].

Apparato sperimentale

Il motore Stirling considerato in questo elaborato presenta una configurazione di tipo Beta [13], ed è composto quindi da un pistone di potenza, responsabile dello scambio di lavoro durante le fasi di compressione ed espansione, e un dislocatore (*displacer*), che sposta il fluido tra lo spazio freddo e lo spazio caldo durante le fasi di rigenerazione. La sorgente calda è costituita da una resistenza elettrica posta all'interno della camera calda, la cui potenza è imposta mediante un regolatore di tensione. La sorgente fredda è invece costituita da un circuito aperto ad acqua, che circonda la camera fredda, e

da un circuito aggiuntivo che porta l'acqua, attraverso la biella, a raffreddare la parte inferiore del displacer. Il rigeneratore è inserito sul pistone del displacer ed è costituito da una spugnetta metallica di rame. L'apparato di misurazione è dotato di un trasduttore di pressione (posto nello spazio freddo), un trasduttore di volume, un contagiri, un debimetro, e tre termocoppie, che misurano rispettivamente le temperature dello spazio caldo, dello spazio freddo, e la differenza di temperatura subita dall'acqua di raffreddamento tra l'ingresso e l'uscita del circuito. Il fluido di lavoro utilizzato nel motore è aria, che è caricata in condizioni ambiente semplicemente aprendo la parte superiore del cilindro. Durante le prove sperimentali al di fuori dello spazio caldo è stato posto un isolamento radiativo al fine di ridurre le perdite per irraggiamento verso l'ambiente. Inoltre al motore non è stato applicato nessun carico, in modo che, una volta raggiunto il funzionamento di regime, il lavoro prodotto è bilanciato dalle sole peridite del sistema.

I dati acquisiti sono stati filtrati attarverso un programma di post processing, e sono stati utilizzati per calcolare le prestazioni della macchina. In particolare la potenza scambiata nel sistema di raffreddamento è stata calcolata come:

$$\dot{Q}_f = \dot{m}_{acqua} C p_{acqua} \Delta T_{acqua}, \tag{1}$$

mentre il lavoro compiuto dal motore è stato stimato a partire dal diagramma p-V come:

$$L = \int p \, \mathrm{d}V. \tag{2}$$

A partire da questi dati è stato così possibile stimare il calore in ingresso nel sistema Q_c (come somma del calore uscente e del lavoro) e il rendimento del motore.

Il modello CFD

Equazioni di governo

Per modellare il problema fluidodinamico, è necessario combinare il sistema di equazioni di conservazione per il generico continuo con le relazioni costitutive che descrivono le proprietà specifiche del fluido. Considerando un fluido comprimibile, monofase, e newtoniano, il set delle equazioni di governo del fenomeno è costituito da:

- l'equazione di continuità, che garantisce la conservazione della massa:

$$\frac{\partial(\varrho)}{\partial t} + \nabla \cdot (\varrho \vec{u}) = 0 \tag{3}$$

- l'equazione di Navier-Stokes, derivata per la conservazione della quantità di moto:

$$\frac{\partial(\varrho\vec{u})}{\partial t} + \nabla \cdot (\varrho\vec{u}\vec{u}) = -\nabla p + \mu\nabla^2\vec{u} + \Re \tag{4}$$

- l'equazione di bilancio dell'energia totale:

$$\frac{\partial(\varrho E)}{\partial t} + \nabla \cdot (\varrho E\vec{u}) = -p\nabla \cdot (\vec{u}) + \nabla \cdot (k_f \nabla T) + \rho Q + Q^{s\to f} \tag{5}$$

Il set di equazioni è chiuso mediante l'equazione di stato dei gas perfetti. Nel caso della fase solida invece, l'insieme di equazioni di governo si riduce alla sola equazione di conservazione dell'energia, che descrive in questo caso la sola conduzione di calore:

$$\frac{\rho c_s T}{\partial t} = k_s \nabla T + \rho Q + Q^{f\to s} \tag{6}$$

Le equazioni 3, 3.16 e 3.6 opportunamente corrette, permettono di rappresentare anche la fisica del mezzo poroso del rigeneratore e di descrivere la sua interazione fluidodinamica e termica col fluido di lavoro.

Definizione della mesh

La configurazione della macchina Stirling considerata in questo lavoro presenta una geometria assialsimmetrica che permette di risolvere le equazioni descritte in dominio bidimensionale. La mesh creata è costituita da celle esaedriche, è strutturata, e presenta una buona qualità. La movimentazione della griglia è stata implementata in modo tale che permetta di spostare, con una legge di moto arbitraria, le singole facce di una data zona di celle. Per il motore in esame si nota, da Fig.1, come le zone di moto necessarie siano tre, rispettivamente lo spazio caldo (rosso), il rigeneratore (verde), che ha un moto rigido, e lo spazio freddo (blu).

Definizione dei sotto modelli

Lo scambio di calore tra fluido e rigeneratore è un aspetto molto importante per i motori Stirling. Per descrivere questo fenomeno, sono proposti in questo lavoro due diversi approcci. Il primo approccio, denominato *Single region*, consiste nell'assumere a priori una distribuzione di temperatura della matrice solida del rigeneratore, che verrà poi mantenuta costante durante

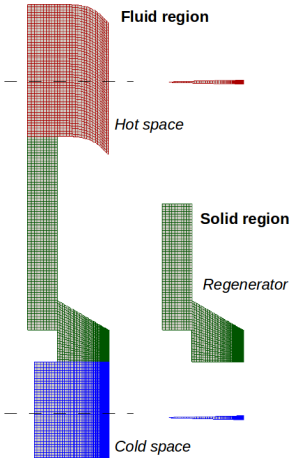

Figura 1: Mesh per la regione fluida e la regione solida. Sono evidenziate le diverse zone: spazio freddo (blu), spazio caldo (rosso) e rigeneratore (verde).

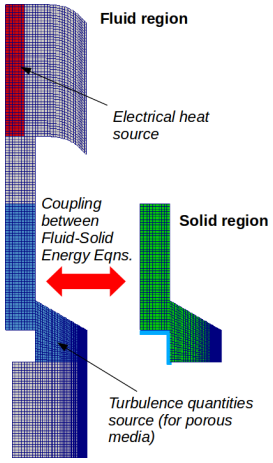

Figura 2: Definizione delle zone di applicazione dei termini sorgenti necessari per il modello

le simulazioni. In questo modo le equazioni di governo 3 - 3.16 sono risolte per la sola fase fluida, mentre non si esprime nessun bilancio per il solido. Il secondo approccio, detto *Multi region*, è più accurato e consiste nell'adozione di due domini di diversi, rispettivamente per il fluido e la fase solida, su cui è risolto l'insieme di equazioni 3 - 3.6. Nelle zone in cui coesistono entrambe le fasi, come nella matrice porosa del rigeneratore, le griglie computazionali si sovrappongono e si introducono modelli per tenere conto delle loro interazioni (Fig. 2). In questo modo la distribuzione di temperatura nella matrice solida non è più costante ma è determinata dal bilancio energetico globale del sistema accoppiato fluido-solido.

Per poter affrontare la simulazione del rigeneratore con un approccio alla macro scala, sono stati inclusi idonei modelli per l'effetto di permeabilità e lo di scambio di calore tra le diverse fasi del mezzo poroso:

1. **Modello per la permeabilità:** questo modello è incluso nella equazione di moto per mezzo del termine sorgente di resistenza $\Re$. Il valore di questo termine dipende dalle proprietà della microstruttura e dalle condizioni fluidodinamiche istantanee. Se la resistenza rappresentata dal mezzo poroso viene espressa in termini di un coefficiente di attrito, l'equazione di moto può essere chiusa mediante la seguente espressione:

$$\Re = \frac{1}{2}\frac{\rho}{d_c} C_f u. \tag{7}$$

In questo lavoro per il calcolo del coefficiente d'attrito è stata utilizzata la correlazione proposta da Gedeon e Wood [14]

$$C_f = \frac{129}{Re} + 2.91 Re^{-0.103}. \tag{8}$$

2. **Modello di scambio termico:** questo modello è incluso come termine sorgente nelle equazioni di bilancio energetico delle due fasi. Il suo valore dipende dalle condizioni istantanee fluidodinamiche e dalle temperature medie delle fasi e può essere determinato, come nel caso della resistenza, mediante una relazione adeguata che esprima la dipendenza del trasferimento di calore dai numeri di Re e Pr:

$$Q^{s \to f} = -Q^{f \to s} = Nu \, \frac{k_f}{d_c} \, \sigma \, u(T_s - T_f), \tag{9}$$

dove è stata utilizzata la seguente correlazione (Gedeon e Wood [14])

$$Nu = 0.51 + 0.4 Re^{0.66}. \tag{10}$$

Per modellare gli scambi termici nello spazio caldo e freddo sono stati adottati specifici modelli. La sorgente calda, costituita dalla resistenza elettrica, è stata modellata introducendo un termine sorgente nel bilancio energetico del fluido (Eq. 3.16) per tutte le celle della zona dove si trova la resistenza (Fig. 2). Per evitare che la temperatura del fluido raggiunga valori troppo elevati, è stata adottata una limitazione sulla potenza massima introdotta; quando questa limitazione si attiva, l'energia viene temporaneamente accumulata e ceduta al fluido solo una volta che la sua temperatura ritorna al di sotto del limite massimo. In questo modo è riprodotto l'effetto di accumulo termico che si verifica nel filo metallico della resistenza, e che impedisce alla temperatura di salire quando il fluido ha velocità troppo basse.

Per quanto riguarda la modellazione dello scabiatore freddo, si è adottata una condizione al contorno di temperatura costante sulle superfici dello scambiatore per entrambe le regioni (fluido e solido). In particolare, nella regione fluida, è stata disegnata una mesh avente uno strato limite raffinato, in modo da descrivere accuratamente il trasferimento di calore a parete.

Validazione del modello e analisi

Il modello è stato validato sia sulla base di quantità globali, quali la potenza prodotta e calore rimosso dal circuito di raffreddamento, sia rispetto alle misure locali di temperatura nella macchina. In Fig. 3 è mostrato il confronto

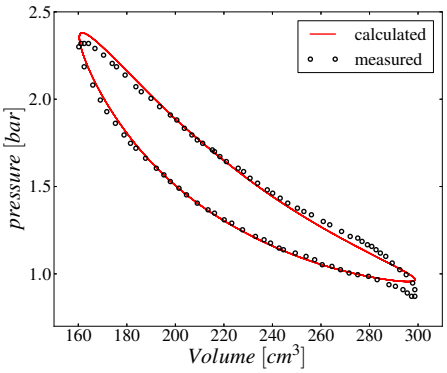

Figura 3: Confronto fra il diagramma p-V misurato e simulato

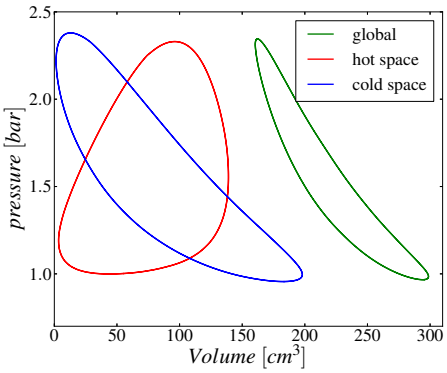

Figura 4: Risultati simulazione, cicli p-V per: spazio caldo, spazio freddo e ciclo globale

tra il diagramma p-V misurato e quello simulato, per i quali si può notare un accordo soddisfacente.

In Fig. 4 invece, sono visibili i diagrammi p-V ottenuti per lo spazio caldo e freddo, insieme al ciclo globale tracciato usando la pressione media e il volume totale della macchina. I dati quantitativi di validazione sono riportati in Tabella 5.1. La potenza meccanica del dispositivo è stata sperimentalmente determinata a partire dalla sola pressione misurata nello spazio freddo; per questo motivo sono riportati sia la potenza meccanica valutata utilizzando la pressione calcolata nella stessa posizione $P_{mec,freddo}$, sia l'effettiva potenza meccanica P_{mecc} ricavata come differenza tra la potenza dello spazio di espansione e la potenza dello spazio di compressione. Per quanto riguarda la temperatura rilevata nello spazio caldo, si deve considerare che la misura sperimentale $T_{caldo,rad}$ è influenzata dall'irraggiamento della resistenza elettrica, poichè la termocoppia non risulta schermata. Per tener conto di tale errore di misura, è stato sviluppato un modello analitico semplificato, che ha portato a stimare la reale temperatura del fluido pari a T_{caldo}, riportata in tabella. Se si considera questa stima, la temperatura del fluido calcolata nella posizione del trasduttore risulta ragionevole.

Una volta validato, il modello ha permesso di trarre alcune conclusioni sul motore studiato: si è rilevato ad esempio che la parte inferiore del rigeneratore funziona in pratica da scambiatore freddo e che le velocità del fluido risultano molto basse nello spazio inferiore, svantaggiando lo scambio termico con le pareti fredde del cilindro. Inltre sono state individuate le zone di stagnazione e di ricircolo dell'aria.

Il modello è stato poi adottato per lo studio degli effetti che diversi pa-

Tabella 1: Confronto tra dati sperimentali e risultati della simulazione.

Grandezza	**Misura**	**Simulazione**
Power cooling system Q_f [W]	84.9	82.9
Mechanical power $P_{mec,freddo}$ [W]	13.2	14.2
Mechanical power P_{mec} [W]	-	9.82
Hot temperature $T_{caldo,rad}$ [W]	818	-
Hot temperature T_{caldo} [W]	692	681

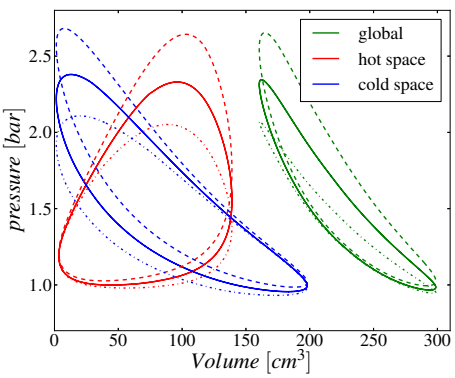

Figura 5: Effetto della variazione della conduttività termica del rigeneratore: $k = 30\ W/(m^2K)$ (continua), $k = 10\ W/(m^2K)$ (tratteggio), $k = 100\ W/(m^2K)$ (puntini).

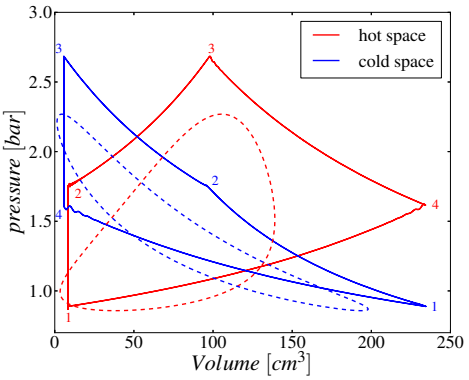

Figura 6: Effetto dell'introduzione del movimento reale in un caso ideale

rametri di progettazione e condizioni operative hanno sulle prestazioni della macchina; i risultati delle analisi sono riportati in Tabella 2. Tra i vari risultati ottenuti si è rilevato che la proprietà del rigeneratore che più influisce sulle prestazioni del motore è la sua conduttività termica effettiva. Tale proprietà dipende sia dal materiale di cui è costituito il rigeneratore, sia dalla natura del mezzo poroso utilizzato. In particolare una bassa conduttività della matrice porosa permette di stratificare meglio la temperatura all'interno della matrice solida del rigeneratore, così che gli scambi termici col fluido di lavoro avvengono con gradienti di temperatura ridotti, limitando le irreversibilità. In Fig. 6.4 sono mostrati i cicli di lavoro calcolati con diversi valori di conduttività della matrice porosa; da essi si può notare come l'area del ciclo globale sia tanto più grande quanto minore è il valore di conduttività utilizzato. Questo si traduce in una maggiore efficienza di primo principio η_I del ciclo, ma anche in una maggiore efficienza di secondo principio η_{II}, dal momento che le irreversibilità sono minori.

Tabella 2: Studio parametrico: risultati delle simulazioni.

Parameter	**Value**	$\mathbf{P_{mech}}[W]$	$\mathbf{Q_{cold}}[W]$	$\mathbf{Q_{hot}}[W]$	$\mathbf{T_{cold}}[K]$	$\mathbf{T_{hot}}[K]$
Caso base		9.8	82.9	92.7	314.6	681.8
Conduttività $[W/(m^2K)]$	10	18.8	64.4	83.2	315.8	763.0
	100	1.3	91.6	92.9	318.3	608.2
Fluido	Elio	10.2	82.5	92.6	320.4	623.8
	Idrogeno	13.2	80.1	93.3	313.9	644.2
Pressione $[bar]$	0.7	10.2	72.1	82.3	308.0	722.9
	1.5	2.2	90.5	92.7	326.4	576.3
$\mathbf{Q_{caldo}}$ $[W]$	50	-4.8	54.5	49.6	329.3	527.5
	150	23.7	109.1	132.8	304.5	894.2

L'analisi effettuata su diversi fluidi di lavoro ha evidenziato come, per il motore in esame, l'idrogeno porti a prestazioni miglior di elio ed aria. Questo comportamento è dovuto all'alta conduttività termica di questo fluido, che garantisce un efficace scambio termico col rigeneratore, ed alla sua bassa viscosità dinamica, che permette di ridurre le perdite di attrito tra fluido e matrice porosa.

Infine è stato simulato un motore con comportamento ideale, sia per quanto riguarda la legge di moto, che per i suoi componenti: ciò ha permesso lo studio delle singole irreversibilità introdotte in un motore reale. In particolare sono stati studiati gli effetti della permeabilità del rigeneratore, della presenza di scambiatori reali, e dell'utilizzo del movimento reale, vincolato dal meccanismo albero-manovella. Per quanto riguarda quest'ultimo caso, in Fig. 6 si mostra il confronto tra i cicli di lavoro ottenuti per il caso ideale, e per il caso in cui, in corrispondenza di componenti ideali, è stato implementato il movimento reale. Questa analisi ha permesso di stimare che le perdite dovute all'utilizzo di un movimento non ideale pesano per circa il 41% della potenza totale in uscita, dato che trova riscontro in letteratura.

Conclusioni

In questo tesi è stato sviluppato, sulla base del codice OpenFOAM, un modello CFD per la simulazione di un motore Stirling in configurazione Beta. Al fine di considerare le particolari caratteristiche di questa macchina sono stati implementati diversi sottomodelli che riguardano il movimento della mesh, lo scambio di calore, la modellazione della turbolenza e il comportamento dei mezzi porosi. Il modello è stato validato con successo su di un piccolo motore Stirling Beta di 300 cc, confrontando sia due grandezze globali che

misure locali. Successivamente alla valutazione, il modello è stato applicato per effettuare uno studio sull'influenza che diversi parametri del motore hanno sulle prestazioni della macchina. Sono stati analizzati: le proprietà rigeneratore, il fluido di lavoro, la pressione media di esercizio e la potenza introdotta dalla sorgente calda. Inoltre è stato indagato l'effetto negativo introdotto dalla non idealità di alcuni componenti e dalla legge di moto reale. I risultati forniti dal modello CFD per i casi studiati sembrano essere ragionevoli e in accordo con quanto previsto sulla base dei modelli teorici esistenti. Il presente lavoro deve però essere inteso come una validazione preliminare del modello CFD: lavori futuri saranno concentrati sulla simulazione e l'ottimizzazione di più complesse configurazioni reali.

Contents

List of Figures

List of Tables

Nomenclature

α	crank angle [Deg]
$\dot{Q}$	heat power [W]
η	efficiency
μ	dinamic viscosity [Ns/m^2]
μ_t	turbulent viscosity [Ns/m^2]
ω	dissipation rate [J/(kg s)]
Π_v	porosity
$\Re$	source term of the momentum equation [Pa/m]
τ_s	surface shear stress [N/m^2]
ϱ	density [kg/m^3]
A	surface [m^2]
b	con rod length [m]
C_f	friction coefficient
c_s	solid specific heat [J/(kg K)]
Cp	fluid specific heat at constant pressure [J/(kg K)]
d_c	characteristic dimension [m]
D_h	hydraulic diameter [m]
E	total energy [J]
F_m	mesh motion flux for a generic quantity
h	heat transfer coefficient [W/(m^{2}K)]

i	internal energy [J]
k	turbulent kinetic energy [J/kg]
k_{eff}	effective termacl conductivity [W/(mK)]
k_f	fluid thermal conductivity [W/(mK)]
k_s	solid thermal conductivity [W/(mK)]
m	crank length [m]
m_{water}	water mass flow [kg/s]
Nu	Nusselt number
P	power [W]
p	pressure [Pa]
Pr	Prandtl number
R	perfect gas constant [J/(mol K)]
Re	Reynolds number
S_ϕ	source term for a generic conservation equation
S_{fluid}	source term for the fluid energy equation [J]
S_{solid}	source term for the solid energy equation [J]
T	absolute temperature [K]
t	time [s]
u	velocity [m/s]
u_b	boundary velocity [m/s]
V	volume [m^3]
W	work [J]
y	position on the y axis [m]

Introduction

In the last decades people has become more and more aware of the importance of a sustainable way to exploit Earth resources and satisfy the global energy demand. The gradual depletion of traditional non-renewable energies along with the increasing degradation of the environment has strongly improved the demand of the public for "Green products". Nowadays a great effort is made by researchers and scientists in order to improve the efficiency of the machines fueled by non-renewable energy sources, to reduce pollutant emissions and to promote the development of renewable technologies. In this context, the Stirling technology is experiencing a renewed interest in industry and academy, due to a wide range of possible applications in energy generation from renewable resources and waste-heat recovery. As a matter of fact, compared to the other available technologies, a Stirling engine is characterized by different interesting aspects and strengths, such as: the possibility of operating with different heat sources, quiet operation with low level of noise and vibrations, low-emissions and possibility of operating in absence of oxygen. On the other hand, the main limitations are related to the low specific power of the device, the slowness of the start-up phase and problems of mechanical reliability.

The ideal Stirling cycle is a close regenerative cycle in which the working fluid undergoes cyclic compression and expansion at different temperature levels. The cycle consists of four transformations: a) isothermal compression, b) isochoric regenerative heating, c) isothermal expansion and d) isochoric regenerative cooling. The ideal cycle is not only characterized by the same efficiency of the Carnot cycle (which represents the maximum efficiency theoretically achievable) but it exhibits also an higher specific work, due to the replacement of the isoenthropic transformations with the isochoric ones. However, the performances of the Stirling cycle are considerably penalized when it comes to real applications, because of different issues: a) irreversibility of the real thermodynamic transformations, b) non-ideality of the real heat transfer transformations (isothermal heat addition/removal and regeneration) and c) non-ideality related to mechanical/fluid-dynamic aspects, in particular related to the impossibility of imposing a discontinous motion to

pistons/regenerator [1, 2]. In particular, while the first class of problems is common to all the thermal machines, the other two are typical of the devices working on the basis of a Stirling cycle. The regenerator is considered by many researchers as the key component to improve the efficiency of the next generation of Stirling engines systems. Different works, both theoretical and experimental, has been focused on its study and optimization in order to minimize the fluid-dynamic losses and to enhance the heat transfer and heat storage properties. Moreover, with regards to the law of variation of volumes, different studies showed that the adoption of a crankshaft for imposing the alternative piston/regenerator motion leads to a significant reduction (40-60 %) of the area of the p-V cycle with respect to the ideal one.

The design of a Stirling device is particularly challenging, since different and complex physical phenomena are involved. The theoretical models proposed in the literature, even if useful for the description and the understanding of the main operations of the machine are, on the other hand, too simplified to be applied for a detailed design of the device. For this reason, the practical conception and optimization of the machine layout is usually performed on a real prototype. In this context, the adoption of CFD tools can give a substantial contribution during the design phase of a new machine, since it allows to enhance the understanding of the physical phenomena providing useful guide-lines for its optimization. Moreover, CFD simulations allow to test different layouts and solutions, in order to identify the more promising configuration and geometry before the first metal is cut. The application of CFD tools to Stirling engines is only recent and still suffers from many challenges: only few examples can be found in literature on the subject and none of them came out with a well established model, especially for the regenerator component. In addition, most of the commercial softwares do not present satisfying tools to be used in Stirling modeling and problems and restrictions still lie in existing functions. In the wide panorama of the CFD softwares, the finite volume open-source code OpenFOAM holds interesting features which can suit the requirements of Stirling analysis. In fact, this software, being open-source, allows the complete access to the source code so that the user has the possibility, if needed, to customize the existing solvers and implement new classes in order to satisfy particular modeling requirements [15, 16].

In this thesis work, *Chapter 1* will be dedicated to an overview of the Stirling technology, concerning the theoretical thermodynamic cycle, the losses in real devices, and existing engine configurations and applications. In *Chapter 2*, a thorough review of the existing models applied to the Stirling technology will be performed; this preliminary analysis will allow to define the

strengths and weaknesses characterizing the previous works. In *Chapter 3*, a general CFD model for the Stirling machine will be implemented on the basis of the OpenFOAM code. Then, in *Chapter 4*, the developed model will be applied for the simulation of a small 300 cc Beta Stirling engine and validated on the basis of experimental measurements available in the framework of a collaboration with the University of Valenciennes (France). The validation and the analysis of the results obtained will be presented in *Chapter 5*. Finally, in *Chapter 6*, the CFD model will be adopted in order to perform a parametric study on different design and operating parameters of the engine.

Chapter 1

The Stirling cycle machine

1.1 Origin

Stirling cycle origin dates back to 1816, when Robert Stirling, a Minister of the Church of Scotland, received the patent for his new type of machine: the "air engine". His invention, which consisted of a closed cycle engine with a hot and a cold space, was undoubtedly revolutionary for that time and several of its aspects were unique when compared with contemporary reciprocating steam engine installations [2, 13]:

- it did not make use of any valves or piston actuated port openings;
- it operated on a closed cycle;
- ihe power piston was located entirely in the cold zone of the engine;
- it introduced for the first time the "economizer" (now known as regenerator), a metallic matrix with the function of storing part of the heat during one phase of the cycle for re-using during another phase. This was probably the most important innovation of the Stirling's invention and for the first time in a formal way, introduced the concept of thermal regeneration [2].

Because of their reliability, higher efficiency and safeness in comparison to the steam machines, Stirling's engines were soon widely used in Britain, Europe, and USA in a variety of shapes end sizes, especially to run water pumps and small machines [13]. However, in the middle of the nineteenth century, the invention of the internal-combustion engine in form of the gas engine, and the subsequent development of Otto and Diesel engine (1876 and 1892) along with the invention of the electric motor, caused the use of Stirling engines to largely diminish until, by 1914, they were no longer available commercially. The main obstacle for the Stirling engine to maintain its competitiveness

was technological, since the materials of that period could not stand very high temperatures in the hot space, at the expense of the reliability and the efficiency of the engine [2, 17].

A new interest in the Stirling technology rose in the late 1930s when, due to the World conflicts, its characteristic to operate by any kind of fuel and heat source become really attractive, especially for military purposes. In those years the most valuable research and progress were made by Philips, and brought to the development of a small and performing electric power generator used to power radios in isolated places. However few years later, the invention of transistor brought to dramatically reduce the electricity consumption of electronic device, and Stirling generators were soon replaced by portable batteries. As a consequence, after the end of the II World War, founds and research programs in Stirling technology diminished considerably and Philips remained the only company to invest in this field.

In the 1970s and 1980s, during the Oil Crisis, a new phase of research on Stirling engines begun, with a particular focus in automotive application: companies involved were still Philips, but now also General Motors and Ford. The renewed interest was lead by an increasing public concern about the environment and the unstable price of gasoline and diesel. In this contest Stirling engines were attractive compared with internal-combustion engines, because of their possibility to be run by any kind of fuel along with low noise and air pollution level. Nevertheless none of the Stirling automotive programs brought to a commercial product, probably due to the lack of public investments and the difficulty to design control strategies able to modify the engine power output quickly and efficiently. In the following years research and investments in Stirling technologies were reduced and remained prerogative of few companies only. The principal applications were in cryogenic refrigeration, naval propulsion, and small and medium size electrical generation [13, 17].

In recent years, due to the increasing concern in Western countries about sustainability, environment protection and Green Economy, a new favorable period for Stirling development is expected to begin: more and more scientific articles have been recently published and modern instruments are used to study and improve the engine performances, as will be shown in chapter 2.

1.2 Theoretical cycle

Stirling machines work on the basis of a thermodynamic cycle and can operate both as direct or reverse machines. In order to study their operation, it is useful to define a theoretical model in which the various parts of the cycle are idealized, in such a way that it is possible to understand the ideal performance

of the machine and to define its theoretical limits. In this analysis a Stirling engine in alpha configuration (see Sec. 1.4) will be used, however the same transformations occur similarly in all the other possible technical solutions. As it can be seen in figure 1.1 the working space is limited by two opposed pistons and divided in two volumes by the regenerator. Regenerator is a key component for Stirling engines and has the role of alternatively absorb and release heat from and to the working fluid. In order to guarantee large exchange surfaces along with low volumes (see Sec. 1.3), regenerators are usually realized by means of porous materials and general solutions comprise: matrix of fine wires, metallic foams or, sometimes simply the metal wall surfaces enclosing the annular gap. One of the two volumes between the regenerator and the pistons is called the *Expansion space*, an is maintained at a high temperature T_{max}. The other volume is called *Compression space*, and is maintained at a low temperature T_{min}. There is, therefore, a temperature gradient $T_{max} - T_{min}$ across the transverse faces of the regenerator, and it is assumed that no thermal conduction in the longitudinal direction occurs. In addition it is made the hypothesis that the pistons move without friction or leakage loss of the working fluid enclosed between them. The ideal cycle is composed of four thermodynamic transformations shown in figure 1.2:

1-2 ***Isothermal compression***. The compression-space piston from the outer dead point moves towards the inner dead point while the expansion-space piston remains stationary in its inner dead point. In this transformation the working fluid temperature remains constant because heat Q_c is abstracted at T_{min} to the surroundings.

2-3 ***Constant volume displacement***. Both pistons move simultaneously and working fluid is forced to move through the regenerator matrix towards the expansion space. Therefore the fluid volume is maintained constant, while its temperature rises from T_{min} to T_{max} by heat transfer from the regenerator.

3-4 ***Isothermal expansion***. The expansion piston moves towards its outer dead point while the compression-space piston remains stationary in its inner dead point. During this phase temperature is maintained constant because heat Q_e is added to the system from an external heat source at temperature T_{max}.

4-1 ***Constant volume displacement***. Both pistons move simultaneously and fluid is displaced to the compression space through the regenerator matrix. In this transformation fluid volume is maintained constant and its temperature is lowered from T_{max} to T_{min} by heat transfer from the fluid to the regenerator.

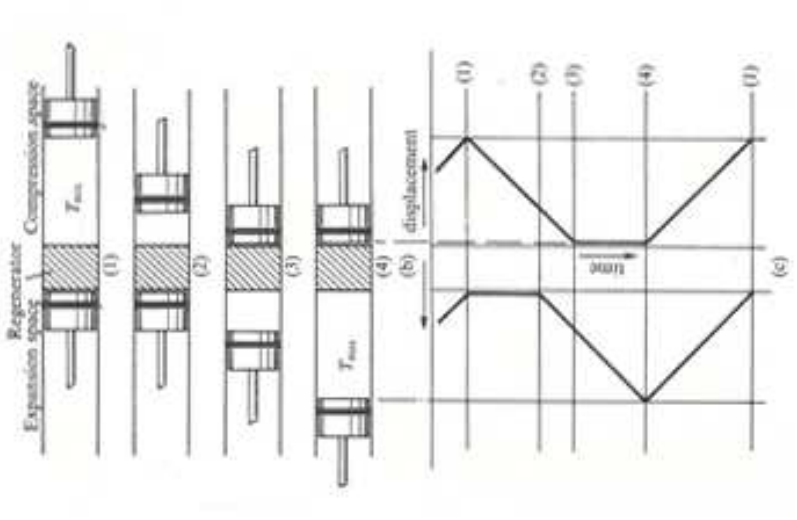

Figure 1.1: Stirling theoretical cycle

In order to guarantee the ideality of the cycle, all the four processes are considered to be thermodynamically reversible and heat exchanged between working fluid and regenerator matrix in process 2-3 and 3-4 has the same magnitude. Therefore the only heat transfers between the system and the surroundings are the heat supply at constant temperature T_{max} in transformation 4-1, and the heat removal at T_{min} in transformation 2-3. This hypothesis imply infinite rates of heat transfer in the regenerator matrix and between the fluid and the working space walls. Considering all the ideal assumptions mentioned, it can be demonstrated that the thermal efficiency of Stirling thermodynamic cycle is equal to the thermal efficiency of a Carnot cycle that works between the same temperatures $\eta = (T_{max} - T_{min})/T_{max}$. The principal advantage of the ideal Stirling cycle over Carnot cycle lies in the replacement of the two isoentropic processes by two isochoric processes, which increase the p-V diagram area significantly and therefore allow to obtain a higher work output. The difference between Stirling and Carnot cycles can be seen in figure 1.2, where Stirling cycle is represented by transformations 1-2-3-4, Carnot cycle by 1-5-3-6 and the striped area in the p-V diagram is the difference between the works of the two cycles [13, 2, 1].

1.3 Real cycle

With regards to the ideal cycle analyzed in the previous section, it must be said that all the hypothesis made were merely ideal assumptions. In any practical engine almost none of those conditions can be achieved and many

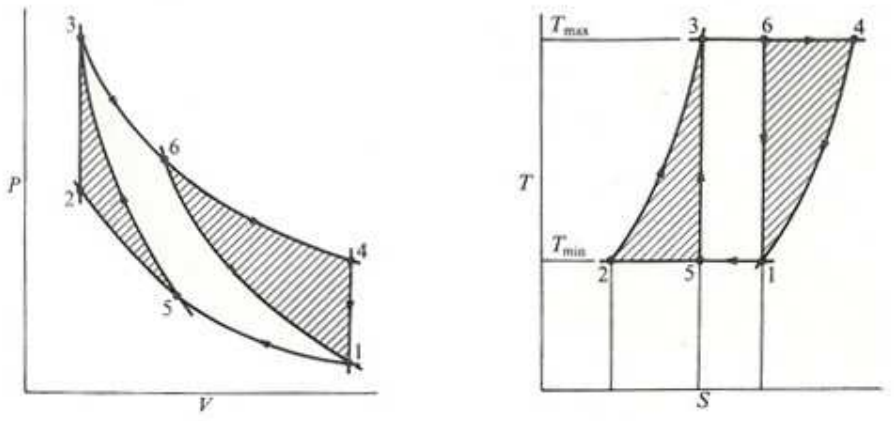

Figure 1.2: p-V and T-s diagram for Stirling cycle (1-2-3-4) and Carnot cycle (1-5-3-6)

factors are involved to reduce the thermal efficiency well below the Carnot value of the ideal case [13]. In this section all the factors that contribute to depart from the ideal conditions will be taken into account; a comparison between real and ideal cycle is shown in Fig. 1.3.

Real motion

The discontinuous motion of the pistons required in the ideal cycle is practically impossible to be reproduced with a continuous moving mechanism. Many different drive methods have been proposed in order to get close to the ideal motion, but a significant difference still remains. The consequence is that the four processes of the ideal cycle are not sharply defined and do not happen separately but overlap over the continuous cycle; the p-V diagram is thus a smooth continuous envelope and its area, which corresponds to the work output, results significantly decreased (40-60%) [13].

Leakage of working fluid

Seals in Stirling engines are typically of the conventional ring type or clearance seals; their design is complicated by the fact that they must usually run without oil or lubrication and their bearing pressures may not be too great, as this would cause local heating and eventual seizure of the moving surfaces. Stirling engine seals design therefore involve some compromise, which may result in unavoidable leakage trough the seals. Thermodynamic effects connected to the leakage losses are principally the reduction of the internal fluid mass of the engine and therefore also of the internal pressures, so that p-V cycle is lowered and work output decreased [2, 13].

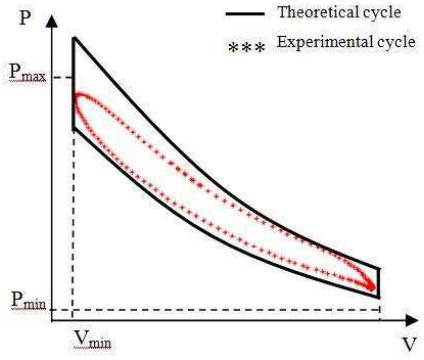

Figure 1.3: difference between Ideal and real Stirling cycle

Aerodynamic and mechanical friction losses

In connection to real seals and a real driving mechanism, it has to be considered the effect of the friction forces in the various mechanical parts of the engine that contributes to reduce the final work output of the cycle. These losses are usually accounted in an 'organic efficiency' and are typical of any real mechanical engine. In addition to the mechanical friction losses, aerodynamic-flow friction losses intervene inside the engine, especially in the regenerator and the heat exchangers. These losses cause differences in the pressure of the working fluid inside the various components of the engine and result in a decrease of the net cycle output; engine components design should therefore pursue efficiency trying not to lead to exceedingly high fluid friction forces and pressure drop [2, 13].

Real gas and turbulence

Another difference with the ideal cycle is represented by the non ideality of the working fluid, which implies non reversible transformations of the gas and introduces gas spring hysteresis losses. The hysteresis loss acts as an additional load on the machine and therefore impairs the work output and the thermodynamic efficiency; even if they usually have small consequences on crank type machine they can imply serious effects on free-piston machines (see section 1.4) where they can alter the phase angle and the amplitudes of the piston and displacer. The losses connected to the working fluid comprehend also turbulence effects: its impact varies widely on the geometry of the machine and the velocity reached inside its different components and has the consequence of dissipating part of the fluid energy inside turbulent micro structures as vortex or eddies [2].

Dead spaces

A dead space is defined as the part of the working space not swept by one of the two pistons: in Stirling devices includes cylinder clearance spaces, void volumes, regenerator, heat exchanger volumes and the volume associated to ducts and ports. Its inevitable presence in a real engine imply a direct loss for the cycle because, unlike in the ideal cycle, the fluid can not expand or be compressed totally and partly remains within these spaces reducing the work output of the engine [13].

Real heat exchangers and regenerator

Heat exchangers are the components having the most significant effect on the performance and the costs of the engine. By using real heat exchangers the heat transfer rate with the fluid can not be assumed infinite and compression and expansion processes will not result isothermal. Therefore the temperatures experienced by the working fluid may be substantially different from the temperatures at which heating and cooling is available and, at high temperatures, material limits can further increase this difference. In fact, in Stirling engine some parts of the machine are exposed continuously to high temperatures, and not just momentary as happen in Otto and Diesel engines, resulting in a limitation of the higher fluid temperatures due to walls metallurgical limits. In order to improve the heat exchangers efficiency it might be increased their exchange surface area however, it must be taken into account that large heat exchangers imply higher dead space and fluid-friction losses, therefore the practical design should be a compromise between these factors. Another important loss in the hot heat exchanger, if combustion is used as the heat source, is represented by the exhaust gas flow, because it has no useful purpose in the engine and therefore represents a direct loss and a reduction of the global efficiency.

Regenerator can be considered as an additional heat exchanger in Stirling engines, and is affected by similar losses. During the regenerations, finite heat transfer rates between fluid and solid matrix make impossible to heat and cool the working fluid to temperatures of the working spaces as was in the ideal case. Real regenerator temperatures lie in between the temperatures of the cold and hot spaces limiting the heat transfer and reducing regeneration efficiencies. The main causes of the withdrawal from ideality can be accounted to finite exchange surface, limited heat capacity of the porous material and internal conduction in the solid matrix which, redistributing the solid temperatures, enlarges the temperature differences between solid and fluid phase and results in increased irreversibilities. The design of the regenerator, similarly to

the one of the heat exchangers, results from the compromise between different requirements: it should guarantee a sufficient heat transfer between the fluid and the solid matrix, but, at the same time, it should be compact (in order to minimize dead space losses) and be characterized by low fluid-dynamic resistance [2, 13].

Thermal losses
Thermal losses in general reduces the machine efficiency and can be accounted to conduction convection an irradiation phenomena. Conduction losses occur through the walls of the engine in particular in expansion space and regenerator, but in most cases do not alter significantly the working gas temperatures, resulting in a negative effect of the thermal efficiency only. Convection losses can have important consequences if the machine presents hot external surfaces, so that usually insulation is used to limit this phenomenon. Irradiation losses can have different importance depending on the type of heat source and engine, and in some cases, can represent one of the major causes of losses in the hot exchanger and expansion space [2].

1.4 Stirling engine configurations

The driving methods of Stirling machines can usually be divided into two groups: kinematic and free-pistons drivers. Under kinematic category are accounted all the machines with elements such as cranks, connecting rods and flywheels, which move together to vary the working spaces in a prescribed manner. Free piston drivers, instead of crank engines, use the working gas pressure variations to move the reciprocating elements, and work is removed by a linear alternator or hydraulic pump. This kind of solutions are more complicated compared to crank mechanism but are reliable, can be self-starting and in most of the configurations do not need external seals. Despite these advantages it must be mentioned that very few free-piston devices are commercially available and that further research is needed in this field. Both kinematic and free-piston engines can be classified into tree general mechanical configurations, known as Alpha, Beta and Gamma arrangements [2, 13] which are shown in Fig. 1.4

Alpha configuration has two cylinders and two separate pistons that move the air back and forth between the hot and the cold side of the engine through the heat exchangers and the regenerator. This configurations have mainly been pursued by the proponents of automotive Stirling engines such as Ford and Philips, and its main advantage consists in the

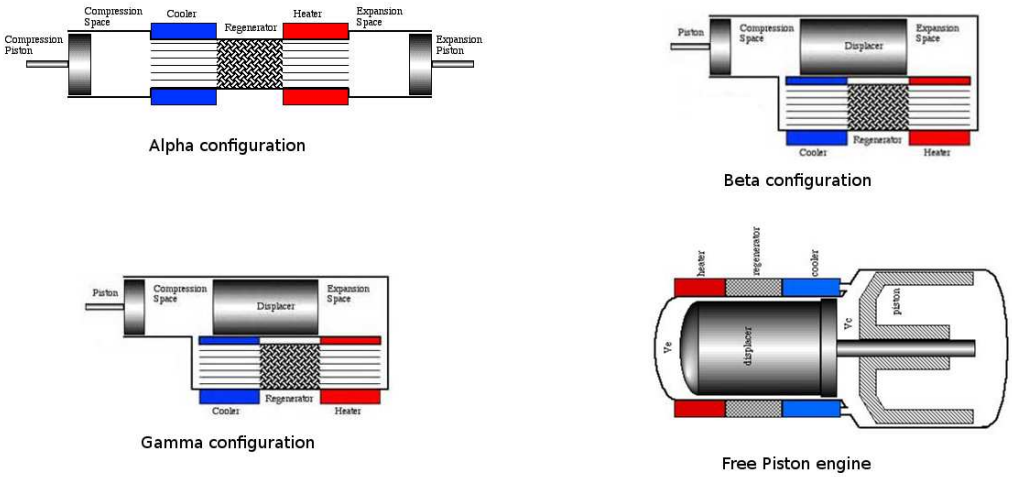

Figure 1.4: Schemes for Stirling Alpha, Beta, Gamma configurations and for a Free Piston engine

simplicity in which it can be compounded into compact multiple cylinder configurations, enabling an extremely high specific power output [2].

Beta configuration has only one piston, named 'power piston', and in the same cylinder presents a displacer, with the aim of moving the working fluid from one space to another. This is the original configuration used by Robert Stirling in his 'Air engine' and has historically enjoyed a wide popularity. One important advantage of this solution, if compared with the alpha configuration, is that it can require less or smaller seals resulting in reduced friction and leakage losses. In addition, since the displacer does no work but only displaces the fluid, it can be structurally lighter than a piston requiring correspondingly smaller rods, links and bearings so that appreciable savings in weight and mechanical-friction losses can be made [13].

Gamma configuration uses a displacer as the Beta configuration, but in this case piston and displacer move in separate cylinders. This solution tends usually to have larger dead volumes than Alpha and Beta and therefore a reduced specific power; however it shares with beta configuration all the advantages of using a displacer and in addition presents an increased flexibility for the design of the crankshaft and connecting rod systems and allows the separation of the displacer rod seal to a

fixed location in the displacer cylinder [2, 13].

Despite several technical solutions have been presented in the Stirling history, there is no configuration that resulted absolutely better than the others, because each one is characterized by peculiar advantages and drawbacks; therefore all these three configurations have been widely studied and used, each one applied as the better compromise for a specific application field.

1.5 Stirling applications

Stirling technology is characterized by different advantages and can become an interesting solution when its strengths are matched to the right applications. In general it can be said that Stirling engine make sense where [17]:

- there is a premium on low noise operation;
- there is a very good cooling source available;
- multi fuel capacity is desired;
- a medium-low temperature waste heat is available;
- the engine can run at constant power output and a warm-up period is acceptable.

The principal disadvantage of the Stirling engines is that technologically advanced solutions are expensive and complex; simpler versions are less costly but are not comparable in terms of efficiency and specific power output with internal combustion engines. In addition Stirling engines with high thermal efficiency and specific output suffer problems in heat transfer methods and seal technologies and it appears unlikely that they will compete with Diesel engines in terms of cost per unit of power. Therefore Stirling engines nowadays are mostly used in very specific applications where their advantages are exalted [13]; among the current fields of use should be mentioned:

Cryogenic engines: Stirling engine used as reversible machine is not competitive in refrigerators range but, when it comes to cryogenic applications, it stands over all the other technologies. Stirling cryocoolers cover a wide range of powers from miniature models to large industrial machines, and guarantee temperatures below 100K reaching even less than 10K in research applications [17].

Small electrical generation: As prime movers machines, Stirling engines are now available as small electrical generators used for various purposes in isolated locations and where maintenance is difficult. Among the others, it deserve a particular attention the application of Stirling engines in concentrated solar power, where it represents the best technological solution to exploit solar dish concentration. Most recent application are small and medium size cogenerative engines powered by different fuel including vegetable waste [13].

Marine engines: Stirling engines are attractive for marine purposes because of the large available cooling supply represented by the water, however in very large size application they can not compete with the most efficient diesel engines. Therefore nowadays their use is restricted to small boats or yachts where their silent functioning is appreciated; the quietness of the functioning has been valuable also for military purposes, and it is worth mentioning the application of Stirling engines on military submarines by the Swedish defence contractor [17, 13].

Chapter 2

A review of the Stirling models

[...] Stirling conceptual simplicity is misleading, and sophisticated computer analysis is required in order to predict its performance satisfactory

Israel Urieli

In this chapter the methods available for the analysis of Stirling engines are reviewed. It must be said that Stirling cycle presents considerable analytical difficulties compared with the analysis of Otto and Diesel cycles, mostly due to the fact that the working gas undergoes many conditions in the different components and phases of the cycle. In addition, all the irreversibilities explained in Sec. 1.3 should be taken into account and modeled at the same time, since their effects are linked and heavily affect the engine performances. In the years, these difficulties along with the alternative fortune of Stirling technologies (see section 1.1) have brought to the development of relatively few models and, despite the most recent formulations date back to the 1980s, the same models are still cited and applied in many of the modern researches. Only in recent years, with the diffusion of CFD analysis, it has been possible to develop new and more accurate simulation tools, which are supposed to gradually overcome all the limitations and assumptions characterizing the former analysis. As many authors [2, 6, 18] and also a recent NASA review suggested [7], all the Stirling models can be classified by their engine design methods and basic assumptions into five categories of increasing sophistication: zero order analysis, first order analysis, second order analysis, third order analysis and fourth order analysis.

2.1 Zero order analysis

This model is the simplest and was formulated by Beale in 1971 in an attempt to establish a similitude between all the Stirling machines [2]. The principal

assumption is that most of the engines operate under similar parametric conditions, therefore the power output can be always expressed by

$$P_0 = Be\ p_{min}\ V_{sw}\ f, \tag{2.1}$$

where Be is the Beale number and is assumed constant and equal to 0.015, p_{min} is the mean operating pressure (bar), V_{sw} is a parameter representative of the compression and expansion swept volumes (cm^3) , and f is the frequency of the system (Hz). Despite many attempts have been made in order to correlate this analysis with experimental measurements, no valuable results were obtained and this analysis remained merely a theoretical dissertation.

2.2 First order analysis

This analysis was published in 1871 by Gustav Schmidt [19] and for many years, almost until 1960, it stood as the reference model for Stirling engine developers; even today, because of its simplicity, this model is widely used for the initial sizing of the engines [2]. The central attraction of this analysis is that it produces closed-form solutions for the performance which can be easily manipulated by the designer. The principal assumption made in this model is that the hot space and the heater are at the upper source temperature T_h, while the cold space and the cooler are both constant at the lower sink temperature T_k. This assumption implies that the heat exchangers, including the regenerator, are perfectly effective and thus ideal. The engine is configured as series of five components representing respectively the compression space c, the cooler k, the regenerator r, the heater h and the hot space e. Therefore any interconnecting volumes (eg ducts) will be included in the closer clearance volume. Each component is considered homogeneous and gas within is represented by a mass m and its thermophisical properties T, p, V, with the assumption that a perfect gas state equation is applicable. It is further supposed that no pressure drop occurs in any component and that friction losses, mechanical losses and fluid leakage are negligible over the entire engine. All these ideal assumptions have the aim to simplify the problem in order to easily calculate the work done by the cycle and the heat transferred to the fluid.

Work is done on the surroundings by virtue of the varying volumes of working spaces V_c and V_e. Total work can therefore be calculated by the sum of these two works over a complete cycle:

$$W = W_c + W_e = \oint p\mathrm{d}V_c + \oint p\mathrm{d}V_e = \oint p\left(\frac{\mathrm{d}V_c}{\mathrm{d}\theta} + \frac{\mathrm{d}V_e}{\mathrm{d}\theta}\right)\mathrm{d}\theta \tag{2.2}$$

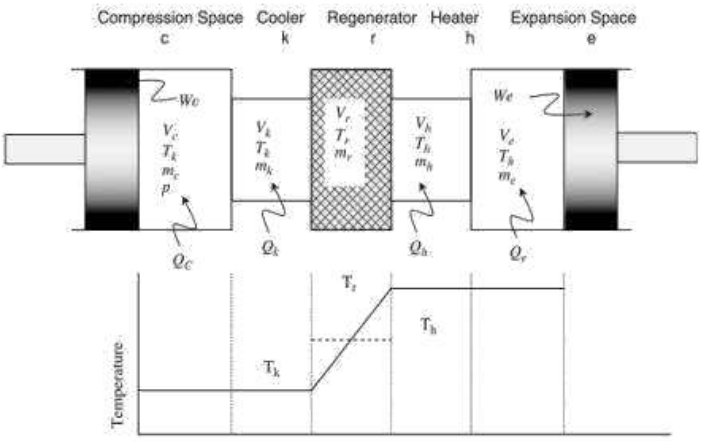

Figure 2.1: Isotermal model scheme

In equation (2.2) p is the the pressure of the working fluid, constant on the total system, and θ is the crank angle. Pressure p then, can be explicitly calculated by

$$p = MR\left(\frac{V_c}{T_k} + \frac{V_k}{T_k} + \frac{V_r ln(T_h/T_k)}{(T_h - T_k)} + \frac{V_h}{T_h} + \frac{V_e}{T_h}\right)^{-1} \tag{2.3}$$

where M is the total mass and R the ideal gas constant. Equation (2.3) is obtained by substituting ideal gas lows of every space in the total mass balance. Therefore work output W can be estimated by simply knowing the temperatures, the volumes of the spaces and the kinematic low with which the volumes vary. Finally, solving the energy balance over each space, it can be demonstrated that the heat exchanged in one space is equal to the work done by the space itself (equation (2.4 a,b)), therefore all heat input to the isothermal cycle occurs in the expansion space, and all heat output occurs in the compression space, while heat exchangers in this analysis does not exchange any heat and result, therefore, redundant.

$$Q_c = W_c = \oint p\frac{\mathrm{d}V_c}{\mathrm{d}\theta}\mathrm{d}\theta \qquad Q_e = W_e = \oint p\frac{\mathrm{d}V_e}{\mathrm{d}\theta}\mathrm{d}\theta \tag{2.4 a,b}$$

It is possible consequently to define the thermal efficiency of the machine as

$$\eta = \frac{W}{Q_e}. \tag{2.5}$$

Despite its simplicity, this model is not much reliable and do not take into account the most of the irreversibilities of the engine. In general it can be

said that first order analysis provide a quick way to estimate the relationship between the overall size of an engine and its power output, but they are not very useful as detailed tools for Stirling engines. Hence the following models will try to gradually remove all the ideal assumptions made in this first analysis in order to obtain more complete information on the machine performances.

2.3 Second order analysis

These design models, as the isothermal analysis of section 2.2, have the main purpose to determine the power output and efficiency of the machine by solving balances on a simplified system. The major improvement of the second order methods relative to first order, is that individual loss mechanism are identified and quantified, and therefore a more accurate information of the machine performances is available. The most important hypothesis of first order analysis is that expansion and compression spaces are isothermal: this assumption is removed in a series of models that can be grouped under the name of *'Adiabatic analysis'*, among which should be cited the analysis proposed by Finkelstein (1960) [20], Walker and Kahan (1965) and Lee and Berchowitz (1978) [2]. A further improvement of these models is then represented by a series of later works in which, still on the same bases of the previous analysis, various other losses are taken into account and studied. These methods, named as *'Quasi stationary analysis'* were first introduced by Urieli and Berchowitz (1984) [2] and then widely used in the following years.

2.3.1 Adiabatic analysis

In this class of models the engine is configured as a five component system as in the isothermal model, however it is assumed that compression and expansion spaces walls are adiabatic and thus the temperatures T_c and T_e can vary over the cycle. Heat exchangers and regenerator instead, are assumed to behave ideally and therefore gas has in these spaces, the same temperature distribution as in the isothermal model. These simple assumptions bring to formulate equations which are no longer explicitly integrable and, therefore, the problem can be expressed only by means of differential equations. Since the describing set of differential equations is non linear, numerical methods should be used in order to solve the mathematical problem. In general the method of solution is the same of isothermal analysis, and solving equations are derived from the global mass balance, the energy balance for each space, the state equations for ideal gas, and the conservation of the mass fluxes

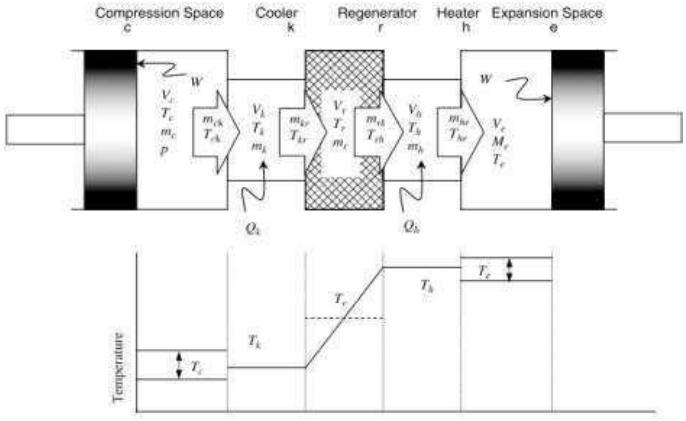

Figure 2.2: Adiabatic model scheme

across the cells interfaces. Here these equations are not shown because they are not useful for the purposes of this discussion; on the contrary it is worth accounting the consequences that this formulation of the problem implies. At first, with this formulation, the heat is transferred or subtracted to the fluid only in heat exchangers spaces, behavior which is closer to reality. Then, it must be noticed that the temperatures in compression and expansion spaces are not constant and result directly form the process, introducing an initialization problem of the temperature of these spaces; the only guidance for a correct choice is that, in a stabilized functioning of the machine, their values at the end of the cycle should be equal to the value they had at the beginning of the cycle. Hence is usual to assign arbitrary (but consistent) initial temperature conditions, and integrate the equations through several complete cycles until a cyclic steady state has been attained. This is equivalent to the transient 'warm up' operation of an actual machine which starts from the same initial condition and go through successive transient cycles until the values of all the state variables repeat unchanged cyclically. Experience has shown that the most sensitive measure of convergence to cyclic steady state is the residual regenerator heat Q_r at the end of the cycle, which should be zero. For completeness in this discussion, it should be mentioned the existence of some *'semi-adiabatic analysis'* [2], in which the wall temperatures of the working spaces are assumed to be constant and equal to the heat source and heat sink temperatures respectively. Thus the adiabatic assumption of the working spaces is removed, but the most of the heat is still exchanged in the heat exchangers which, as the regenerator, are assumed to behave ideally as before. This semi-adiabatic models can actually result in efficiency predictions closer to the experimental measurements than either the purely

adiabatic cycle or the isothermal cycle.

2.3.2 Quasi steady state analysis

This model is an improvement of the adiabatic analysis and aims to study various losses that were ignored previously, with a particular attention to the heat exchangers [2]. Heat exchangers and regenerator are, as said before, probably the most important components of the engine and, at the same time, the most critical: their design is complicated because they should transfer the highest heat quantity to improve efficiency and, at the same time, occupy small volumes in order to reduce pressure drop and dead space losses (see section 1.3). Their development is therefore a compromise between these two aspects and, practically, in none of the technical solutions it can be assumed an ideal heat transfer with the working gas. In order to model the real heat exchange it must be considered the fundamental equation for heat transfer

$$\dot{Q} = U(T_w - T_f), \tag{2.6}$$

where $\dot{Q}$ is the rate of heat transfer, U is the overall thermal conductance and T_w and T_f are the respective wall and fluid temperatures. Since in Stirling engines the major means for transferring heat to the working gas is forced convection, equation (2.6) can be rewritten as

$$\dot{Q} = hA_{wg}(T_w - T_f), \tag{2.7}$$

where h is the heat transfer coefficient and A_{wg} is the exchange surface area. The apparent simplicity of this equation, however, is misleading, since coefficients h are only available empirically, being a complicated function of the transport properties, the flow regime and the heat exchanger geometry. It must be said that design of heat exchangers is well established in industry and lots of empirical correlations have been published, both for thermal conductance and flow friction factor. However all of them are obtained assuming steady flow state, while in Stirling engines flow is unsteady and varies considerably over the cycle. Furthermore, because of the relative motion of the two pistons, at some periods of the cycle the gas can flow simultaneously in both directions. In absence of periodic-flow heat transfer and flow friction data, in this analysis is assumed that, at each increment in the cycle, steady flow conditions prevail, thus the name 'Quasi steady state'. Therefore at each time step, the heat transferred between heat exchangers and working fluid is evaluated by means of the equation (2.7) and added to the energy balance of the corresponding cell. The same equation is then applied also for the regenerator, with the additional consideration that its temperature is

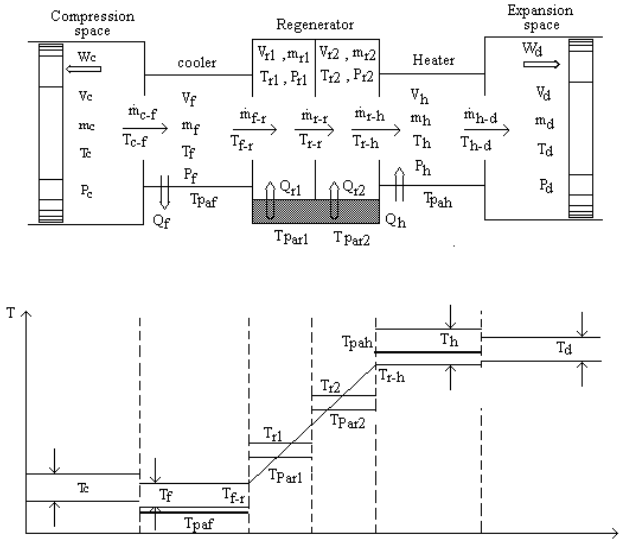

Figure 2.3: Quasi steady state model scheme

variable during the simulation and can be calculated by solving equation

$$\frac{\partial T_w}{\partial t} = -\frac{\dot{Q}}{c}, \tag{2.8}$$

where c is the thermal capacity of the solid matrix. As illustrated in Fig. 2.3, the regenerator is here divided in two cells, in order to more accurately model the temperature stratification which characterizes it. This analysis also takes into account the frictional drag force that occurs in the heat exchangers and most importantly in the regenerator matrix; these losses cause a difference of pressure inside the engine and are responsible of a reduction in the work output. Pressure losses Δp are here evaluated by

$$\Delta p + \frac{2 f_r \mu g V}{A d^2 \rho} = 0, \tag{2.9}$$

where f_r is the friction factor (empirically derived), μ the gas viscosity, g the mass flow, V the void volume, A the wetted area, d the hydraulic diameter and ρ the gas density. The compression space temperature is arbitrary taken as the baseline pressure and is solved each time step; the pressure distribution in the engine is then obtained from its value by simply adding the Δp calculated in the same instant for the various spaces. It must be noted that Δp changes its sign depending on the direction of the fluid and, therefore, the pressure in the compression space is alternatively the maximum and minimum pressure of the system. One last consideration is done to evaluate the flow dissipation $Diss$, that is the internal heat generation which occurs when

the gas is forced to flow against the frictional drag force. This therm can be expressed as a function of the pressure drop by means of Eq. (2.10)

$$Diss = \frac{\Delta pgA}{\rho}, \tag{2.10}$$

and should be included in the energy balance of each cell in which a pressure drop occurs.
The overall analysis brings to the formulation of a set of non linear differential equations more numerous than the adiabatic model, therefore the numerical solution needs more computational effort. As before, a consistent set on initial conditions should be chosen, and equations are integrated until cyclic steady state has been attained. It is interesting to notice that the time needed for convergence to cyclic steady state is dependent mainly on the thermal capacitance of the system, in particular that of the regenerator matrix c. Various accelerating techniques have been presented in literature, in order to decrease the computational time required to reach convergence. Finally it should be taken into account that in general, the more the analysis is accurate and complete, the more the system of equations is complex and the numerical solution is prone to various effects of numerical instability. These effects are often difficult to locate or identify and, in many cases, are function of the specific system being solved; therefore it is difficult to define universally applicable techniques to solve these problems.

2.4 Third order analysis

Third order methods, also known as nodal analysis, group all the 1D simulations of the Stirling engines and usually consist of three basic steps [21]: (1) discretization of the engine geometry as a network of nodes and control volumes; (2) definition of the set of differential equations for the conservation of mass, momentum, and energy, which is closed by the equation of state for the working gas; (3) solution of the the system of differential equations by means of some adequate numerical method. Third order methods have been introduced with the purpose to consider simultaneously the many different complex processes coexisting in a Stirling engine, which were considered decoupled in the previous analysis. Nevertheless they still require empirical correlations to model the heat transfer coefficients and friction factors [18]. These methods are more sophisticated and by far more expensive in computational effort and time with respect to the second order analysis: the domain is usually divided in many nodes and more equations have to be solved for each control volume, resulting in numerical stability problems. The main difference between the methods accounted in this class lies in the

way they approach the numerical problem in order to reduce the computation time and promote stability and convergence of the solution. In general third class methods can be divided in two subclasses: one more rigorous and the other less rigorous [21, 18]. The rigorous third order analysis solve all the equations and include empirical formulations for friction factors and heat transfer coefficients; the less rigorous analysis instead, simplify the numerical computations by omitting some of the therms from the governing differential equations. In this way it is possible to decouple certain losses from the main calculation and thus improve the speed of computation. Common simplifications in existing models are: ignoring inertial terms in the momentum equation; ignoring both inertial terms and flow friction terms, which allows not to solve the momentum equation; ignoring the kinetic energy in the energy equation.

Numerical methods normally applied, use a finite differencing of the spatial derivatives to convert the partial differential equations to a system of ordinary differential equations, so that each conservation equation is represented by a difference equation at each node. In literature, numerical methods for solving this system of ordinary differential equations can be divided in two categories: *explicit* and *implicit*. In the explicit integrations, the thermodynamic information at the new time is computed from time derivatives that were evaluated at the previous time. These techniques are sometimes affected by numerical oscillations and instabilities, especially if time steps are too large [18, 22]. Implicit methods instead, solve the system of ordinary differential equations by computing the thermodynamic information at a new time from time derivatives that are evaluated at the same time. These methods are usually numerically stable and therefore can use larger time steps than the explicit methods. In addition to the previous numerical methods, should be cited a group of analysis as the ones done by Organ (1981) [1] and Larson (1981) that apply the *method of characteristics* to solve the set of nonlinear partial differential equations. This method is used to transform the partial differential equations into a system of ordinary differential equations that are valid only along characteristics curves and allows to simultaneously solve all the conservation equations. The method of characteristics can be applied at different levels of complexity to Stirling engines and it is claimed to be more general and more precise in determining the mathematical solution of the equations.

Third order methods can generate a more complete information about the machine than second order analysis, and can be used to compute gas conditions inside the engine which can not be measured in practice. Nevertheless there is no evidence that they always give better results compared with the previous analysis because, in some cases, second order codes can obtain com-

parable precision in a shorter computational time [6]. It must be said however, that technology improvements of the last two decades largely diminished the computational time required in third-order analysis and numerical methods have been refined in order to improve convergence and stability; therefore nowadays, mono-dimensional models are adequate engineering tools and are used especially in fast optimization applications and performance mapping; among mono-dimensional softwares should be cited Sage and DeltaE [7]. Nevertheless this type of analysis can not account the effects of the geometry on the internal flows as well as distributions of working fluid properties over longitudinal axes, thus resulting in an incomplete information for the machine design. A better understanding of flow features and heat transfer throughout the engine can be useful to improve efficiency, reliability, and supplement experimental testing, therefore a multi-dimensional approach is worth developing.

2.5 Fourth order CFD analysis

As anticipated in the previous section, third order analysis can give adequate information on the performances of the engine, but are characterized by inherent limits. They still require the definition of heat exchange and flow friction models and do not take into account the real properties distribution inside the engine. The importance of a multi-dimensional (fourth order), CFD approach is thus explained. Computational Fluid Dynamics is a fairly new tool: its development and practical use has been in the years limited by the computing power of calculators and, thanks to technology fast enhancement, in the last two decades this type of analysis has improved considerably. Todays CFD softwares can be considered very efficient and advanced tools to support the design and optimization of technologies in many application fields. CFD simulations typically consist of five main steps. First define and design the geometry (domain) of the problem. Second, discretize the continuous geometry into a mesh grid. Third define the physical laws and boundary conditions governing the problem. Fourth, convert the partial differential equations of the governing laws into a set of algebraic equations. Last run the simulation and post-process the results analyzing whether they represent the physical solution of the initial problem. Despite CFD is actually used with success in many fields (internal-combustion engines, aerodynamics, acoustics etc), its application to Stirling engines is only recent, and still suffers from many challenges [23, 24, 25]. The first issue is that a Stirling engine is inherently a multi-physic and multi-scale problem, in fact is characterized by the interaction of more than one material (working fluid, walls and especially regenerator) and the simultaneous simulations of various

components, which can have different scales. In addition heat transfer and fluid mechanics should be solved simultaneously, because they are strictly connected and influence each other. Mesh grid should be designed carefully, because the rate at which conjugate heat transfer can be solved is directly related to the smoothness an quality of the grid at the interface; moreover the mesh, in Stirling engines, is not stationary and the simulations involve moving parts. It must be said that not all industrial softwares can support and correctly solve all these problems together and, in any case, they should be used with care. It is not uncommon the necessity of human intervention to define additional functions and codes to supply software deficiencies and avoid inaccurate results. Another challenge facing CFD analysis of Stirling engines is that, due to the oscillatory nature of the flow, it is necessary to model the entire engine as a whole and not as single separate components [23]. The modeling of a sole component in fact, requires known unsteady boundary conditions for an entire cycle. Since a given boundary may have flow going in both directions, the direction of the characteristics at these boundaries are difficult to define, but at the same time, incorrect specifications of these brings to solution instability, non-convergence of solutions, and/or convergence to inaccurate results. Moreover, these problematic boundaries can, in some cases, move during the functioning of the engine, further complicating the numerical boundary treatment. It can be said that artificial boundary condition specification in non-linear turbulent flows such as Stirling flows, is an important but non yet resolved area of research. As a consequence of these difficulties, in recent years only few researches tried to simulate the unsteady functioning of single components [9, 8], while most recent publications are moving towards the direction of modeling the whole engine at once [11, 10, 12]. Current researchers' effort focus mainly on solving the challenges facing accurate simulations of Stirling engines in a reasonable time. Simulation duration is of major importance because only if this is limited, results can be used for practical purposes as the optimization of design variables and parametric analysis of engine performances. In literature there can be find few cases in which a CFD analysis was successfully used to study a Stirling engine. The first successful three-dimensional whole Stirling engine simulation was reported by Mahkamov (2006) in the United Kingdom, after having obtained encouraging results with a 2D axisymmetric geometry [11]. Two gamma-type Stirling engines were simulated using commercially available software with good experimental agreement but limited information and verification is available. Seal leakage, appendix gap, and other loss mechanisms were not included in this work. The second reported three-dimensional Stirling engine simulation was conducted by Zhang and Ibrahim (2004) in China , but it took approximately 3 months to reach a steady-harmonic con-

verged solution on a simplified, academic geometry that did not include the appendix gap, solid walls, or internal displacer [10]. Two dimensional models were then developed by Arlanda et al. and Houkema to model and optimize respectively a solar Stirling engine and the regenerator of a Stirling machine used for domestic combined heat and power generation [23]. Though they used simplified geometry and models, the results have been encouraging and gave practical information for the engines improvement. A more complete model was reported by Dyson et al. (2008) and concerned a fully converged three dimensional simulation of a free-piston Stirling engine [12]. The latest advances in computer processor and hardware were used in these simulations and the authors claimed to have obtained accurate results in relatively short time; this work however did not include a thermal non-equilibrium regenerator model yet. As a matter of fact, Stirling CFD simulation is still an open problem and different aspects need further improvements, especially the convergence time of simulations and the regenerator model.

In conclusion, despite the numerous problems that faces, it can be said that CFD analysis still remains an appetizing tool to study Stirling engines. As previous researches demonstrated, CFD can generate a far more complete and punctual information on the engine compared with second and third order analysis, and allows to investigate internal behaviors of the machine which are not accessible with experimental tests. In addition to a mono-dimension third-order analysis, CFD introduces the modeling of the system geometry. This allows to study and correctly account the real spatial flow distribution of the working fluid inside the engine and provides detailed pressure, velocity and temperature fields in the various parts of the machine. Moreover, by means of properly generated grids, it is possible to solve thermal exchanges, friction factors, and boundary layers effects which were previously modeled or neglected. At the same time CFD analysis can be used to numerically determine the one dimensional equivalent friction factors and heat transfer terms in the various components; in this way, one dimensional analysis can be made more accurate and can be used for fast optimization and performance mapping.

2.6 Closure

The review and analysis of the literature done in this chapter leads to the conclusion that third-order mono-dimensional methods and CFD modeling are characterized by important capabilities and, when combined, represent useful tools for the design of a Stirling device, supporting all the phases of the development: initial design, tuning of the model coefficients, optimization and final prototype demonstration before the first metal is cut.

Chapter 3

Development of the model

In this chapter the development of a CFD model for the simulation of a Stirling machine will be described. The model has been developed on the basis of the open-source finite volume code OpenFOAM [15], by means of the implementation of specific submodels in order to take into account the specific features of this type of machine. In particular specific mesh motion strategies were developed for the description of the motion of the power piston and of the regenerator, in order to reproduce the variation of the volumes of the working spaces. Moreover, heat-transfer models were implemented for taking into account the presence of the heat source/sink of the cycle and the regenerator.

In the following sections, at first the governing equations for the problem in exam will be presented. Then the strategies implemented for the mesh generation and motion will be described. Finally the different sub-models needed for the simulation will be analyzed, including the models for the simulation of the flow through the porous matrix of the regenerator. In particular, with regards to the modeling of the solid-fluid thermal interaction in the regenerator, two approaches will be proposed: *Single regione* and *Multi region*.

3.1 Governing equations

In order to model the fluid-dynamic problem, the system of conservation equations for the generic continuum needs to be combined with the constitutive relations describing the properties of the specific medium. Working fluids usually adopted in Stirling applications are air, hydrogen or helium, which do not undergo state transition or mix with other species under working conditions. Considering a Newtonian compressible single-phase fluid, the mathematical set of the governing equations consists in [26]:

- Continuity equation

$$\frac{\partial(\varrho)}{\partial t} + \nabla \cdot (\varrho \vec{u}) = 0 \tag{3.1}$$

  which guarantees the mass conservation in the domain. Conservation of mass is always important, but in Stirling engines results fundamental, because the system is closed and inaccuracies in mass calculation can bring to instabilities and/or incorrect solutions.

- Navier-Stokes equation, derived from the conservation of momentum

$$\frac{\partial(\varrho \vec{u})}{\partial t} + \nabla \cdot (\varrho \vec{u}\vec{u}) = -\nabla p + \mu \nabla^2 \vec{u} + \Re \tag{3.2}$$

- Total energy equation

$$\frac{\partial(\varrho E)}{\partial t} + \nabla \cdot (\varrho E \vec{u}) = -p\nabla \cdot (\vec{u}) + \nabla \cdot (k_f \nabla T) + S_{fluid} \tag{3.3}$$

  where E represents the total energy of the fluid. In Stirling engines total energy can by expressed by the sum of internal energy and kinetic energy only, because potential energy effects can be neglected and no other forms of energy are present, so that

$$E = i + \frac{1}{2}u^2,$$

  where i represents the internal energy and u the magnitude of the fluid velocity.

This set of equations is closed by means of the perfect gas equation of state:

$$p\ V = n\ R\ T \tag{3.4}$$

The variation of the fluid dynamic viscosity on the bases of the fluid temperature has been accounted by using the Sutherland model expressed with two parameters

$$\mu = A_s \frac{\sqrt{T}}{1 + T_s/T} \tag{3.5}$$

where A_s and T_s are tabulated. On the other hand, when a solid medium is considered, the set of governing equations reduces to the energy conservation equation, which describes the conductive heat-transfer process:

$$\frac{\partial \rho c_s T}{\partial t} = k_s \nabla T + S_{solid} \tag{3.6}$$

The set of Eqns. 3.1 - 3.3 is general, and is solved for each cell in which the fluid domain is divided; the introduction of Eq. 3.6 instead allows to describe the physics of the solid porous media and will be described in Sec. 3.5. The source terms $\Re$, S_{fluid} and S_{solid} of Eqns. 3.2-3.3-3.6 are applied only in the cells where particular components of the machines are located. In addition it should be considered that fluid-dynamic and heat transfer simultaneously influence the performances of the machine and that the respective governing equations therefore, can not be decoupled in the solution.

In order to solve this system of differential equations, boundary conditions should be defined; in Stirling engines, if leakage is not taken into account, all the boundaries are *Wall*, because the geometry is closed. Therefore on boundaries, fluid velocity is equal to the local wall velocity; for temperatures are used zero gradient conditions if the wall can be considered adiabatic or fixed temperature conditions if the wall is maintained externally at a constant temperature (Sec. 3.4). Boundary conditions are summarized in the following table.

Table 3.1: Boundary conditions.

Field	**Boundary patch**	**Boundary type**	**Expression**
pressure	all	Neumann	$\partial p/\partial \vec{n} = 0$
velocity	fixed	Dirichlet	$\vec{u} = 0$
	moving	Dirichlet	$\vec{u} = u\vec{_W}$
temperature	adiabatic	Neumann	$\partial T/\partial \vec{n} = 0$
	fixed temperature	Dirichlet	$T = T_W$

3.2 Mesh generation and Mesh motion

In the CFD analysis it is primarily the grid quality that determines the speed and accuracy of the solution; a valid mesh in fact, is a pre-requisite for a good numerical solution and is of fundamental importance for motion of the mesh. In Stirling engines, geometry can be complex and always presents moving parts, therefore meshes obtained with automatic meshing softwares are usually not refined enough and often require human intervention. In addition, because of the very different heat capacity between working fluid and regenerator (Sec. 3.5), Stirling simulations require many cycles to reach a cyclic steady state regime and, therefore, many iterations have to be solved. Consequently mesh generation should always be a compromise between an accurate description of the real geometry and the speed of the resolution.

Here below are listed some guidelines which come from the experience gained in this work and from the procedure described by Dyson (2005) [24].

[1] Use structured grids, better if orthogonal; wherever possible try to reduce the number of bad cells and in general the total number of cells required.

[2] Include as much geometry as is practical to avoid having to redo the grid a second time when simplifying assumptions are found to matter

[3] Mesh is compressed and strained during the simulation, therefore the effective minimum and maximum dimensions of the cells over a complete cycle should be accounted in grid developing. Wherever possible use a layering addition/removal function on the piston patches, so that smallest and largest dimensions of the cells are automatically corrected.

[4] Limit mesh motion to piston/displacer swept zones; avoid moving grid inside regenerator and heat exchangers for faster run-times.

[5] Avoid grid adaption and remeshing because they slow down the simulation considerably

[6] Refine grid close to non adiabatic walls and wherever the geometry suggests remarkable friction effects so that it is possible to correctly solve the thermal and dynamic boundary layers. Use sizing function to smoothly expand the cell size from these boundaries inwards. (see Sec. 3.4)

[7] Do not overly refine mesh in regenerator zone because here boundary layers do not occur and the interaction between fluid and solid matrix needs always to be modeled. A fine mesh in this zone would only slow down the computation time without leading to a better solution. (see Sec. 3.5)

[8] For the first simulations avoid modeling engine details (eg. seals, appendix gaps) which require extremely fine grids without having a significant influence on the fluid velocity field or the general performances of the engine. In this way it is possible to use a coarser grid and run faster simulations, so that parametric analysis on the most important parameters can be done. In a later time, by knowing the fields distribution over the engine, a more complete and refined mesh can be tested, to account also the effects of those small parts that were previously omitted.

In order adopt a mesh motion mechanism, the integral form of the generic conservation equation for a tensorial property ϕ defined in an arbitrary moving volume V bounded by a closed surface S states [27, 28]:

$$\frac{d}{dt}\int_V \phi dV + \oint_S ds \cdot (\vec{u} - \vec{u}_b)\phi = -\oint_S ds \cdot q_\phi + \int_V S_\phi dV \tag{3.7}$$

where $\vec{u}$ is the fluid velocity, $\vec{u}_b$ the boundary velocity and q_ϕ and S_ϕ are the surface and the volume sources/sinks of ϕ respectively. Mesh motion in fact introduces additional fluxes through the volume faces since implies the motion of the control volumes boundaries, generating a 'grid convection'. The relationship between the rate of change of the cell volume and the mesh motion flux is governed by the space conservation law 3.8:

$$\frac{d}{dt}\int_V dV - \oint_S ds \cdot \vec{u}_b = 0 \tag{3.8}$$

On the other hand the mesh fluxes F_m, can be calculated by means of the volume swept by the face f in motion with a velocity $\vec{u}_b$ during the current time step, therefore:

$$\oint_S ds \cdot \vec{u}_b = \sum_f \int_{S_f} ds \cdot \vec{u}_b = F_m \tag{3.9}$$

In the most common mechanical configurations (alpha, beta and gamma), the mesh should move with respect to a single axis (in the direction of the movement of pistons or displacer), and its deformation is limited to the expansion and compression zones. In these zones is recommended to define a structured computational grid, so that only one dimension of the cells will change during the movement, limiting the mesh fluxes to a single direction. Therefore, at first it was necessary to define a function which could vary one dimension of the cells in a prescribed zone, without deforming the neighboring zones. Then, a second function was implemented, with the aim to calculate the mesh fluxes and add their contribute to the conservation equations. With OpenFOAM it was possible to define a moving function which takes as entries a cell zone and an axis, and moves rigidly the zone boundaries. It is given to the user the possibility to apply any law of movement which should be defined separately for each boundary. For Stirling engines has been implemented a preset crank mechanism law in which the lengths of con rod and crank should be specified. By knowing the motion laws of the zone boundaries, the moving function calculates for each crank angle, the effective position of the mesh points and then derives the height of each cell and its position simply dividing the distance between the boundaries by

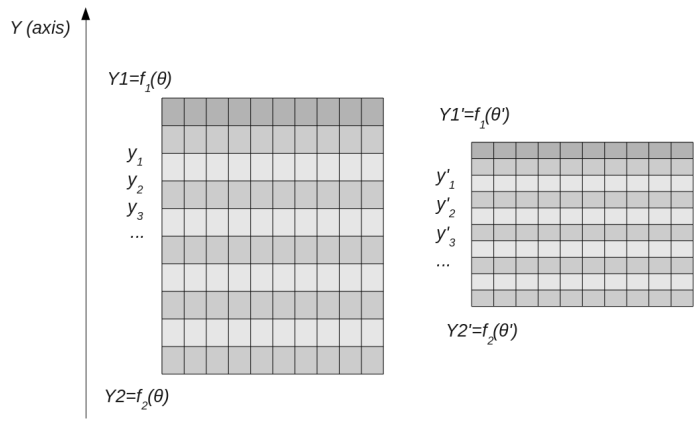

Figure 3.1: Mesh motion function

the number of cells along the same axis (Fig. 3.1). The mass fluxes through the cell faces in the direction of the movement are calculated considering the difference between the position of every point in two successive time steps as:

$$\dot{m} = -\rho \; A \; \frac{y^{t+1} - y^t}{\Delta t} \tag{3.10}$$

where $\dot{m}$ is the bulk flux, ρ is the fluid density of the cell boundary, $y' - y$ is the algebraic difference between the calculated position and the initial position of the boundary in the direction of the movement, Δt is the time duration of the movement considered.

3.3 Pressure drop modeling

Compared to third order analysis, which requires the definition of proper pressure drop sub-models for taking into account the frictional losses in the ducts, the CFD analysis allows, in most of the cases, to directly simulate these losses. This comes from the fact that, if domain geometry truly represents the real engine, viscous forces are automatically solved during the simulation; nevertheless this is not valid for the regenerator zone which will be analyzed separately in Sec. 3.5. Friction forces between fluid and solid walls in fact, are inherently accounted in CFD analysis when flow velocity field is solved with the correct boundary conditions: each wall should guarantee the adherence condition, which means that fluid velocity on the wall $u_{f,W}$ is equal to the velocity of the wall itself u_W

$$u_{FW} = u_W.$$

For walls which are not moving, the boundary condition is simplified by imposing a zero velocity to the fluid. Correct boundary conditions however, are not sufficient to ensure a proper calculation of friction losses because the friction factor depends also on the correct solution of the dynamic boundary layer. Assuming a Newtonian fluid, the surface shear stress may be evaluated from the knowledge of the velocity gradient at the surface [26]

$$\tau_s = \mu \frac{\partial u}{\partial y}\Big|_0 \tag{3.11}$$

where μ is the fluid dynamic viscosity. Friction coefficient then can be expressed as

$$C_f = \frac{\tau_s}{\rho u_\infty^2/2} \tag{3.12}$$

where ρ is the fluid density and u_∞ the fluid velocity outside the boundary layer. It is thus clear that frictional effects depend on fluid local properties, on fluid velocity but also on the velocity gradient on the surface. Close to the walls therefore, mesh should be fine enough to properly describe velocity changes into the boundary layer and correctly represent all its thickness. A general rule to define the correct dimension of cells in the boundary layer does not exist, but after the first simulation a check of the velocity field should be done, in order to establish if more (or less) cells are needed to smoothly represent the wall layers. It is immediately clear that this indication contrasts with the need to limit cells number to increase simulation speed (Sec 3.2); therefore friction losses should be correctly evaluated with fine meshing layers only if their effect is important and influences the machine performances. With regards to Stirling engines it can be said that, unless particular geometries are used, compression and expansion spaces are not affected by high pressure drops and therefore a coarse mesh can be used in these zones. Heat exchangers instead, are often built by means of numerous small ducts and wide exchange surfaces, therefore pressure drops in these components can be important and fine meshes, along with correct geometry design, have to be used; anyway a fine computational grid in these zones is required in order to solve the thermal boundary layer, as described in the following section. An inevitable pressure drop in a Stirling engines however, occurs in the porous matrix of the regenerator; here friction effects can not be calculated by solving a boundary layer because it would require an unacceptable computational effort to describe the real internal geometry of the pores. Therefore in order to calculate friction forces in regenerator zone it is necessary to define a model, which will be described in section 3.5.

3.4 Heat exchangers modeling

Heat exchangers have a primarily role on the performances of the engine, since they directly influence the energy transfer between the heat source/sink and the working fluid. There are many technical solutions on the market and the most common involve small ducts or finned surfaces but, in simplest laboratory solutions, electrical resistances, along with simply direct heating/cooling of the surfaces, are often used. It is possible to classify all heat exchangers in two different classes according to the parameter which can be externally controlled: *constant power heat exchangers* (eg. electrical resistance) and *constant temperature heat exchangers*. Based on this classification, two different ways to represent this components in the model are here analyzed.

3.4.1 Constant power heat exchangers

This class of heat exchangers includes all the technological solutions which can control the power given or removed from the fluid over each engine cycle. These solutions are not common in commercial machines but can be very useful in research and development devices, where a direct control on the power through the exchangers allows an easier calculation of the engine performances. It must be considered that it is very difficult to model the real geometries of the exchangers so that, solving all the boundary layers and fields, the exact amount of heat desired is transferred in the exchanger. The simplest way to represent these elements, if they are inside the fluid flow (e.g. electrical resistance), is to add a source term S_{fluid} to the fluid energy equation where the power is effectively exchanged, so that heat transfer over every cycle is always controlled. (see Eq. 3.3).

$$S_{fluid} = \dot{Q}_{imposed} \tag{3.13}$$

In case the power is exchanged mostly along the boundary surfaces, it is better to represent the exchanger as a fixed boundary condition of the third specie:

$$\dot{q} = -k\frac{\partial T}{\partial n}. \tag{3.14}$$

Since heat transfer is externally controlled and fixed over a cycle, no boundary layers have to be solved in these zones and consequently, if friction losses are not important (Sec. 3.3), a coarse mesh can be used.

The use of this sub-model (Eq. 3.13) however, leads to correct solutions only in terms of average temperatures over a cycle. The temperature distribution of the working fluid within each cycle instead, may be different from

the physical solution. In fact the power is given/removed from the fluid at a constant rate, without considering that, during a real cycle, heat is exchanged at different rates on the base of the fluid velocity. Therefore it can happen that, in a particular moment, more/less power than reality is exchanged with the fluid, leading to and error in temperature solution that is as large as smaller is the fluid heat capacity. In fact, heat capacity C is inversely proportional to the temperature difference caused by a heat transfer and, since fluids are characterized by very small C, the inaccuracy in the instantaneous heat transfer can lead to large local errors in the fluid temperatures. This problem has been corrected by applying a limitation to the temperature of the fluid in the source zone, so that it can not exceed a maximum/minimum value. The transfer of the correct power is then ensured by using a storage: if in some phases of the cycle the total power can not be exchanged because of the temperature limit, the exceeding power is accumulated in a virtual memory and introduced in the fluid when its temperature is distant from the restrictive value. In this way, the effect of energy accumulation into the solid material of the exchanger, which occurs when the heat transfer with the fluid is not efficient, is reproduced; therefore fluid temperatures are preserved to reach unphysical values and the solution results closer to the reality.

3.4.2 Constant temperature heat exchangers

This class of heat exchangers includes the most of commercial solutions, which usually adopt ducts or finned surfaces. In such components the controlled parameter is the temperature of the exchanger surfaces, which depends on the heat/cold source used, and determines the heat transfer with the fluid. The model of these heat exchangers can be therefore represented by means of a proper temperature boundary condition on the exchanger walls, which should be as close as possible to the real walls temperature distribution. On the other hand, the operation of these heat exchangers is strongly determined by the thermo-fluid-dynamics inside the heat exchanger and, consequently, these phenomena should be accurately described. For this purpose a proper computational mesh is required, with sufficient refining and boundary layers to allow the correct solution of the velocity field and the fluid-wall heat transfer. Nevertheless, the adoption of a refined mesh implies an increased computational effort which, in some cases, can become very high; therefore a compromise between the accuracy of the solution and the computational time should be pursued. The modeling of these heat exchangers can be further extended by using a multi-region approach to represent the solid walls of the exchangers; in this way it is possible to simulate also the walls conductivity and thermal inertia, describing more accurately the global

operative conditions. This approach on the other hand leads to an additional increase of the computational effort and to longer convergence times, because of the high characteristic time of the solid materials transient phase. If both the boundary condition and the mesh refining are correct performed, no additional assumptions should be done on the exchanger behavior, and heat transfer coefficients are automatically accounted during the simulations.

3.5 Regenerator modeling

Regenerator is the key component for an efficient operation of a Stirling machine. It behaves as a heat exchanger which alternatively supply and remove heat from the working fluid and, at the same time represents a loss for the system since introduces additional dead volumes and pressure drop (see Sec. 1.3). In order to increase exchange surfaces using small volumes, many different solutions have been researched and adopted. On the market it is possible to find regenerators made of stacks of woven-wire screens, random fiber porous materials, packed sphere matrices, wrapped-foil or segmented-involute-foil regenerators, metallic foams and compositions of these technologies. The common characteristic of all these possibilities is the presence of very small ducts and paths through which the working fluid is forced to pass. Try to accurately model these geometries in a whole engine simulation is impossible and anyway meaningless, because even if the internal random geometries were known, their correct representation would require an enormous amount of cells in order to solve field distributions inside such small spaces. Therefore it is not possible to use the same approach adopted for the heat exchangers and both fluid friction forces and heat transfer should be completely modeled. The first consequence is that no boundary layers have to be solved in this zone, and thus the mesh can be coarser than heat exchangers.

3.5.1 Regenerator pressure drop

In order to model fluid friction losses and therefore pressure drop in a porous matrix it is common use to introduce a negative source term $\Re$ in the momentum equation of the cells representing the zone, as shown in equation (3.15).

$$\frac{\partial(\varrho\vec{u})}{\partial t} + \nabla \cdot (\varrho\vec{u}\vec{u}) = -\nabla p + \mu\nabla^2\vec{u} + \Re \tag{3.15}$$

Many models have been developed to correlate the source term $\Re$ characterizing the various porous media to the flow characteristics, but most of them are derived for steady flow conditions; Stirling regenerators instead are subjected to periodic-flow conditions, which on the other hand have not been

exhaustively studied yet. In recent years more and more research efforts have been spent in this sense both by means of experimental tests and CFD works, even though simulations have the additional problem to define cyclic boundary conditions (see Sec. 2.5). These works report that both friction factor and heat transfer coefficient can behave differently in equivalent periodic-flow and steady-flow cases. Nowadays a fair range of semi-empirical correlations for periodic-flow friction factor in porous media has been developed, even though not all the possible technical solutions have been covered; among these models are worth mentioning the empirical correlations obtained by Gedeon [14]. In the CFD model perspective, if a periodic flow correlation is not available, it is possible to use a steady-flow correlation. The error introduced can be reduced by using a relatively fine mesh in the regenerator zone and running the simulation with a small time step; in this way the periodic behavior of the fluid in the porous media can be represented by a sequence of many steady state solutions and the approximation is acceptable.

Finally, it must be said that is always important to compute fluid friction forces in the regenerator zone by using a correlation obtained for a porous material as similar as possible to the one modeled, because porous matrices usually have different behaviors and, in general, pressure drop through regenerator can be one of the most important pressure losses of the entire machine.

3.5.2 Regenerator heat transfer

Regenerator heat transfer model is perhaps the most important part of the Stirling model, because the amount of heat transferred by the porous matrix in each cycle can be considerable and approximately ranges between 3 to 40 times the heat transferred in the heater [1]. In literature models the most common solution is to assume solid/fluid thermal equilibrium and solve a single modified energy equation in the zone such as the following [24]:

$$\begin{aligned} &\frac{\partial}{\partial t}\left(\Pi_v \rho_f E_f + (1-\Pi_v)\rho_s E_s\right) + \nabla \cdot \left(\vec{u}(\rho_f E_f + p)\right) \\ &= \nabla \cdot \left[k_{\text{eff}} \nabla T - \left(\sum_i h_i J_i\right) + (h\tau \cdot \vec{u})\right] + S_f^h \end{aligned} \tag{3.16}$$

where f and s indicate respectively fluid and solid properties, and k_{eff} is an effective solid/fluid average conductivity. This representation is not considered satisfactory, because very often fluid and solid matrix are not in thermal equilibrium and furthermore, heat conduction inside the porous media is not taken into account. Here below two different methods to model regenerator heat transfer are proposed, the first, very simple, is called *Single region*

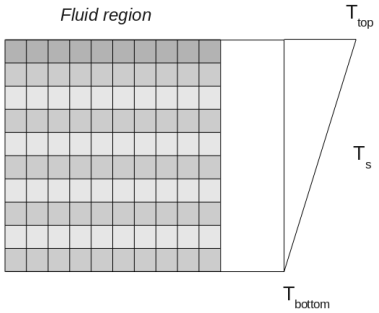

Figure 3.2: Regenerator zone: Single region approach to model fluid-solid heat transfer

model, the second, more accurate, but more expensive from a computational point of view, is called *Multi region model*.

Single region approach

In this simplified approach, a single mesh is adopted for the solution of the fluid domain. The temperature distribution in the solid matrix of the regenerator is assumed as a-priori known (linear distribution between a minimum and a maximum value) and is maintained constant during the simulation. In the fluid domain instead, a source term S_{fluid}, which represents the heat transfer between the fluid and the solid matrix, is added in the regenerator zone, as was done for the heat exchangers in equation (**??**). The energy equation in this area should be however corrected in order to account the presence of the porous media, and can be expressed by:

$$\frac{\partial(\Pi_v \varrho E_f)}{\partial t} + \nabla \cdot (\Pi_v \varrho E_f \vec{u}) = -p\nabla \cdot (\vec{u}) + \nabla \cdot (k_{\text{f eff}} \nabla T) + S_{fluid} \qquad (3.17)$$

where Π_v is the volumetric porosity of the solid matrix, and $k_{\text{f eff}}$ is the fluid effective thermal conductivity which takes into account the pores geometry and the material of the regenerator. Source term S_{fluid} is then computed on the basis of the assumed solid temperature T_s distribution as:

$$S_{fluid} = hA(T_s - T_f) \qquad (3.18)$$

where h represents the heat transfer coefficient, which is assumed constant through the simulation and must be defined a-priori, and A is the surface exchange area between fluid and solid matrix. This approach is very simplified and approximate because can not account regenerator physical properties and the solution strongly depends on the T_s distribution chosen. The lower accuracy of this model however is balanced by a faster computation time and a faster convergence to a regime state.

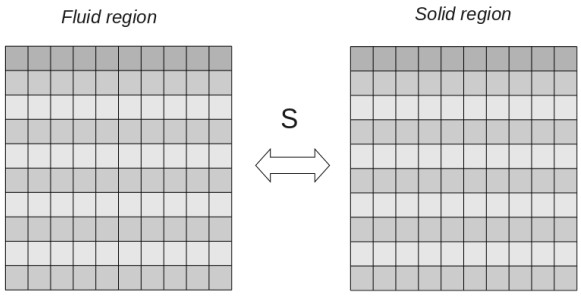

Figure 3.3: Regenerator zone: Multi region approach to model fluid-solid heat transfer

Multi region approach

This approach uses two overlapping meshes for the solution of the fluid and the solid regions respectively. Therefore temperature distribution of the regenerator is computed by solving an energy balance for the solid matrix. Fluid energy equation is corrected in the regenerator zone to consider the porous media, as was done in Eq. (3.17); similarly a correction is necessary for the solid energy balance in order to consider the effective physical properties of the porous material and Eq. (3.20) is derived. Then the energy equations are coupled by means of an energy source term S representing the heat power exchanged between the two phases calculated with Eq. (3.21).

$$\frac{\partial(\Pi_v \varrho E_f)}{\partial t} + \nabla \cdot (\Pi_v \varrho E_f \vec{u}) = -p\nabla \cdot (\vec{u}) + \nabla \cdot (k_{\mathrm{f,eff}} \nabla T) + S \tag{3.19}$$

$$\frac{\partial((1-\Pi_v)\varrho E_s)}{\partial t} = \nabla \cdot (k_{\mathrm{s,eff}} \nabla T) - S \tag{3.20}$$

$$S = hA(T_s - T_f) \tag{3.21}$$

With regards to Eqns. (3.19) and (3.20) it is important to highlight that the effective fluid thermal conductivity $k_{\mathrm{f,eff}}$ is usually very close to the real fluid thermal conductivity k_f because, in absolute terms, it is always very small. The solid effective thermal conductivity $k_{\mathrm{s,eff}}$ instead, can range between very different values and order of magnitudes, depending on the nature of the porous matrix and its porosity. This difference between fluid and solid phase comes from the fact that in the porous region, solid matrix occupies only a small portion of the total volume and presents many inner voids, therefore its effective thermophysical properties can be really different from the original material properties. It is important therefore to find in the literature an appropriate model to determine, for the specific nature of the porous material, the effective conductivity $k_{\mathrm{s\ eff}}$. In order to estimate heat

transfer coefficient h accurately, a correlation for periodic heat transfer in porous media should be researched, even tough, as said for the friction factor estimation (Sec. 3.5.1), literature does non cover exhaustively all the possible technical solutions.

Multi region approach is certainly more accurate and complete than single region approach. As a matter of fact, it is able to account the material properties of the porous media (eg heat capacity and conductivity) and does not depend on a constant temperature distribution, because solid temperature field is calculated for each time step of the simulation. In addition, if porous matrix is initialized with the real initial temperature, this model allows to study the thermal transient that leads to the convergence state. Multi-region approach is however slower, both because zone coupling requires additional computational effort and because many cycles are needed to reach convergence due to the high thermal inertia of the solid matrix which slows down the thermal transient. In order to speed up convergence time it is useful to initialize the porous matrix with a temperature distribution as close as possible to the convergence distribution, so that the characteristic time of the solid thermal transient is reduced, but in this way is not possible to analyze the transitory phase.

3.6 Turbulence modeling

The necessity to model the whole engine at once and to reduce the simulation time (section 2.5), precludes the possibility to use LES or DNS analysis to study Stirling technology. The most common way to describe turbulence phenomena in CFD problems is to use a turbulence model. In turbulence modelling, an averaging operation is applied to the Navier-Stokes equations to form an equivalent set of equations for the averaged flow quantities [29, 28]. This leads to the Reynolds Averaged Navier Stokes (RANS) equations, which present an additional term in the momentum equation, the Reynolds Stress term. The Reynolds Stress term represents the effect of the stochastic component of the flow on the mean flow, and can be replaced by a turbulence model to achieve closure. In this work the k-ω SST model, proposed by Menter [30], has been applied. This is a widely-adopted two-equation eddy-viscosity model based on the solution of the transport equations for two quantities, namely turbulent kinetic energy and specific dissipation rate, and can be adopted as low-Re model without any extra damping functions. In addition the model is robust and recommended for simulations where boundary layers effects are important ensuring a good functioning even at distance from the walls.

However, when a turbulence model is applied to describe the flow char-

acteristics through a porous media (e.g. through the regenerator) specific sub-models needs to be introduced. As a matter of fact, a turbulent flow entering in a porous media experiences a drastic change of its turbulent properties, due to the fact that the integral length-scale reduces of orders of magnitude, becoming similar to the pore dimension of the media [31]. In most practical applications, when the flow velocity in the porous media is kept low in order to maintain the pressure drop in an acceptable range of values, the flow regime in the media is laminar. In this case, the presence of the porous media determines the re-laminarization of the turbulent flow passing through that. This is particularly important in a Stirling machine because it means that the turbulence generated in one space is not transferred into the other and, therefore, the positive effect of the turbulence to promote the heat transfer with the walls of the spaces is minimized. In order to take into account this phenomenon a simplified sub-model has been introduced. It consists of an additional source term applied in the specific dissipation rate equation, which has the effect to determine the re-laminarization of the flow passing through the porous media. The transport equations of the turbulent kinetic energy and the dissipation rate are shown respectively in Eqs. 3.22-3.23; the sub-model for the description of turbulence in the porous matrix is represented by the source term S_ω of Eq. 3.23 which, expressed as a function of the dissipation rate itself, decreases the values of ω as fast as the higher they are.

$$\frac{\partial(\varrho k)}{\partial t} + \nabla \cdot (\varrho k \vec{u}) = \nabla \cdot \left[\left(\mu + \frac{\mu_t}{\sigma_k} \right) \nabla k \right] + P_k - \beta^* \varrho k \omega \tag{3.22}$$

$$\frac{\partial(\varrho \omega)}{\partial t} + \nabla \cdot (\varrho \omega \vec{u}) = \nabla \cdot \left[\left(\mu + \frac{\mu_t}{\sigma_\omega} \right) \nabla \omega \right] + P_\omega - \beta_1 \varrho k \omega^2 + S_\omega \tag{3.23}$$

$$\begin{cases} S_\omega = 0 & default \\ S_\omega = -10\ \omega & in\ porous\ media\ cell\ zones \end{cases}$$

3.7 Numerical solution

The PISO (Pressure-Implicit with Splitting of Operators) algorithm [28] was adopted for the pressure-velocity equation coupling. The convection term in the equations was discretized using an upwind interpolation scheme [16]. For the discretization of the equation in time an explicit first-order accuracy Euler scheme [27] was adopted. The Courant number was set equal to 0.5 in order to satisfy both accuracy requirement and stability issues.

Chapter 4

Application of the CFD model

In this chapter, the model described in chapter 3 will be applied to a real case. The study was done on a small $300cm^3$ Stirling machine used for research and didactic purposes at the laboratory TEMPO (University of Valenciennes, France). This choice was motivated by the simplicity of the engine geometry, which made it possible to describe the machine adopting a low number of mesh elements, reducing the effort required for the CFD simulations. On the other hand, this engine includes all the components of a typical Stirling machine, allowing to perfom a validation of the Stirling sub-models developed in this work [32].

4.1 Experimental device

The considered Stirling engine is a Beta type machine (see Sec. 1.4) and is illustrated in Fig. 4.1 and 4.3. This machine is a reversible device and can operate both as a prime mover or as a receiver. The hot source is represented by an electrical resistance located inside the hot room, whose power can be externally chosen by means of a voltage regulator. The cold source instead, consists of an open water circuit which surrounds the cold room, and of an additional circuit realized at the bottom of the displacer, in which the water flows through the con rod. The regenerator (Fig. 4.2) is inserted on the displacer piston and is made of a random fiber copper matrix (porous media); the matrix is shaped as a funnel and contained in an internal geometry, smaller then the cylinder dimensions, while the external geometry closes as a cylinder with the same width of the working spaces. The space enclosed between the internal and external geometry is filled with air. The measuring apparatus is equipped with a pressure transducer, a volume transducer, a tachometer, a debimeter, and three thermocouples. The pressure transducer is located in the cold space and has 0.2 % of incertitude in the measure. The volume transducer consists of a position sensor connected to the power piston

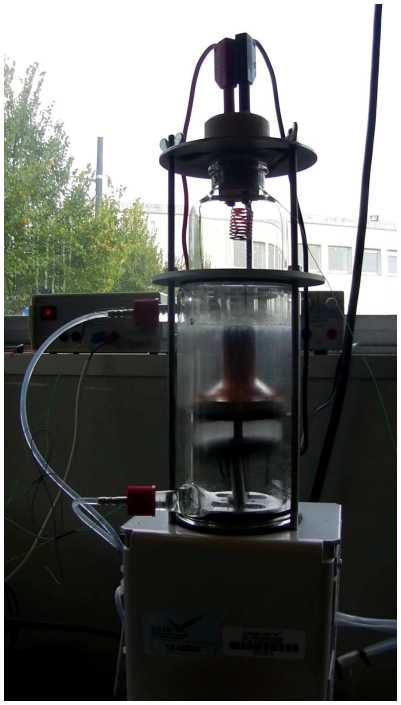

Figure 4.1: Stirling engine used for the validation of the model

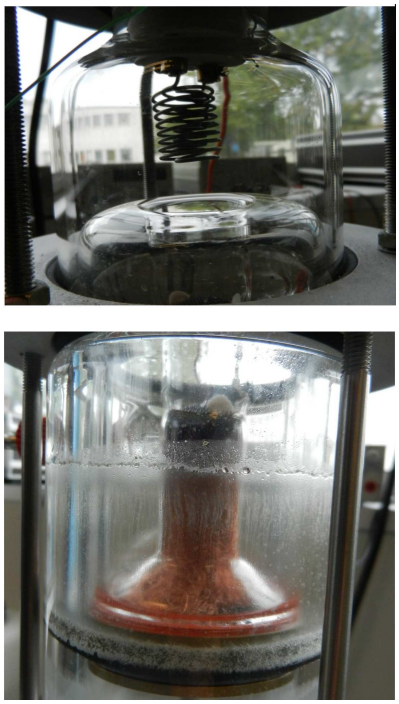

Figure 4.2: Particulars of the engine: electrical resistance and regenerator

which delivers a continuous tension signal, then internal volume is computed by means of the piston movement law. In order to monitor the temperatures of the working spaces, two thermocouples have been used, located respectively in the top part of the hot room, and inside the power piston in the cold space. A differential thermocouple is used to measure the water temperature difference between the entrance and the end of the cooling circuit so that, measuring the water mass flow with the debimeter, it is possible to compute the average power exchanged by the cooling system. The working fluid used in the engine is air and is charged at ambient conditions by simply opening the top part of the cylinder. During the experimental tests, the machine was used as a prime mover, powered by the heat produced by the electrical resistance. Outside the hot room a radiative insulation was adopted, in order to reduce the radiative losses towards the surroundings. In addition no load was applied to the engine so that, when the regime functioning was reached, all the work output was balanced by the system losses [32].

After data acquisition a post processing program was used to filter the rough signals and to compute the engine average performances. In particular

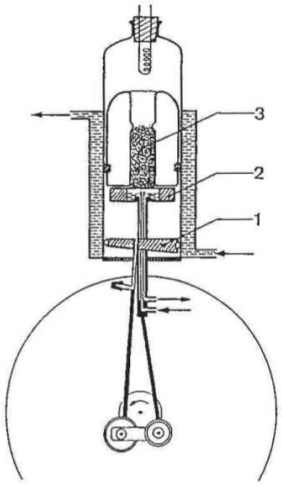

Figure 4.3: Scheme of the experimental device: 1) power piston 2) displacer piston 3) regenerator matrix

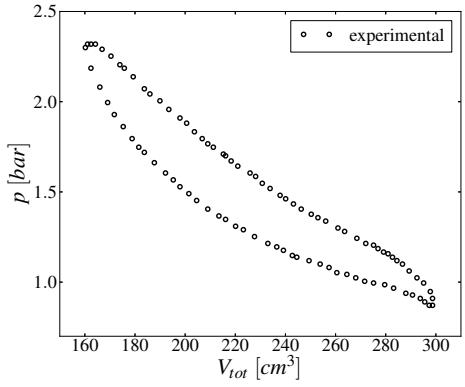

Figure 4.4: Data plot of the filtered experimental pressure-volme cycle

power exchanged in the cooling system was calculated as:

$$\dot{Q}_{\text{cold}} = \dot{m}_{\text{water}} Cp_{\text{water}} \Delta T_{\text{water}}, \tag{4.1}$$

Work output W_{out} was estimated integrating the pressure-volume diagram, than power output P_{out} was obtained by simply dividing W_{out} for the cycle period τ:

$$P_{\text{out}} = \frac{W_{\text{out}}}{\tau} = \frac{1}{\tau} \int p \, \mathrm{d}V. \tag{4.2}$$

Then, solving a global balance over the engine, it is possible to estimate the effective power $P_{\text{el eff}}$ given to the fluid by the electrical resistance as the sum of $\dot{Q}_{\text{cold}}$ and P_{out}. Finally, from these results, the thermodynamic efficiency and the global efficiency of the engine were derived respectively as

$$\eta_{\text{thermo}} = P_{\text{out}} / P_{\text{el eff}} \tag{4.3}$$

$$\eta_{\text{global}} = P_{\text{out}} / P_{\text{el}} \tag{4.4}$$

Tables 4.1 and 5.1 summarize respectively the geometrical characteristics of the engine and the working parameters measured during the experimental tests.

Table 4.1: Geometrical properties of the experimental engine

Hot space	*mm*	Displacer	*mm*
diameter	60	*con rod length*	100
height	49.2	*stroke*	48
Cold space	*mm*	Power piston	*mm*
diameter	60	*con rod length*	197
height	35.7	*stroke*	48
Regenerator	*mm*	Engine volume	cm^3
inner diameter	22	*maximum*	300
outer diameter	60	*minimum*	160
height	59		
porosity	0.796		
material	copper		
nature	random fiber		

Table 4.2: Experimental results

rotation speed	235	rpm
hot room temperature	818	K
cold room temperature	322	K
maximum pressure	2.2	bar
minimum pressure	0.9	bar
power electrical resistance	265.5	W
power cooling system	84.9	W
power output	13.2	W
thermodynamic efficiency	13.5	%
global efficiency	5.0	%

4.2 CFD Model

4.2.1 Mesh definition

The engine considered presents a simple configuration and an axial-symmetric geometry, therefore it is possible to reduce the size of the problem adopting a wedge-type discretization. The resolution in a 2D domain allows not to solve redundant equations and, consequently, the computational effort required for the simulation is largely diminished. The mesh was generated by means of a parametric script which, on the basis of the main geometrical parameters of the machine, creates a structured hexaedral grid as shown in Fig 4.5. It has been decided not to model the seal of the piston and the appendix gap between displacer and cylinder so that cell number is kept to the minimum. The computational mesh created in this way presents a good quality, and is characterized by the following parameters: maximum non-orthogonality over a cycle 49, maximum aspect ratio 13.3 and a maximum skewness of 2.7. A second mesh has been created for the regenerator zone in order to use the Multi region approach described in Sec. 3.5; this second mesh is obtained by duplicating the fluid mesh in correspondence to the porous matrix, so that presents the exact geometry and number of cells of the original grid. The creation of the mesh with this method allows to establish a one to one coupling between the cells of the fluid and the solid matrix and thus to reduce the computational effort of the simulation.

The mesh motion was handled by means of the implementation of a flexible

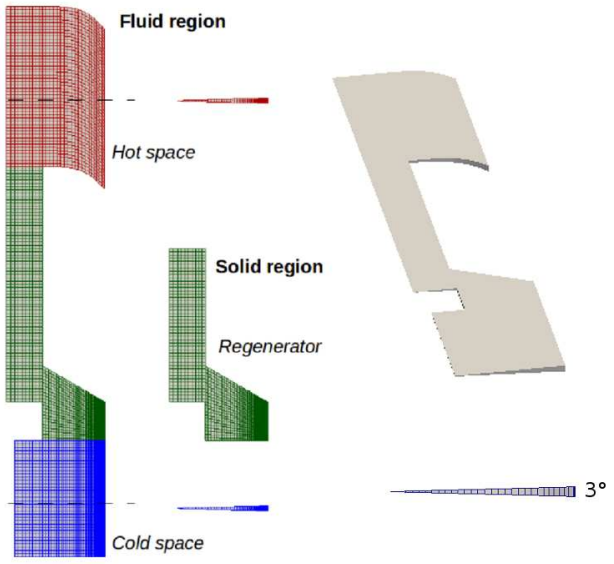

Figure 4.5: Computational mesh

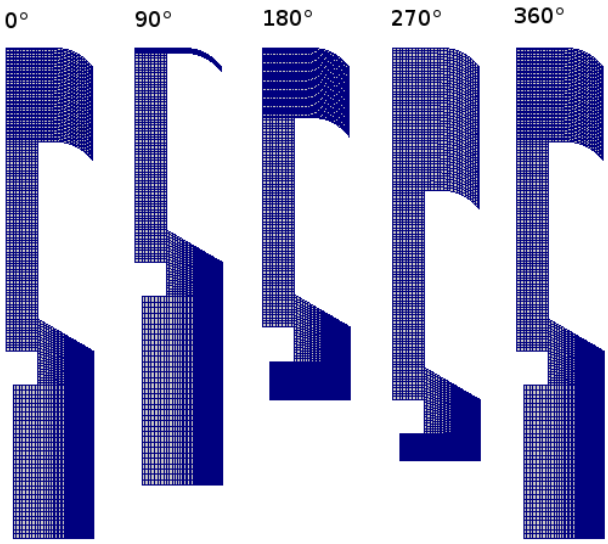

Figure 4.6: Description of the mesh motion as a function of the crank angle

framework which allows to define an arbitrary number of moving zones and to prescribe their motion according to user-defined motion laws (Sec. 3.2). In Fig. 4.5 the three moving zones needed for the modeling of this Beta-type machine are highlighted, namely the hot space (red), the cold space (blue) and the regenerator (green). The motion of each space is specified by defining the direction and the displacement for the top and bottom boundaries of the zone. In particular, as shown in Fig. 4.6, regenerator moving zone is subjected to a rigid displacement, since its volume is constant during operation and, therefore, the internal mesh is not deformed in this zone; hot and cold spaces instead are responsible of the air volume variation during expansion and compression phases and consequently mesh in these zones is strained and relaxed during the simulation. The motion law adopted is the one for ordinary crank mechanisms expressed by Eq. (4.5), which accurately describes the real movement of the piston and the displacer.

$$s = m(1 - \cos\alpha) + b(1 - \sqrt{1 - (m/b)^2 \sin\alpha^2}) \tag{4.5}$$

In Eq. (4.5) s is the crank position, m the crank length, b the con rod length, and α the crank angle, which varies according to the rotation velocity. These parameters have been set using the actual real values listed in Table 4.1 imposing a phase displacement between piston and displacer of 90 degrees; the rotation velocity was then maintained constant during the simulation at a value of 235 rpm, equal to the average speed recorded during measurements (Table 5.1).

Table 4.3: Mesh comparison

mesh	cell dim $[mm]$	cell n^o	P_{output} [W]	Q_{cold} [W]	T_{cold} [K]
fine	1	6075	9.91	81.9	312.3
normal	2	1223	9.82	82.9	314.7
coarse	3	520	8.2	66.1	332.3

The grid independence of the solution was assessed considering three different meshes, having a cell dimension of respectively 3, 2 and 1 mm. As it is possible to observe in Table 4.3 the results obtained with the fine mesh and the normal mesh do not present significant differences, therefore, during this study, it was decided to adopt the normal mesh of 2 mm.

4.2.2 Heat exchangers

Both hot and cold heat exchangers have been modeled according to the indications of Section 3.4.

Hot exchanger

The hot source is an electrical resistance located inside the hot room (Fig. 4.2). This type of heat source, as mentioned in Sec. 3.4 can be approximated as a constant power source, and the most appropriate model for this component is to add a positive source term in the energy balance of the cells representing the resistance (Eq. **??**). A direct solution of the heat transfer in fact, would be very difficult, since it would require to closely represent the geometry of the resistance (in order to automatically solve the boundary layers) and, furthermore, to know the resistance temperature distribution. A constant power approach instead, allows to control the energy entering the system during each cycle and can use a simple and approximate geometry to represent the resistance. As long as the power of the source term is constant during the simulation, the average parameters over a cycle are stable, and do not depend on the geometry of the cells in which the source is added. Nevertheless, if instantaneous parameters are accounted, the geometry chosen influences the results, because locally the same source power is distributed on a different number of cells. In order to establish how much this difference weights on the output parameters, two different configurations to model the resistance have been compared: *linear* and *distributed* (fig 4.7).

The first configuration approximates the resistance as an hollow cylinder which, on the wedge mesh, is reduced to a line of cells; the second instead, models the resistance as a full cylinder which, in two dimensions, is repre-

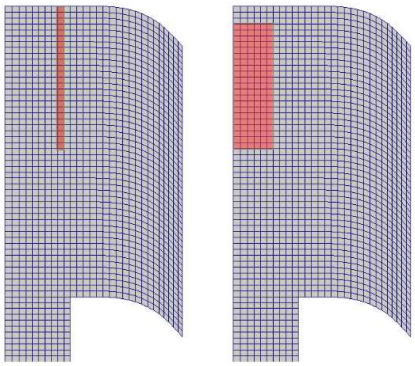

Figure 4.7: Geometry of the electrical resistance: linear and distributed

sented by a wedge. The difference between the two geometries is basically that the second distributes the same amount of power input onto a larger volume, resulting in lower local temperatures of the air. In both cases a limitation was used for the maximum power introduced in the fluid (as suggested in Sec. 3.4), to ensure that the temperature in the cell zone does not exceed a maximum value. When this situation occurs, energy is temporarily accumulated, and then introduced in the fluid system when temperature returns below the maximum limit. In this way, the effect of energy accumulation, which occurs in the metallic wire of the resistance and preserve the temperature to rise in case of low speed gas flow (e.g. at the top dead center), is reproduced. The temperature limit chosen is 1000 K, which can be assumed as a reasonable value for the electrical resistance surface. By means of the limitation, local temperatures obtained with linear and distributed configuration were not significantly different, nevertheless the distributed configuration seemed to have a more realistic behavior and was chosen to run the simulations.

The upstream power given to the electrical resistance during the experimental tests is 265.5 W however, if this power was given entirely to the fluid in the model, it would lead to incorrect results, because various losses occur in the real engine, both upstream and downstream the resistance-fluid exchange, so that the effective power absorbed by the air is largely diminished. Among all these losses the most relevant are the conduction through the walls, especially through the top closure of the hot space, the natural convection outside the hot room and the radiation. Although these losses can be accounted in a CFD analysis, their solution would require a more refined mesh, a detailed representation of the resistance geometry and the introduction of additional solid meshes to study the wall heat transfer. In addition, no temperature measurements of the walls are available to validate the correct behavior of the losses sub-models. As a result of these considera-

tions, for the first validation of the general model it was decided to account all the fluid losses by reducing the power input of the electrical resistance. In order to estimate this power, a black box approach was adopted, calculating the power given to the fluid during the simulation $P_{\text{el eff}}$, as the sum of the cooling power and the power output measured experimentally.

$$P_{\text{el eff}} = \dot{Q}_{\text{cold,exp}} + P_{out,exp} \tag{4.6}$$

As a consequence of this approach, all the walls of the engine should be considered adiabatic (Sec. 4.2.4), but the computational mesh resulted simplified and faster and many simulations could be done in order to test properly the model. By using the data of table 5.1 it has been computed a $P_{\text{el eff}}$ of 98.1 W; however, as it will be explained in Section 4.2.8, the power output measured experimentally overestimates the real power output, so that in the simulations it was given to the hot source a reduced input power of 93.6 W.

Cold exchanger

The cold exchanger is obtained by means of a water circuit, which cools both the external surface of the cold space and the base of the displacer. The heat transfer takes place through five surfaces, as shown in Fig. 4.8: 1) the external surface, 2) the con rod, 3) the base of the displacer, and 4-5) two surfaces which are in direct contact with the regenerator matrix. The best way to model these heat exchangers is a constant temperature boundary condition, however, in order to set the boundary values with a physical meaning, some considerations need to be done.

The *external surface* of the cold room is the largest exchange surface and is efficiently cooled by a swirling flow of water; this part contains the most of the circuit volume and it is reasonable to assume that the temperature of the wall is close to the average temperature of the water; therefore the boundary condition is set to 16^0C. In order to correctly solve the boundary layers on this surface, the mesh close to this wall has been refined, and a grading has been used to smoothly enlarge cells dimensions towards the center of the cold space.

The *con rod surface* is really small compared with the external surface. The geometry and the dimension of the two ducts that pass through it to bring water towards the base of the displacer is not known, therefore it is difficult to estimate a heat transfer coefficient to the water side. On the other hand, it must be considered that the heat transfer of this surface is really small and that, consequently, an accurate model for this surface is not necessary. Therefore it has been chosen to use water average temperature

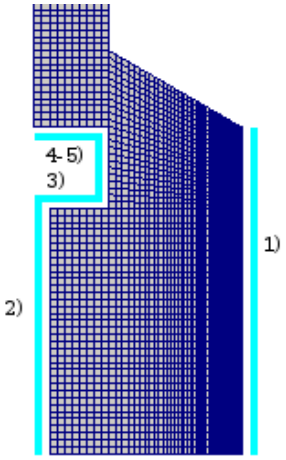

Figure 4.8: Cooling system surfaces

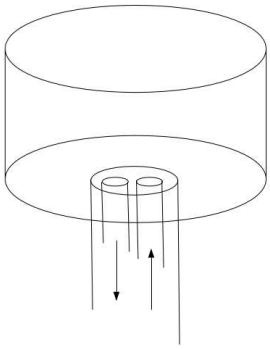

Figure 4.9: Supposed geometry for the base of the displacer

of 16^0C for the boundary condition and the mesh on this surface was not refined.

The *surface at the base of the displacer* is characterized by a small power transfer as well, because the air is almost still in this zone of the engine; therefore the same conditions of the previous surface has been used.

The study of the *internal surfaces* is more complicated because the real geometry of the vane at the base of the displacer is not known: while creating the mesh, this zone was assumed to be a cylinder, so that the internal exchanging surfaces are two (fig. 4.9). A further complication is that these surfaces are in direct contact with the regenerator porous matrix; this fact is relevant because in this way, part of the heat that should be stored in the regenerator flows by conduction to the cooling system. The amount of heat transferred by these two surfaces is not negligible and rather represents the majority of the power exchanged with the water; in fact, the porous media behaves similarly to a finned surface, enhancing the exchange of the cold walls, so that the lower part of the regenerator basically becomes an extension of the cooling system itself. Because of the large heat transfer, the surfaces of the water chamber at the base of the displacer will be at a higher temperature then the water, and some considerations need to be done in order to estimate the real value. At first, it is useful to start analyzing the water flow from the con rod to the displacer base. In fact, despite the real geometry is unknown, it is reasonable to assume that the water stream experiences an abrupt slowdown in this region, because the flow suddenly enters, from the tiny duct of the con rod, to a much larger space. It is re-

ally difficult to describe the real water behavior inside the chamber but, as a consequence of the velocity difference, it is reasonable to assume that the heat transfer coefficient here is smaller than the one in the con rod. On the other hand it can be assumed that the same heat transfer coefficient is higher than 100 W/m^2K, which represents a very low heat transfer. The surfaces temperature therefore must comply with the condition that, by exchanging a certain power with the system, the coherent heat transfer coefficient inside the base of the displacer must be comprehended between these two values. The method used to determine the surface temperature is thus the following:

1. assume a first attempt value for the temperature on the two surfaces T_{wall}, to be used as boundary condition;
2. run the simulation till the output values validate the experimental results;
3. compute with the simulation the heat removed by the two surfaces per each cycle;
4. compute the heat transfer that water should have on the two surfaces to remove the power of the former passage, and check if it is consistent with the minimum and maximum values established.

The heat transfer coefficient in the con rod can be estimated by assuming that the water flows inside two identical ducts of 2 mm diameter. Therefore, from the water mass flow, it is possible to calculate the velocity inside the ducts, which results 2.7 m/s. The corresponding Re_D number relative to the duct diameter is 5080, which implies a turbulent behavior ($Re_D > 2100$), therefore the correlation of Gnielinski has been used to compute the Nu_D number. With these assumptions the heat transfer coefficient in the ducts of the con rod results $h = 12600\ W/m^2K$; therefore the heat transfer coefficient of the water inside the lower part of the displacer will have to comply the condition $100 < h_w < 12600\ W/m^2K$.
Starting from the average power exchanged by the surfaces and setting a temperature T_{wall} on the air side, it is possible to compute the corresponding heat transfer coefficient to the water side using a lumped parameter approach.

$$\dot{Q} = \frac{T_{wall} - T_{water}}{R_{tot}} \tag{4.7}$$

In Eq. (4.7), T_{wall} is the supposed boundary conditiond, $\dot{Q}$ is computed during the simulation, T_{water} is the average temperature of the water (16^0C) and R_{tot} is the global thermal resistance. This resistance is composed by

two contributes, convective and conductive through the walls, and can be expressed as

$$R_{tot} = \frac{1}{h_w A_w} + R_{cond} \tag{4.8}$$

In Eq. (4.8) R_{cond} depends on the geometry and the material of the wall and can be calculated since it was assumed a cylindrical design. In order to simplify the calculations it has been assumed that the walls are made of steel and that the two surfaces have the same temperature; therefore the only unknown parameter left in Eq. 4.7 is h_w, which can be explicitly calculated.

By means of all the considerations done, the surface temperature of the two surfaces has been estimated of 350 K; the consequent convective heat transfer to the water side is about 1700 W/m^2K, which is considered a reasonable value and respects the bounds imposed. It is clear that the solution obtained is, in a certain way, the result of the assumptions made on the water circuit geometry however, it was the most that could be done under these uncertainties and it must be noted that the obtained results have a good agreement with all the experimental data, which means that the assumptions are not far form reality.

4.2.3 Regenerator

The regenerator has been modeled by means of the sub-models described in Sec. 3.5. Since this component moves along with the displacer, in both the calculations of permeability and heat transfer a relative velocity should be used, in order to account the real difference of velocity between the fluid phase and the solid phase. All velocities of this section are therefore considered relative.

In order to account its permeability effect, a resistance source term $\Re$ has been included in the momentum equation of the cells which compose the regenerator zone of the fluid region (Eq. 3.15). The value of $\Re$ depends on the properties of the micro-structure and the instantaneous fluid-dynamics conditions of the air. If the flow resistance is expressed in terms of a friction factor correlation, the momentum equation can be closed by means of the following expression [26]:

$$\Re = \frac{1}{2}\frac{\rho}{d_c} C_f u^2 \tag{4.9}$$

To evaluate C_f, a suitable correlation should be used, with the aim to express the friction factor for the chosen porous material, as a function of the fluid-dynamics of the system. Therefore it was researched the literature to find a suitable correlation for the considered regenerator, which is made of random fibers of copper, with a porosity of 0.796 and a wire diameter of 200 μm.

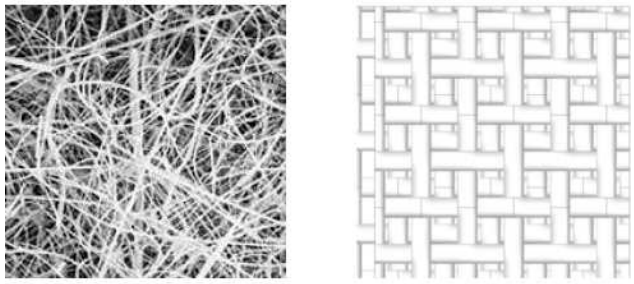

Figure 4.10: Random fiber porous matrix and Staggered wire screen matrix

Unfortunately no studies have been found for this type of matrix, while different papers were published on other porous materials. Between them, the most similar solution to the random fibers, was the wire screen matix. The main difference between random fibers and wire screens is that the first has homogeneous properties in every direction while the second, obtained by staking several layers of woven wires, presents an anisotropy along the axis normal to the layers, due to the contact resistance between the wires. Due to the lack of a specific correlation for the prorous matrix considered, it has been decided to use a correlation for staggered wire screens in the anisotropic direction, which resembles the most similar to the chaotic distribution of the random fibers and takes into account the contact resistances between wires (Fig. 4.10). The correlation selected is the one of Gedeon and Wood [14](Eq. 4.10), obtained experimentally for air flow through a wire screen matrix under periodic conditions. This equation is close to the correlation obtained for a similar matrix by Tanaka and has been recently corroborated by the numerical simulations of Costa [5, 33].

$$C_f = \frac{129}{Re_{D_h}} + 2.91 Re_{D_h}^{-0.103} \tag{4.10}$$

In Eq. (4.10) Re_{D_h} number is calculated using the hydraulic diameter D_h defined by

$$D_h = d_w \Pi_v / (1 - \Pi_v), \tag{4.11}$$

where Π_v is the volumetric porosity and d_w the wire diameter of the matrix.

To model the regenerator thermal behavior, both the two approaches *Single region* and *Multi region* have been used. The application of the approaches to the real case is shown in Fig. 4.11.

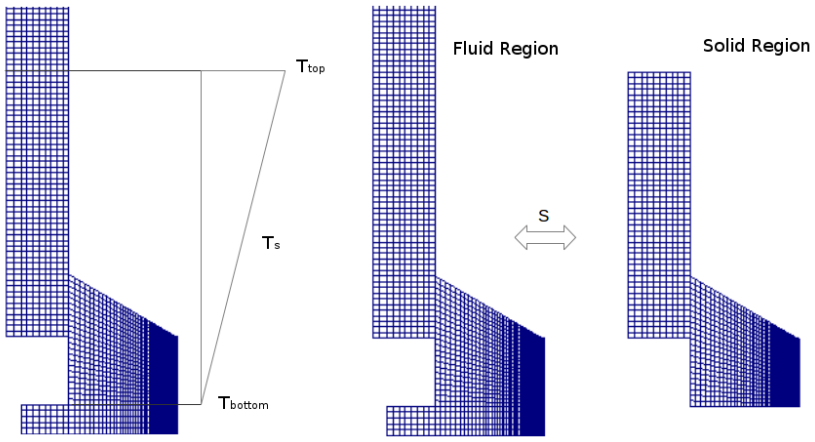

Figure 4.11: Approaches to model the thermal behavior of the regenerator: Single Region (left) and Multi Region (right)

Single region approach

This approach is really simple, needs a single mesh, and simulates the fluid-regenerator heat transfer by adding a source term S_{fluid} to the energy equation of the cells located in the regenerator zone.

$$S_{fluid} = hA(T_s - T_f) \tag{4.12}$$

This way to proceed implies the assumption of some parameter. At first, it should be defined a temperature field distribution for the regenerator zone, which will remain constant during the simulation, and will allow to define, for every cell, the value of T_s. Than it is necessary to estimate an average heat transfer coefficient h between the porous matrix and the working fluid. In the case studied it was assumed that the temperature T_s is distributed linearly between a maximum temperature T_{top} and a minimum temperature T_{bottom}; the regenerator in reality will have a different temperature distribution due to its non regular geometry and the enlargement in the lower part, but a linear assumption can still be considered a good approximation. In order to establish the value of T_{top} and T_{bottom} and h, which simultaneously influence the system behavior, an iterative method is adopted. Since the simulations are really fast it is possible to solve many cases and vary the parameters till the output is close to the experimental parameters. The values found with this analysis are $T_{top} = 480\ K$, $T_{bottom} = 340\ K$ and $h = 2000\ W/m^2K$.

Multi region approach

This approach is more complex and models the fluid-regenerator heat transfer by means of two overlapping meshes, respectively the fluid region and the solid region, including a source term S in the energy equation of the fluid and the solid phase (Eqns. 3.19 - 3.20). Its value depends on the instantaneous fluid-dynamics conditions and on the averaged temperatures of the phases, and can be evaluated by means of Eq. 4.13:

$$S = Q^{s \to f} = -Q^{f \to s} = Nu \ \frac{k_f}{d_c} \ A \ (T_s - T_f) \tag{4.13}$$

which includes in Eq. 3.21 the definition of Nusselt number

$$Nu_{D_h} = \frac{h \ D_h}{k_f}. \tag{4.14}$$

Nusselt number sholud be evaluated by means of a suitable relationship which express the dependency of the heat transfer in the chosen porous material as a function of Re and Pr. Nevertheless, it was not possible to find any correlation for random fiber porous matrices in the literature, therefore, similarly to what done during the definition of the permeability sub-model, it was decided to use a correlation obtained for staggered wire screen matrices. The chosen correlation (4.15) is taken form the same experimental study of Gedeon and Wood [14] and has been equally corroborated by following studies [4, 33].

$$Nu_{D_h} = (1 + 0.99 Re_{D_h}^{0.66} \ Pr^{0.66}) \ \Pi_v^{1.79} \tag{4.15}$$

Multi region approach in addition, requires the estimation of the effective thermal conductivities $k_{\text{f eff}}$ and $k_{\text{s eff}}$ of the fluid and the solid in correspondence to the porous zone. Since the fluid phase occupies the most of the porous zone, it is reasonable to assume that its thermophysical properties will not vary substantially in this zone and, therefore, it has been used the normal thermal conductivity of the fluid ($k_{\text{f eff}} = k_f$). For the solid phase instead, the effective value of the thermal conductivity can be very different from the material conductivity, because the solid geometry presents many void spaces. This problem has been studied for many porous materials but, once again, not exhaustively for random fiber matrices; therefore, as for the other sub-models, it was decided to use a correlation for wire screen matrices because of their similarity to the random fibers. A review of the existing models for the effective thermal conductivity of wire screens matrices has been done in 2006 by Chen [34] and is summarized in figure 4.12. As it can be seen, the output values of the models can vary between several orders of magnitude, difference that can be explained by a good or scarce contact

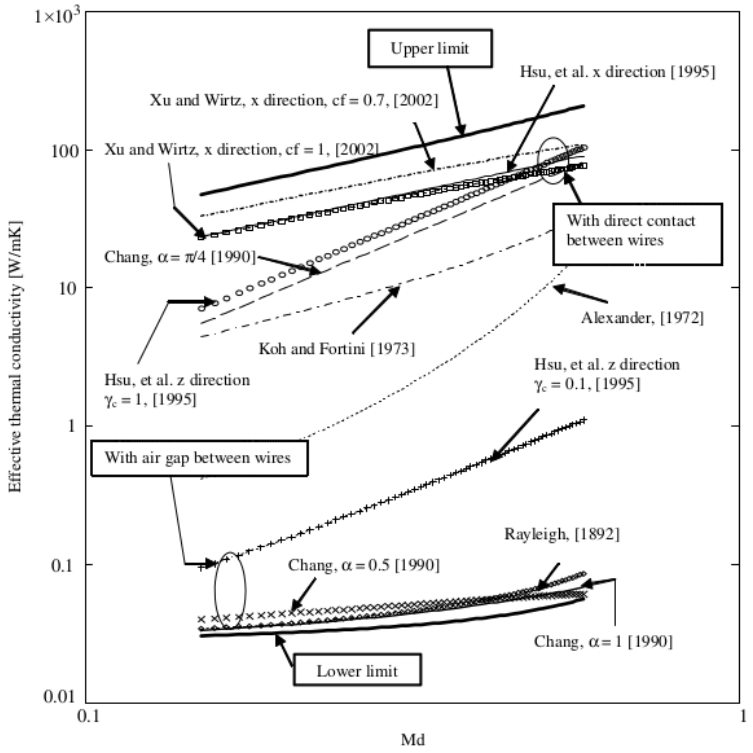

Figure 4.12: Predictions of the effective thermal conductivity of wire screen from existing models

resistance between the wires and by the transport direction considered (wire screens are anisotropic). With the purpose to closely address the behavior of the random fiber matrix of the regenerator, it has been chosen to use the correlation of Hsu at al. in the z direction, because this equation takes into account that the wires are in direct contact and that the contact resistance prevails on the conduction along the wires. The value of $k_{\mathrm{s\ eff}}$ calculated with this correlation is of 30 W/mK, which is the 7.8 % of the thermal conductivity of the copper; this value, obtained for the z direction of the wire screen, has been used in the three dimensions of the random fiber matrix in order to account the isotropic behavior of the real regenerator.

4.2.4 Walls

In section 4.2.2 it was explained the decision to account all the energy losses of the system by reducing the power input in the electrical resistance zone. A direct consequence of this decision is that all the boundary walls, with the exception of the cooling surfaces, must be considered adiabatic. For the cold

piston this assumption is not far from reality, because its surface is close to the ambient temperature and its movement occurs within a closed cylinder. For the displacer walls and especially for the hot space walls, the adiabatic hypothesis does not represent the reality, however can be accepted for the first validation and, avoiding to model the losses singularly, allows to run faster simulations.

4.2.5 Hot space thermocouple

The temperature in the hot space is experimentally measured by means of a K-type thermocouple positioned, as shown in Fig. 4.13, very close to the electrical resistance (at about 1 cm). Since the thermocouple is not shielded from radiation, its measure is representative not only of the temperature of the fluid, but also of the temperature of the resistance which, during the functioning of the engine, is incandescent. In the simulation it is possible (and easy) to probe the temperature of the fluid in the same position of the thermocouple, but it can be difficult to model convective and radiative effects of the thermocouple. Therefore it is important to give a rough estimation of the error related to the thermocouple measurement in order to compare, during the validation of the model, only the effective temperatures of the fluid. Since the problem is rather complex and characterized by uncertainties, many assumptions were introduced, and the solution should be taken as an indicative estimation of the real behavior of the system.

At first, it is possible to write the energy balance for the thermocouple as:

$$\frac{\partial U}{\partial t} = Q_{rad} + Q_{conv} + Q_{cond} \tag{4.16}$$

then, since the system moves with high frequency and the cycles are stabilized, a steady state simplification can be adopted. In addition the power exchanged by the thermocouple through its connecting wires is considered accounted into the thermocouple calibration, therefore Eq. (4.16) can be rewritten as:

$$Q_{rad} + Q_{conv} = 0 \tag{4.17}$$

To estimate the heat exchanged by irradiation, a lumped parameter approach has been used, in which radiative power is regarded as an electric current and equivalent losses relative to the transmission and emission of radiation are accounted (Fig. 4.14). Therefore the radiative power exchanged between the electrical resistance and the thermocouple is expressed by:

$$Q_{rad} = \frac{\sigma(T_T^4 - T_R^4)}{R_{eq,TR}} \tag{4.18}$$

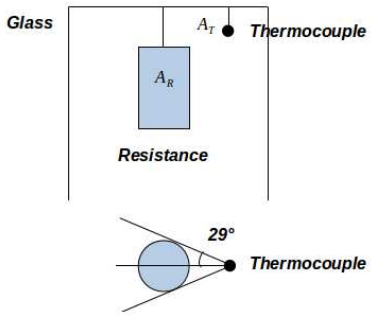

Figure 4.13: Scheme used to estimate radiative exchange

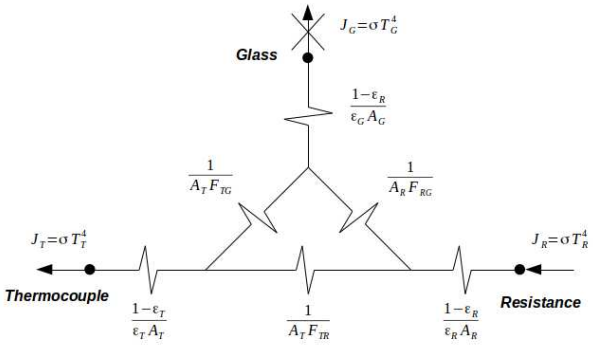

Figure 4.14: Lumped parameters scheme

The elements considered in the scheme are the thermocouple T, the electrical resistance R and the glass walls of the hot space G. Since the hot space presented a radiative insulation during the experimental measure, and since the resistance emits mostly in the infra-red range, which is partially reflected by the glass of the walls, it can made the rough approximation that none of the irradiance of the resistance is lost to the surrounding $J_G = 0$. It must be considered that the hot space walls are heated also by convection and conduction with the working fluid, and their emitted radiation contributes to rise the error committed by the thermocouple. However, as a first approximation, this contribution is neglected, being aware that the final solution might be an underestimation of the real error of the thermocouple. Another hypothesis is that both the thermocouple and the electrical resistance behave as black bodies ($\varepsilon_R = 1$ and $\varepsilon_T = 1$), therefore their representing resistances can be neglected in the solution of the scheme. The areas A_T and A_R are estimated by approximating the resistance with a cylinder of the same dimensions, and the thermocouple by a sphere of $1mm$ of diameter. In order to estimate the view factors is assumed that $F_{RG} = 1$ and $F_{TG} = 1$, since both the thermocouple and the resistance can be considered small bodies completely surrounded by the container glass walls; F_{TR} instead, has been evaluated geometrically as the ratio between the resistance surface seen by the thermocouple and the total resistance surface. By means of all the assumptions made, the equivalent resistance R_{eq} between the electrical resistance and thermocouple can be easily calculated as a parallel between resistances:

$$R_{eq,TR} = \frac{1}{A_T F_{TR}} // \left(\frac{1}{A_R} + \frac{1}{A_T} \right) \tag{4.19}$$

The convection power estimation has been solved as forced convection

over a spherical surface:

$$Q_{conv} = h_C A_T (T_T + T_F) \tag{4.20}$$

At first a simulation has been run, monitoring the fluid velocities in correspondence to the thermocouple position in order to compute an average Re number in that position. Then, using the correlations for external forced convection on a spherical surface, the Nu number was calculated. Finally from the definition of Nu was possible to evaluate an average value of the heat transfer coefficient h_C. Eq (4.17) can thus be written as:

$$\frac{\sigma(T_T^4 - T_R^4)}{R_{eq}} + h_C A_T (T_T + T_F) = 0 \tag{4.21}$$

where T_T is the thermocouple temperature, T_R the electrical resistance temperature and T_F the working fluid temperature. Equation (4.21) can be solved directly for the variable T_F considering that the thermocouple temperature measured is $T_T = 818K$, and assuming that the temperature of the resistance is about $T_R = 1000K$. The related temperature of the working fluid calculated with this model is of $T_F = 690K$, therefore the error on the thermocouple measurement seems to be not negligible and the hot temperature in the simulations should be validated against the corrected temperature $T_{hot} = T_F$ well below the experimental measure of the thermocouple.

4.2.6 Cold space thermocouple

The thermocouple which measures the temperature of the cold space is inserted in the power piston, however it is not possible to simulate its behavior by means of a probe because the real position of the sensor is not known. In the simulation therefore, the cold space temperature has been monitored as the average temperature of the piston surface, which should not be far from the one indicated by the thermocouple.

4.2.7 Pressure transducer

Pressure transducer is inserted in the power piston and, therefore, measures the the pressure of the cold space. Since pressure does not present significant gradients in this space, in the simulation the same information has been obtained by computing for each time step the volumetric average pressure of the space.

4.2.8 Power output

The indicated work output of the experimental cycle is calculated by integrating the measured p-V diagram. This diagram however is obtained by means of the pressure measured in the cold space and would represent correctly the effective behavior of the engine only if the pressures were the same in all the components of the engine. Because of the presence of the porous matrix, which in the regeneration phases implies a significant pressure drop, this assumption is not true in Stirling engines, and work output calculated in this way can sometimes be really different from the real value. The most correct way to compute the indicated work output is by means of Eq. (4.22)

$$W_{out} = \int p_C \, \mathrm{d}V + \int p_H \, \mathrm{d}V \tag{4.22}$$

which calculates the total work as the sum of the works done by the cold space and the hot space separately, taking into account their pressure difference. While the experimental apparatus does not allow to measure the pressure of the hot space, in the simulation it is possible to monitor this value, as done for the cold pressure, by computing the volumetric average pressure of the hot room. Therefore, for the validation of the model, the work output calculated as in the experimental tests was adopted; on the contrary, to define the real performances of the machine and during the parametric study, the correct power, calculated from Eq. 4.22, was used.

Chapter 5

Validation of the model and analysis of the results

In this chapter the validation of the developed CFD model will be presented. As explained in the previous chapter, two different approaches has been adopted for the modeling of the regenerator: *multi-region* and *single-region*. In the following sections, these approaches will be compared considering both the accuracy of the prediction and the computational effort required for the simulation. Moreover their strengths and weaknesses will be analyzed, defining when they can be applied in relation to the purpose of the simulation. Finally, on the basis of the predictions of the simulation models the different phenomena occurring in the engine will be investigated and explained.

5.1 Multi Region

5.1.1 Validation

The computational model was validated both on global quantities, such as the power output and the heat transferred to the cold sink in a cycle, and on local measurements of temperature in the machine.

In Fig. 5.1 the comparison of experimental and computed p-V cycles is reported, showing a satisfactory agreement; simulation results are consistent with the measurements also if pressure and volume variations are considered singularly, as shown in Fig. 5.2 and 5.3. Considering the other quantities, shown in Fig. 5.4, 5.5 and 5.6, the comparison was done on the average values over the cycle, since instantaneous experimental data were not available. With regards to the temperature probed in the hot space, it must be considered that the experimental measurement $T_{hot,rad}$ is affected by the influence of the radiative heat transfer since the thermocouple is not shielded against radiation. In order to take into account this measurement error a simple

analytical model was developed, leading to the estimation of the fluid temperature T_{hot} (Sec. 4.2.5); if this estimation is considered, the temperature of the fluid calculated at the thermocouple location seems to be reasonable. The numerical comparison between measured and calculated quantities is reported in Table 5.1.

In Fig. 5.1 the comparison of experimental and computed p-V cycles is reported, showing a satisfactory agreement; simulation results are consistent with the measurements also if pressure and volume variations plotted as a function of the crank angle, as illustrated in Fig. 5.2 and 5.3. Considering the other quantities, shown in Fig. 5.4, 5.5 and 5.6, the comparison was done on the average values over the cycle, since instantaneous experimental data were not available. With regards to the temperature probed in the hot space, it must be considered that the experimental measurement $T_{hot,rad}$ is affected by the influence of the radiative heat transfer since the thermocouple is not shielded against radiation. In order to take into account this measurement error a simple analytical model was developed, leading to the estimation of the fluid temperature T_{hot} (Sec. 4.2.5); if this estimation is considered, the temperature of the fluid calculated at the thermocouple location seems to be reasonable. The numerical comparison between measured and calculated quantities is reported in Table 5.1.

The mechanical power of the device was experimentally determined from the pressure probed in the cold space, however this value is not correct, as explained in Sec. 4.2.8; for this reason in Table 5.1 are reported both the mechanical power evaluated using the pressure of the cold space $P_{out,cold}$, and the effective mechanical power P_{out} determined as the difference between the power of the expansion space and the compression space.

Table 5.1: Multi region: Comparison between measurements and experimental results

Quantity		Measured	Simulated	Rel err %
power cooling system Q_{cold}	W	84.9	82.9	2.4
power output $P_{out,cold}$	W	13.8	14.2	−2.9
power output effective P_{out}	W	-	9.82	-
hot temperature $T_{hot,rad}$	K	818	-	-
hot temperature T_{hot}	K	692	681	1.6
cold temperature T_{cold}	K	322	314.6	2.3

5.1.2 Engine analysis

In Fig. 5.7 the simulated p-V diagram for the hot space and the cold space is shown, along with the global cycle plotted using the averaged pressure and

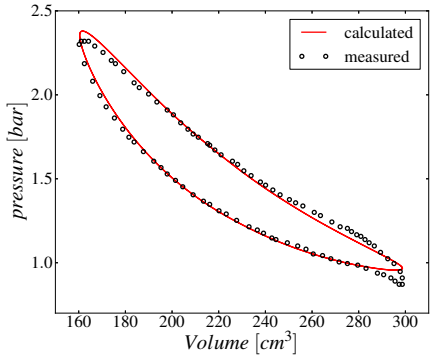

Figure 5.1: Multi region: Comparison of the p-V diagrams between the model and the experimental data measured

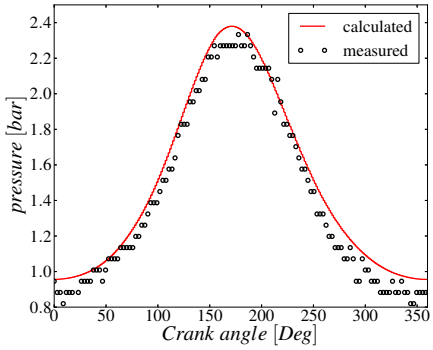

Figure 5.2: Multi region: Comparison of the pressure variation between the model and the experimental data

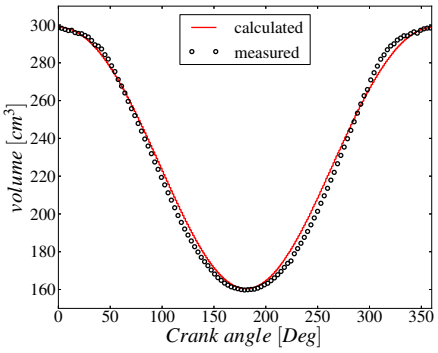

Figure 5.3: Multi region: Comparison of the volume variation between the model and the experimental data

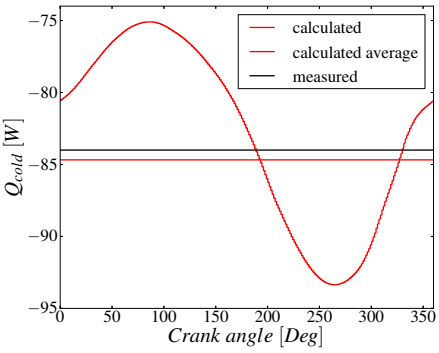

Figure 5.4: Multi region: Comparison of the cooling power between the model and the experimental data

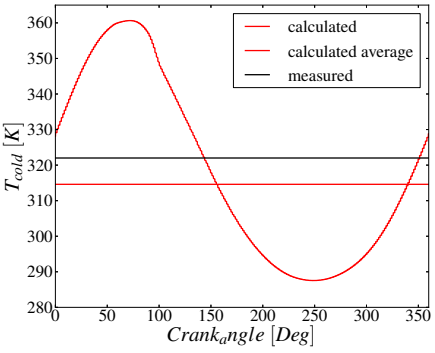

Figure 5.5: Multi region: Comparison of the cold average temperature between the model and the experimental data

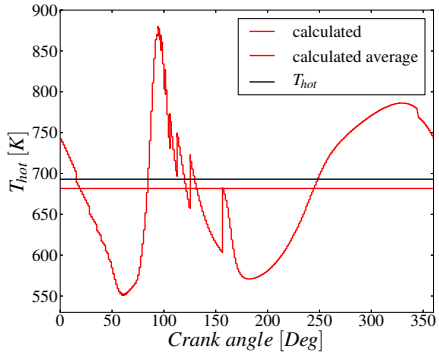

Figure 5.6: Multi region: Comparison of the hot average temperature between the model and the experimental data

the total machine volume. From this figure is possible to study graphically the difference between the positive cycle of the hot space and the negative cycle of the cold space, whose difference represent the effective work output mentioned in Sec. 4.2.8. Fig. 5.8 instead, displays the evolution of the regenerator matrix average temperature. In this simulation the regenerator was initialized with an ambient temperature and it can be noticed that the cyclic stationary state was reached after approximately 450 cycles, requiring 36 hours of computational time. Fig. from 5.9 to 5.12 show the fields of

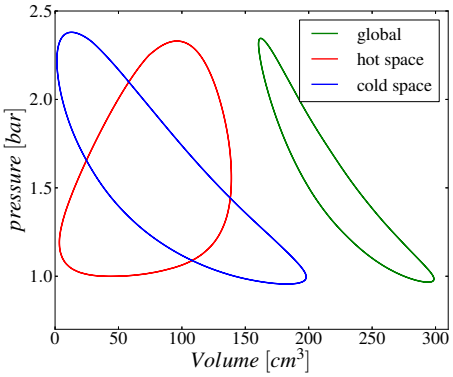

Figure 5.7: Multi region: p-V cycles for the base case: compression space, expansion space and global machine cycle

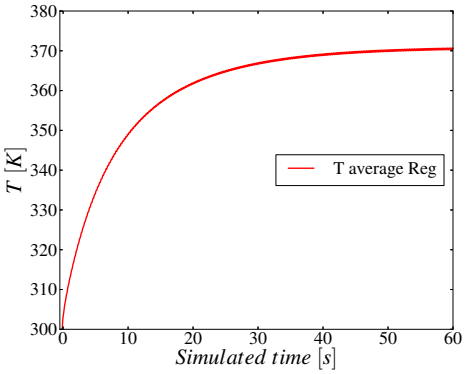

Figure 5.8: Multi region: cyclic steady state achievement of the average regenerator temperature

different fluid-dynamics quantities during the four ideal phases of the cycle. The most interesting phases are the regenerations (Fig. 5.10 and 5.12), when the axial motion of the displacer forces the fluid to move from one of the two spaces to the other passing through the porous matrix. During the isochoric cooling regeneration (Fig 5.12) the displacer moves from the bottom to the top, determining the motion of the fluid towards the cold space. As a result of the air flowing through the porous media, a pressure difference between the hot and the cold space is originated. Moreover the regenerator, whose temperature varies along its axis, accumulates energy from the fluid, cooling it to a temperature close to the one of the cold space; it can be observed that, in the considered engine, this phase results particularly effective since the lower part of the regenerator is in direct contact with the cooling system, enhancing the cold exchange with the air (Sec. 4.2.2). The analogous isochoric heating transformation is illustrated in Fig. 5.10: in this case the energy accumulated in the regenerator matrix during the previous regeneration is given back to the fluid, which passes from the bottom to the top of the

engine. During the isothermal expansion and compression transformations instead (Fig. 5.11 and Fig. 5.9) the working space volumes change significantly, the air is mostly contained in one of the two spaces and a positive or negative work is done on the power piston.

The figures show that the the porous matrix of the regenerator has the effect of increasing the velocity of the fluid, since the presence of the solid phase involves a reduction of the passage area. With regards to the pressure drop inside the engine, it might be observed that it is concentrated entirely in the narrow part of the regenerator, where the friction effect in the porous media is maximum due to the high velocities reached; compared to the pressure drop in the regenerator, no significant friction losses can be observed in the other components of the engine. Moreover, it can be further observed that the highest pressure drop during the cycle occurs in regenerative phases, when the velocities inside the porous matrix are maximum due to the air displacement; in the expansion and compression phases instead, the pressures of the two spaces are closer because air is not forced into the regenerator and the losses are reduced. Lastly, it can be seen that, during a cycle, the two spaces present alternatively the highest and the lowest pressure of the engine, and that this passage occurs at the end of the regeneration phases. This effect is visible also in Fig. 5.13, where are represented the pressure evolutions of the two spaces along with the average pressure of the engine.

It can be further observed that, since the lower part of the regenerator has a larger section area than the upper part, the air velocity decreases significantly before entering the cold space. This fact leads to very low fluid velocities in this part of the engine, where the flow is almost laminar, and results in a very ineffective heat transfer in the boundary layer of the external cooling surface. The power exchanged by the various surfaces of the cooling system is shown in Fig. 5.14, where is displayed how the most of the heat is removed by the surfaces in direct contact with the regenerator matrix, while the surfaces of the cold room are less effective. This can be explained by the fact that the lower part of the regenerator matrix behaves almost as an extension of the displacer cooling system, enhancing considerably its removal power. Therefore, the air entering the cold space is characterized not only by low velocities, but even by low temperatures, resulting in a inefficient heat transfer in this zone. The turbulence solution is consistent with the observations done: it is possible to note that the turbulent viscosity presents very low values in the cold space, which means that flow is almost laminar and that the heat transfer in the boundary layer is not promoted by the turbulence. In addition, it can be noticed that the turbulent viscosity is not transported from one space to the other because drops through the displacer zone; this means that the re-laminarization of the turbulent flow into the porous re-

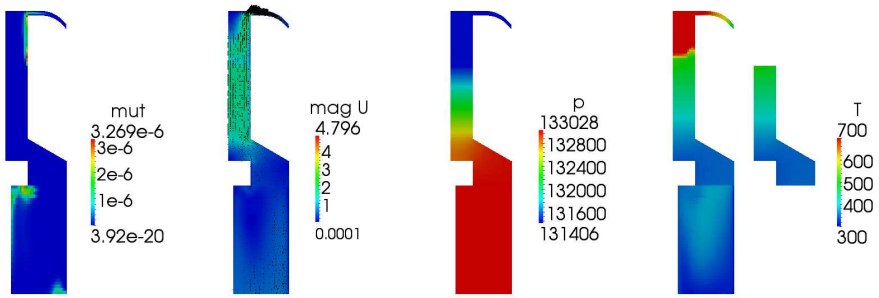

Figure 5.9: Multi region: Fields during the isothermal compression transformation

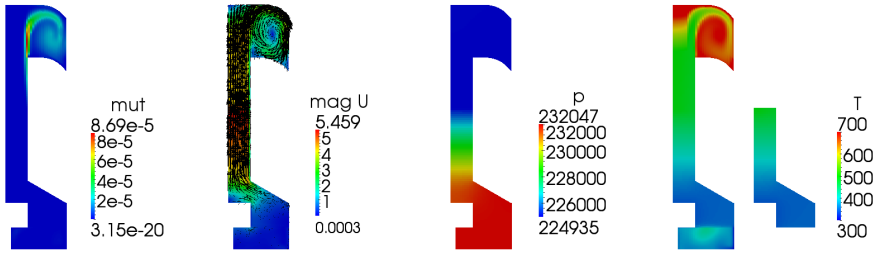

Figure 5.10: Multi region: Fields during the isochoric heating regenerative transformation

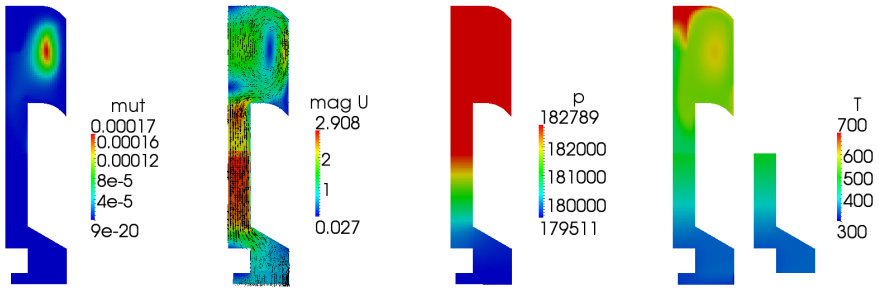

Figure 5.11: Multi region: Fields during the isothermal expansion transformation

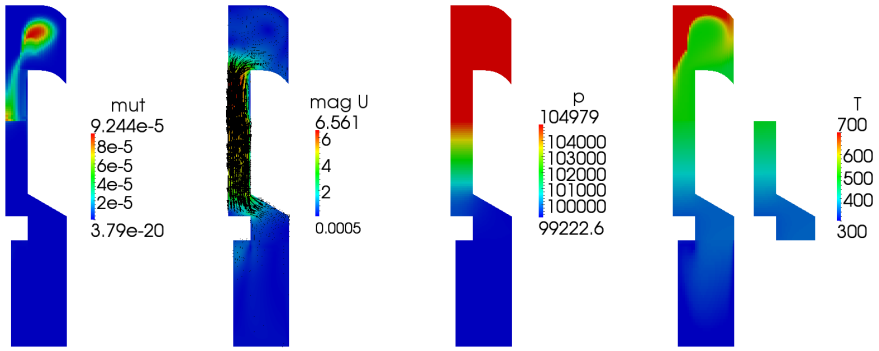

Figure 5.12: Multi region: Fields during the isochoric cooling regenerative transformation

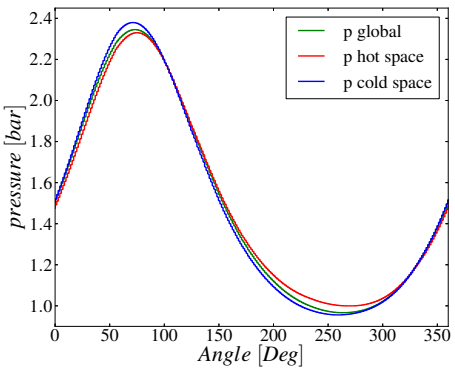

Figure 5.13: Multi region: evolution of the pressures of the hot space and cold space and the average engine pressure

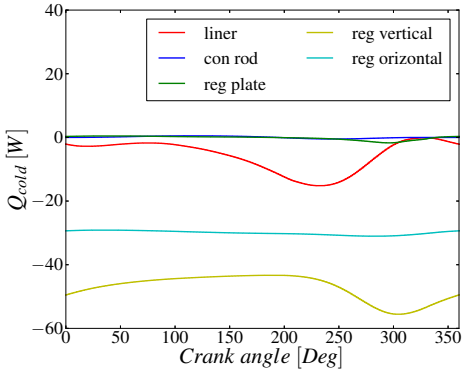

Figure 5.14: Multi region: power exchanged by the different surfaces of the cooling system

generator is correctly taken into account (Sec 3.6). Finally, in figure 5.15 are shown the stream lines of the air during the cycle phases, which highlight where the eddies and the recirculation zones are generated; this information can be important in the design phase and could not be evinced applying simplified non-CFD approaches (first, second and third order analysis).

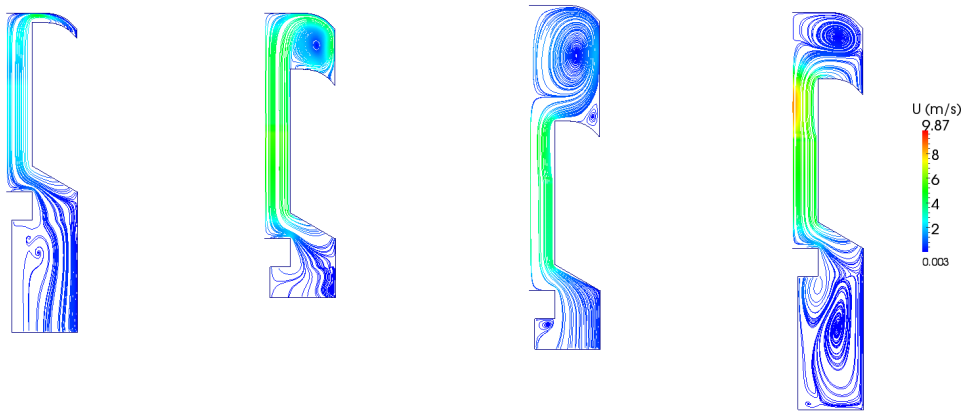

Figure 5.15: Multi region: stream lines during the four cycle phases

Table 5.2: Single region: Comparison between measurements and experimental results

Quantity		Measured	Simulated	Rel err %
power cooling system Q_{cold}	W	84.9	82.43	2.9
power output $P_{out,cold}$	W	13.8	15.4	−11.2
power output effective P_{out}	W	-	9.9	-
hot temperature $T_{hot,rad}$	K	818	-	-
hot temperature T_{hot}	K	692	685.7	0.9
cold temperature T_{cold}	K	322	309.2	4.0

5.2 Single Region

5.2.1 Validation

The single-region model has been validated adopting the same method used in the multi-region approach. The agreement between calculated and measured data is satisfactory also in this case as it is shown in Figures 5.16 - 5.21 and summarized in Table 5.2. The only difference with the multi-region approach consists in the derivation of the Q_{cold} of Fig. 5.19. In fact, as shown previously, the majority of the cooling power in this engine is removed by the regenerator matrix; this means that the energy balance of the regenerator is not zero, but is globally negative. Consequently, in single-region approach, even the source term which simulates the regenerative exchange is globally negative over a cycle. The real value of the power removed therefore, is given by the sum of the power that flows through the cooling surfaces Q_{cold} and the power exchanged with the regenerator sub-model Q_{reg}. The average of this sum over a cycle gives the cooling power and can be directly compared with the experimental measurement.

5.2.2 Analysis

Single-region approach can be analyzed by means of the same parameters used for the multi-region approach. Fig. 5.22 shows the p-V cycles obtained for the two working spaces and the global averaged cycle; it can be noticed that this diagram is very similar to the one obtained with the multi-region approach. Fig. 5.23 instead, represents the evolution of the average temperature of the regenerator zone; if this diagram is compared to the analogous of Fig. 5.8, it can be observed that in the single-region model, the cyclic convergence is reached after the first cycle, in a much shorter time than multi-region.

With regards to the fields of the thermo-dynamic quantities calculated,

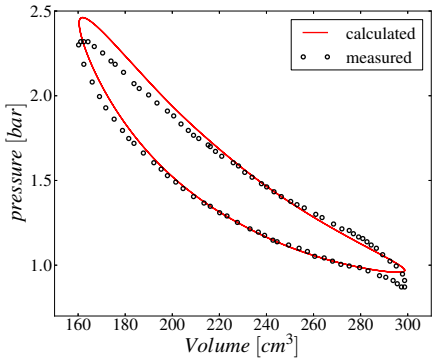

Figure 5.16: Single region: Comparison of the p-V diagrams between the model and the experimental data measured

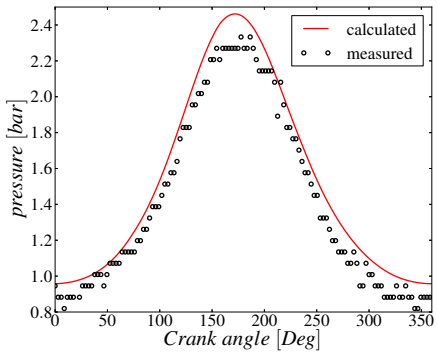

Figure 5.17: Single region: Comparison of the pressure variation between the model and the experimental data

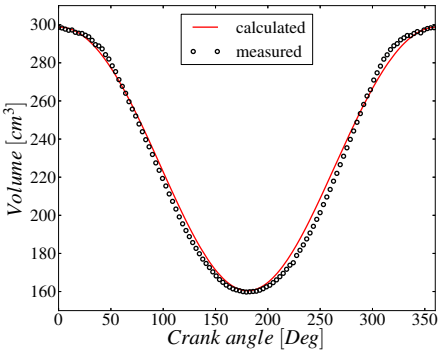

Figure 5.18: Single region: Comparison of the volume variation between the model and the experimental data

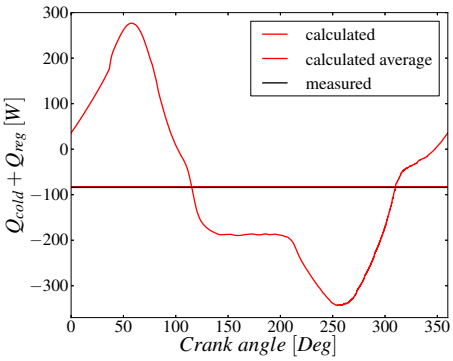

Figure 5.19: Single region: Comparison of the removed power between the model and the experimental data

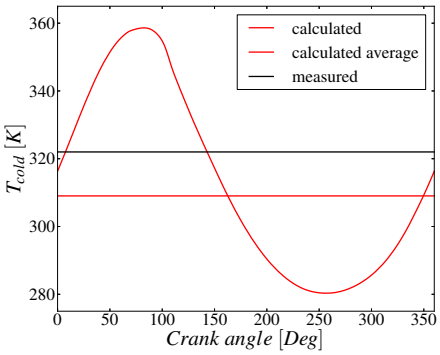

Figure 5.20: Single region: Comparison of the cold average temperature between the model and the experimental data

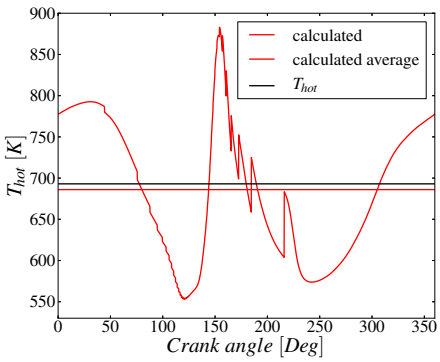

Figure 5.21: Single region: Comparison of the hot average temperature between the model and the experimental data

the output is illustrated in Fig 5.24 - 5.27, which show the four ideal transformations. If this figures are compared with the analogous obtained with the multi-region approach, it can be noticed that the results are very similar. In particular the temperature field, whose solution contains the difference between the models, presents a good similarity. As a matter of fact, all the considerations done on the engine operation with the multi-region model (Sec. 5.1.2), could have been derived even by means of this approach. This lead to the conclusion that, if correctly set, both the models are coherent and can both be used to study the engine behavior. On the other hand, it requires the definition of quantities, such as the temperature distribution in the regenerator, which might not be a-priori known and should be obtained from experimental measurements or from more detailed multi-region simulations.

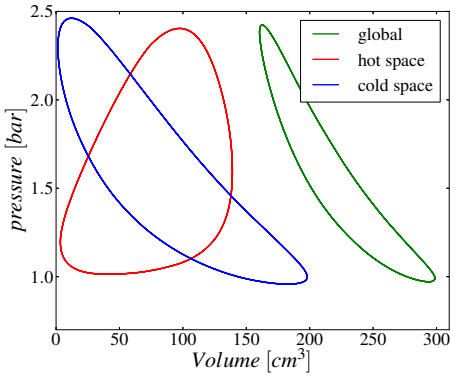

Figure 5.22: Single region: p-V cycles for the base case: compression space, expansion space and global machine cycle

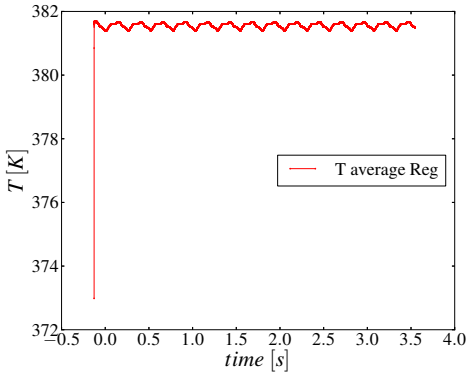

Figure 5.23: Single region: cyclic steady state achievement of the average regenerator temperature

5.3 Models comparison

From the results presented in the previous sections it can be seen that both the models are able to satisfactory simulate the engine behavior, and can be similarly useful to understand the functioning and the efficiency of the various parts of the machine.

Starting from this observation one might be led to the conclusion that single-region model is more convenient, since gives comparable results in a much shorter computation time, reaching an almost immediate convergence.

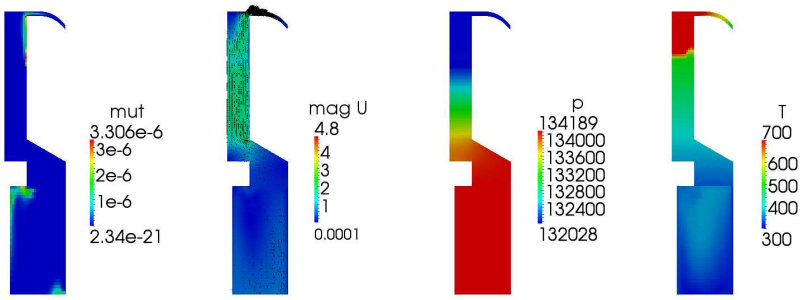

Figure 5.24: Single region: Fields during the isothermal compression transformation

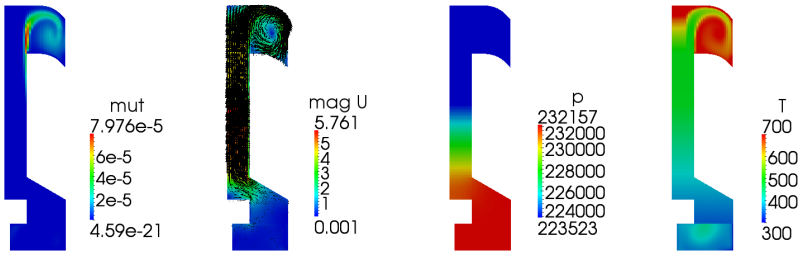

Figure 5.25: Single region: Fields during the isochoric heating regenerative transformation

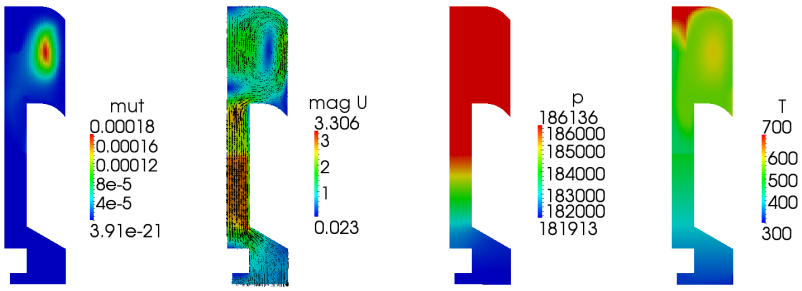

Figure 5.26: Single region: Fields during the isothermal expansion transformation

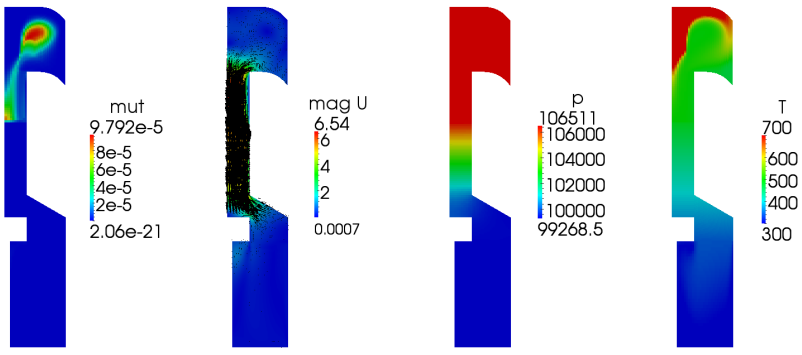

Figure 5.27: Single region: Fields during the isochoric cooling regenerative transformation

However this model holds two inherent disadvantages. The first disadvantage is that it can not be used if the engine behavior is completely unknown in advance; in fact, if the regenerator temperatures can not be reasonably hypothesized, at least two of the other global or local quantities should be known a-priori. In this way it is possible to assume a regenerator temperature distribution and run many simulations till the results match the known quantities. Furthermore, the known quantities should be at least two because, by means of the experience gained during the simulations, it has been noticed that the matching of a single quantity can be obtained by very different combinations of the others, and therefore the solution achieved validating only one datum could be incorrect. The second disadvantage of single-region approach, which is a consequence of the first, is that it can not be used satisfactory for a parametric study, because it would require to evaluate, case by case, the correct temperatures to be set in the regenerator sub-model. The regenerator temperatures chosen in fact, strongly influence the output parameters and, if incorrectly set, can lead to invalid results.

On the contrary, multi-region model does not require any hypotesis on the temperature distribution in the regenerator, since this information is determined by solving an additional energy balance for the solid region. In addition it can account the physics of the regenerator material and its internal heat transfer, which were not included in the single-region approach, resulting more precise and complete. This way to proceed is fully predictive of the engine behavior and can be used to perform an optimization study, where none of the output results are known. The drawback that lies under this approach is the long computational time required to reach the cyclic stationary state of the regenerator. This problem can be partially overcome if the regenerator temperatures, instead of being initialized with the ambient temperature, are initialized by means of a sensed hypothesis of the regenerator temperature distribution of the final solution. Despite the Single region approach, in this case, even if the hypothesis done result incorrect, the simulation will converge to the correct solution, taking more or less time according to the error committed in the initialization assumptions.

Chapter 6

Parametric analysis

In this chapter the developed *multi-region* model will be applied to perform a parametric study involving different aspects related to the machine. In particular different design and control parameters will be considered: mean cycle operating pressure, heat power input, regenerator properties, working fluid. Lastly, the model will be adopted to simulate the operation of an ideal engine configuration, investigating the aspects related to the adoption of an ideal law of variation of the volumes, infinite permeability of the regenerator and ideal heat exchangers.

The case chosen as base for the parametric study is the one representing the real operation of the engine, validated against the experimental measurements in chapter 5. Starting from the setting of this case, simulations were run by changing only one parameter at once, so that its effect on the engine performances is clarified. The base case is characterized by a velocity of 235 rpm, maintained constant in every test case in order to compare the calculated power output, a mean pressure of charge of 1 bar and a power input of 92.7 W. It might be noticed that the power introduced in the system is not always constant in the various tests: this is the consequence of the temperature limitation of the electrical resistance, which automatically decreases the power input when the temperatures rise above a maximum value. With regards to the regenerator properties, the real regenerator consists of a copper random fiber matrix, for which a thermal conductivity of 30 W/mK and a heat capacity of $7e5$ J/m^3K have been estimated.

6.1 Mean pressure

In this section the effect of the mean pressure of the cycle is investigated. This parameter controls the mass of working fluid which operates in the cycle and is usually adopted in practical applications in order to modify the load and, therefore, the mechanical power output of the machine. If the pressure

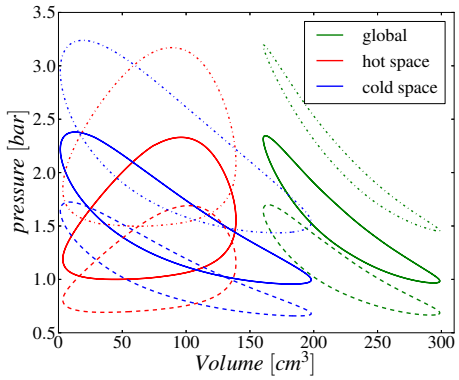

Figure 6.1: Effects of a variation of the mean pressure of the cycle: base case, $1\,bar$ (continuos line), $0.7\,bar$ (dashed line), $1.5\,bar$ (dotted line).

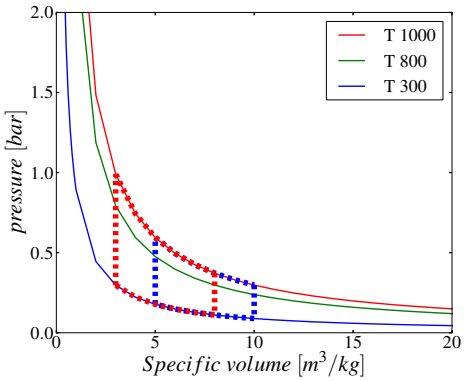

Figure 6.2: Effect of the density variation on the specific work output

of the engine is increased (and consequently the fluid density), the specific work output (J/kg_{fluid}) rises, as shown in Fig. 6.2, because the specific p-V cycle is shifted to the left, and its area is enlarged. As a matter of fact, if the mean pressure rises, the total power output increases because both the specific work output and total mass evolving in the system are higher. This analysis however, is valid only if the power introduced in the heat sources is large enough to maintain the working spaces temperatures at the same constant values; if this does not happen, the higher temperatures decrease and the lower rises, leading the engine to function with very low specific works and reduced efficiencies. This loss can either be considered as a reduction of the weight of the expansion work over the compression work.

With regards to the considered engine, the cooling system has been modeled as a constant temperature source, while the electrical resistance as a constant power source. Therefore, in case of a mass increase of the air due to an higher mean pressure, the cold space temperature will undergo small changes, and a higher mechanical power will be obtained only if heat introduced in the hot space increases accordingly in order to maintain a constant hot temperature.

In the graph reported in Fig. 6.1 the mean pressure of the cycle is varied keeping constant the heat power transferred in the hot space. As theoretically derived, when the mass is increased keeping constant the amount of heat introduced, the temperature of the hot space decreases. In this case the consequent reduction of the specific work due to a lower hot isotherm is more important than the positive effect of the mass increase. Consequently,

Table 6.1: Parametric study on system mean pressure: simulation results.

Pressure	$[bar]$	$\mathbf{P_{mech}}[W]$	$\mathbf{Q_{cold}}[W]$	$\mathbf{Q_{hot}}[W]$	$\mathbf{T_{cold}}[W]$	$\mathbf{T_{hot}}[W]$
Base case	1.0	9.8	82.9	92.7	314.6	681.8
Test	0.7	10.2	72.1	82.3	308.0	722.9
	1.5	2.2	90.5	92.7	326.4	576.3

Table 6.2: Parametric study on system mean pressure: calculated efficiencies.

Pressure	$[bar]$	$\eta_{\mathbf{Carnot}} = \mathbf{1} - \frac{\mathbf{T_{cold}}}{\mathbf{T_{hot}}}$	$\eta_{\mathbf{I}} = \frac{\mathbf{P_{mech}}}{\mathbf{Q_{hot}}}$	$\eta_{\mathbf{II}} = \frac{\eta_{\mathbf{I}}}{\eta_{\mathbf{Carnot}}}$
Base case	1.0	0.54	0.11	0.20
Test	0.7	0.57	0.12	0.22
	1.5	0.43	0.02	0.06

the area of the resulting global cycle is reduced compared to the base case and, since the heat introduced is the same, also the efficiency η_I drops.

On the other hand, the reduction of the mean pressure determines an higher hot space temperature and the functioning of the cycle on a higher hot isotherm; the consequent increase of the specific work results more important than the negative effect due to the decrease of the air mass, therefore the power output increases and a better η_I is obtained. Though the Carnot efficiency rises in this case due to the higher hot temperature, the positive effect on the cycle is more pronounced, resulting also in a better η_{II}

6.2 Power input

In this section the effect of the amount of heat introduced in the device is investigated. Fig. 6.3 shows that the increase of the power input determines a higher work output of the machine. Moreover the efficiency η_I increases, since the weight of the compression space work over the global cycle decreases. On the contrary, a reduction of the heat power at the hot end determines a reduction of the work of the expansion space, which can become not sufficient to overcome the compression work resulting therefore in a negative power output of the machine. The numerical results are summarized in Table 6.3 and 6.4.

6.3 Regenerator parameters

As previously said, the regenerator is the key component for the optimization of the performances of a Stirling device. Its behavior depends mostly on

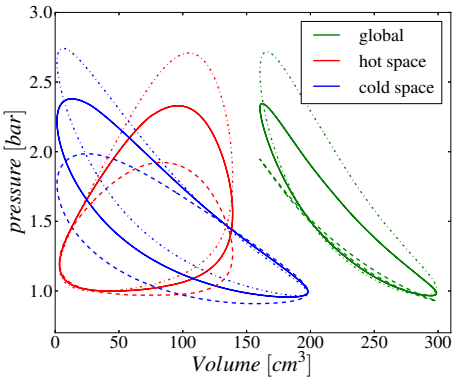

Figure 6.3: Effects of a variation of the amount of heat introduced in the hot space Q_{hot}: base case, $Q_{hot} = 93\,W$ (continuos line), $Q_{hot} = 50\,W$ (dashed line), $Q_{hot} = 150\,W$ (dotted line).

Table 6.3: Parametric study on system power input: simulation results.

Power input	$[bar]$	$\mathbf{P_{mech}}[W]$	$\mathbf{Q_{cold}}[W]$	$\mathbf{Q_{hot}}[W]$	$\mathbf{T_{cold}}[W]$	$\mathbf{T_{hot}}[W]$
Base case	93	9.8	82.9	92.7	314.6	681.8
Test	50	-4.8	54.5	49.6	329.3	527.5
	150	23.7	109.1	132.8	304.5	894.2

Table 6.4: Parametric study on system power input: calculated efficiencies.

Power input	$[bar]$	$\eta_{\mathbf{Carnot}} = \mathbf{1} - \frac{\mathbf{T_{cold}}}{\mathbf{T_{hot}}}$	$\eta_{\mathbf{I}} = \frac{\mathbf{P_{mech}}}{\mathbf{Q_{hot}}}$	$\eta_{\mathbf{II}} = \frac{\eta_{\mathbf{I}}}{\eta_{\mathbf{Carnot}}}$
Base case	93	0.54	0.11	0.20
Test	50	0.38	-0.10	-0.26
	150	0.66	0.18	0.27

two parameters: the material of which is made the regenerator matrix and the morphological properties of the porous material adopted. The effective thermal conductivity of the regenerator matrix is a function of both these parameters, while the effective heat capacity depends only on the porosity and the material used. In this section a separated analysis of the effects of regenerator conductivity and heat capacity will be performed; finally a comparison between real materials will be done, trying to outline useful guidelines for the regenerator design.

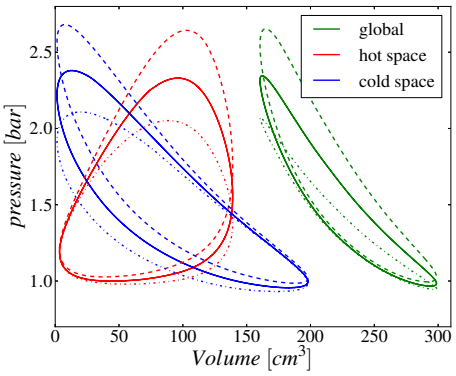

Figure 6.4: Effects of a variation of the effective conductivity $k_{reg,eff}$ of the regenerator: base case, $k_{reg,eff} = 30\,W/(mK)$ (continuos line), $k_{reg,eff} = 10\,W/(mK)$ (dashed line), $k_{reg,eff} = 100\,W/(mK)$ (dotted line).

6.3.1 Thermal conductivity

The effective thermal conductivity of the regenerator matrix influences the efficiency losses related to the heat transfer from the hot source to the cold source; in fact, the internal conduction in the regenerator has the effect to redistribute the heat stored in the porous matrix, leveling its temperature distribution. If the axial conductivity is high, the maximum and minimum temperatures of the porous matrix are closer to each other, while the local temperature differences between fluid and solid increase, leading to higher irreversibilities in the fluid-solid heat transfer. In an ideal machine the axial conductivity of the regenerator should be null, in order to minimize this loss. It must be considered that, in real applications, the effective thermal conductivity of the porous matrix is sensibly lower than the conductivity of the original material because of the presence of void spaces; therefore it should be pursued the technical solution which, combining the material and the porous matrix effects, is characterized by the lowest effective axial thermal conductivity.

In Fig. 6.4 the p-V cycles computed in the case of different effective conductivity of the porous matrix is shown. It can be seen that the area of the global cycle increases as the conductivity decreases. This is due to the fact that, as reported in Table 6.5, a higher temperature is reached in the hot space because of the heat losses towards the cold space are lower. This results in an higher first law efficiency η_I of the cycle, since the temperature difference between the spaces increases, but also in a higher second law efficiency η_{II}, because of the reduced irreversibility source.

Table 6.5: Parametric study on regenerator conductivity: simulation results.

Conductivity	$[\frac{W}{mK}]$	$\mathbf{P_{mech}}[W]$	$\mathbf{Q_{cold}}[W]$	$\mathbf{Q_{hot}}[W]$	$\mathbf{T_{cold}}[W]$	$\mathbf{T_{hot}}[W]$
Base case	30	9.8	82.9	92.7	314.6	681.8
Test	10	18.8	64.4	83.2	315.8	763.0
	100	1.3	91.6	92.9	318.3	608.2

Table 6.6: Parametric study on regenerator conductivity: efficiencies.

Conductivity	$[\frac{W}{mK}]$	$\eta_{\mathbf{Carnot}} = \mathbf{1} - \frac{\mathbf{T_{cold}}}{\mathbf{T_{hot}}}$	$\eta_{\mathbf{I}} = \frac{\mathbf{P_{mech}}}{\mathbf{Q_{hot}}}$	$\eta_{\mathbf{II}} = \frac{\eta_{\mathbf{I}}}{\eta_{\mathbf{Carnot}}}$
Base case	30	0.54	0.11	0.20
Test	10	0.59	0.23	0.38
	100	0.48	0.01	0.03

6.3.2 Heat capacity

The volumetric heat capacity C, defined by the product ρC_p (J/m^3K), measures the ability of a solid material to store thermal energy. For the same value of thermal conductivity, materials with a small C will respond quickly to changes in their thermal environment, whereas materials of large C will respond more sluggishly, taking longer to reach a new equilibrium. In porous materials the density should be corrected to account the void volume, therefore the effective thermal capacity can be expressed as equation (6.1)

$$C_{\text{eff}} = (1 - \Pi_V)\rho C_p \tag{6.1}$$

where Π_V is the volumetric porosity of the material. Since a Stirling regenerator is subjected to cyclic heat transfer, it is important that its response to the temperature variation of the fluid is fast; therefore between two materials characterized by comparable conductivities, it should be chosen the one with the lowest C_{eff}. Fig. 6.5 shows the results obtained by varying the effective heat capacity at constant material conductivity, which are numerically reported in Table 6.7 and 6.8. As it can be seen, very little variations occur in the engine behavior when the regenerator thermal capacity is modified; this leads to the conclusion that this parameter has not a determinant effect on the engine operation. However, it can be noticed that, from the higher to the lower C, the power output undergoes a slight increase, confirming the expected result. An exception is represented by the case with the lowest heat capacity (1.8e4 $J/(m^3K)$) whose power output is the lowest of the tested cases. This is explained by the fact that, in correspondence to very low heat capacities, the porous matrix is not able to store all the heat that could be exchanged with the air. This situation occurs when the effective

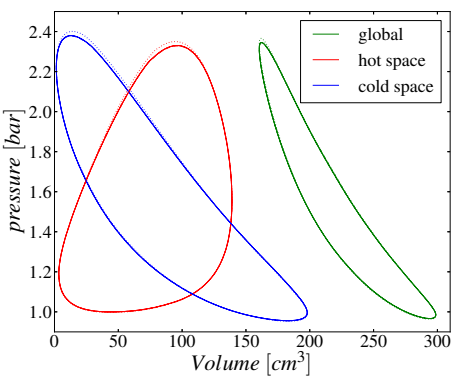

Figure 6.5: Effects of a variation of the effective heat capacity C_{eff} of the regenerator: base case, $C_{eff} = 0.7e6\, J/(m^3K)$ (continuos line), $C_{eff} = 1.3e6\, J/(m^3K)$ (dashed line), $C_{eff} = 3.8e4\, J/(m^3K)$ (dotted line).

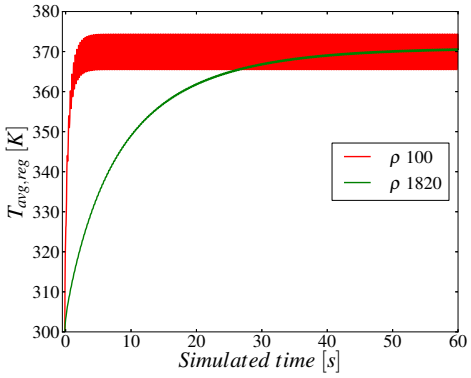

Figure 6.6: Regenerator average temperature during the thermal transient: comparison between low and high values of regenerator heat capacity

Table 6.7: Parametric study on regenerator heat capacity: simulation results.

Heat capacity	$[\frac{J}{m^3K}]$	$\mathbf{P_{mech}}[W]$	$\mathbf{Q_{cold}}[W]$	$\mathbf{Q_{hot}}[W]$	$\mathbf{T_{cold}}[W]$	$\mathbf{T_{hot}}[W]$
Base case	0.7e6	9.8	82.9	92.7	314.6	681.8
Test	1.3e6	9.78	83.0	92.6	314.5	708.1
	1.8e5	9.92	82.8	92.8	314.9	709.9
	3.8e4	10.08	83.1	93.2	314.8	713.7
	1.8e4	9.42	83.1	92.5	315.0	713.5

Table 6.8: Parametric study on regenerator heat capacity: efficiencies.

Heat capacity	$[\frac{J}{m^3K}]$	$\eta_{\mathbf{Carnot}} = \mathbf{1} - \frac{\mathbf{T_{cold}}}{\mathbf{T_{hot}}}$	$\eta_{\mathbf{I}} = \frac{\mathbf{P_{mech}}}{\mathbf{Q_{hot}}}$	$\eta_{\mathbf{II}} = \frac{\eta_{\mathbf{I}}}{\eta_{\mathbf{Carnot}}}$
Base case	0.7e6	0.54	0.11	0.20
Test	1.3e6	0.56	0.11	0.19
	1.8e5	0.56	0.11	0.19
	3.8e4	0.56	0.11	0.19
	1.8e4	0.56	0.10	0.18

Table 6.9: Tested regenerator materials

Material	ρ $[kg/m^3]$	**Cp** $[J/kgK]$	$\mathbf{k_{eff}}$ $[W/mK]$	$\alpha_{\mathbf{eff}}$ $[m^2/s]$	$\mathbf{e_{eff}}$ $[J/m^2Ks^{-0.5}]$
copper	8920	385	30.0	$4.3 \cdot 10^{-5}$	$4.6 \cdot 10^3$
aluminum	2700	902	18.2	$3.7 \cdot 10^{-5}$	$3.0 \cdot 10^3$
inox304L	7850	430	2.0	$2.6 \cdot 10^{-6}$	$1.2 \cdot 10^3$
monel400	8800	477	1.7	$2.2 \cdot 10^{-6}$	$1.1 \cdot 10^3$

heat capacity of the porous material is similar or below the heat capacity of the fluid mass which flows through the regenerator; in this case in fact, in order to exchange the maximum amount of heat, the solid phase should rise above the fluid temperature, which is physically impossible.

Despite its effect on the functioning parameters is very low, the variation of C has significant consequences on the duration of the regenerator thermal transient and on the amplitude of its temperature oscillations. Fig. 6.6 shows that high heat capacities lead to long heat transient and small oscillations, since the energy that can be stored is large and the thermal response is slow, while small heat capacities allow to reach quickly the regime state and determine more pronounced temperature oscillations.

6.3.3 Material

After the parametric study on the regenerator transport and thermophysical properties $k_{reg,eff}$ and C_{eff}, it is important to analyze the effects that different regenerator materials have on the engine performances. The materials to test were chosen on the basis of a similar experimental study performed on a Gamma Stirling engine [3], in such a way it was possible to qualitatively compare the results obtained. The materials and their properties are listed in Table 6.9. The graph of Fig. 6.7 shows the cycles obtained with the different regenerator materials. It is possible to observe that all the materials tested are more effective than copper, of which the base case regenerator is made of. In particular, Monel400 and Inox304L have similar behavior and give the best performances, while aluminum has an intermediate outcome. From the analysis done in Sec. 6.3.1 and 6.3.2 it is possible to observe that, if the lower limit for the heat capacity is respected, both the decrease of effective conductivity and heat capacity have a positive effect on the cycle performances. However, it must be considered that the effect of k_{eff} on the final results is much more valuable than the small variations induced by C_{eff}, therefore the *thermal conductivity* is the property that should be taken into account in order to predict the regenerator behavior. This conclusion is in line with the experimental measurements, in which Monel400 resulted the most perform-

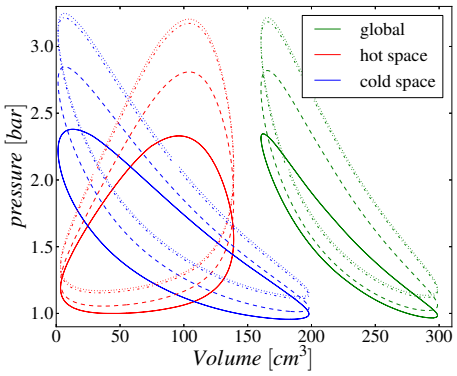

Figure 6.7: Effects of a variation of regenerator material: base case, Copper (continuous line), Aluminum (dashed line), Inox304L (dotted line), Monel400 (fine dotted line).

ing materials, followed closely by Inox304L, while aluminum demonstrated intermediate performances and copper was proven to be the worst solution.

Table 6.10: Parametric study on regenerator material: simulation results.

Regenerator material		$\mathbf{P_{mech}}[W]$	$\mathbf{Q_{cold}}[W]$	$\mathbf{Q_{hot}}[W]$	$\mathbf{T_{cold}}[W]$	$\mathbf{T_{hot}}[W]$
Base case	Copper	9.8	82.9	92.7	314.6	681.8
Test	Aluminum	9.78	82.8	92.6	314.5	708.1
	Monel400	27.35	61.6	89.0	351.4	963.7
	Inox304L	27.27	62.4	89.7	346.0	957.4

Table 6.11: Parametric study on regenerator material: calculated efficiencies.

Regenerator material		$\eta_{\mathbf{Carnot}} = \mathbf{1} - \frac{\mathbf{T_{cold}}}{\mathbf{T_{hot}}}$	$\eta_{\mathbf{I}} = \frac{\mathbf{P_{mech}}}{\mathbf{Q_{hot}}}$	$\eta_{\mathbf{II}} = \frac{\eta_{\mathbf{I}}}{\eta_{\mathbf{Carnot}}}$
Base case	Copper	0.54	0.11	0.20
Test	Aluminum	0.56	0.11	0.19
	Monel400	0.64	0.31	0.48
	Inox304L	0.56	0..30	0.48

6.4 Working fluid

As reported in many studies the choice of the working fluid has important influences on the machine performances; the most tested working fluids in the last decades were helium and hydrogen, which demonstrated in many applications to give better performances than the most common air. All

Table 6.12: Thermo-physical properties of the three working fluids at 370 K

Working fluid	$\rho[kg/m^3]$	$\mathbf{C_p}[kj/kgK]$	$\mu[Ns/m^2]$	$\nu[m^2/s]$	$\mathbf{k}[W/mK]$
Air	0.945	1.011	$216.96 \cdot 10^{-7}$	$23.12 \cdot 10^{-6}$	$31.52 \cdot 10^{3}$
Helium	0.134	5.193	$220.8 \cdot 10^{-7}$	$175.9 \cdot 10^{-6}$	$176.5 \cdot 10^{3}$
Hydrogen	0.066	14.45	$157.4 \cdot 10^{-7}$	$212.8 \cdot 10^{-6}$	$212.8 \cdot 10^{3}$

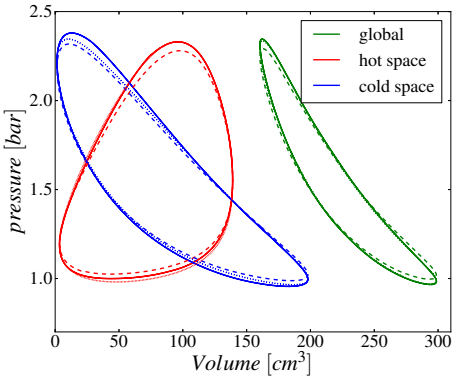

Figure 6.8: Thermodynamic cycles for different working fluids: base case Air (continuous line), Helium (dashed line), Hydrogen (dotted line).

these three fluids therefore were tested in simulations; in order to allow a comparison between the results, the different fluids were initialized with the same conditions of pressure and temperature, as it would be done in a real test case. The results obtained are shown in Fig, 6.8 and summarized in Tables 6.13-6.14.

It can be noticed that hydrogen seems to have the best performances, both in terms of power output and efficiency η_I; moreover if η_{II} is accounted, the improvement is even more pronounced. With regards to the helium, a small increase of the power output and efficiency was calculated but, in general, it seems to have performances similar to the air. In order to explain these behaviors, it is useful to observe Fig. 6.9-6.10 in which are represented the fluid-porous matrix heat transfer coefficient and the regenerator pressure drop as a function of the fluid velocity. These graphs are obtained by means of the correlations of Gedeon and Wood adopted in the regenerator sub-models (Sec. 4.2.3), using fluid thermo-physical properties at 370 K (which resulted the regenerator average temperature in all the three cases). It must be considered in addition that the velocity field of the different fluids were almost identical, and presented the maximum values (7 m/s) during the regeneration phases in correspondence of the porous matrix. At the considered temperature, hydrogen appears to have the best heat transfer coefficients with the

Table 6.13: Parametric study on the working fluid: simulation results.

Working fluid		$\mathbf{P_{mech}}[W]$	$\mathbf{Q_{cold}}[W]$	$\mathbf{Q_{hot}}[W]$	$\mathbf{T_{cold}}[W]$	$\mathbf{T_{hot}}[W]$
Base case	Air	9.8	82.9	92.7	314.6	681.8
Test	Helium	10.2	82.5	92.6	320.4	623.8
	Hydrogen	13.2	80.1	93.3	313.9	644.2

Table 6.14: Parametric study on the working fluid: calculated efficiencies.

Working fluid		$\eta_{\mathbf{Carnot}} = \mathbf{1} - \frac{\mathbf{T_{cold}}}{\mathbf{T_{hot}}}$	$\eta_{\mathbf{I}} = \frac{\mathbf{P_{mech}}}{\mathbf{Q_{hot}}}$	$\eta_{\mathbf{II}} = \frac{\eta_{\mathbf{I}}}{\eta_{\mathbf{Carnot}}}$
Base case	Air	0.54	0.11	0.20
Test	Helium	0.49	0.11	0.23
	Hydrogen	0.51	0.14	0.28

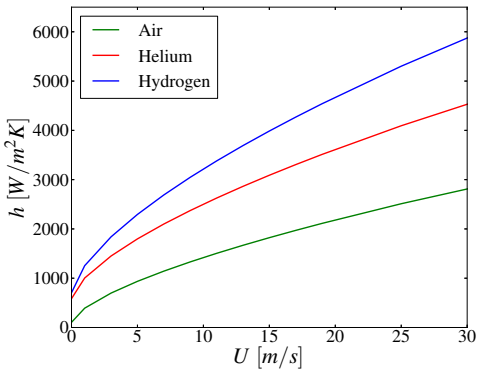

Figure 6.9: Heat transfer coefficient $[W/m^2/K]$ in the regenerator matrix as a function of fluid velocity $[m/s]$

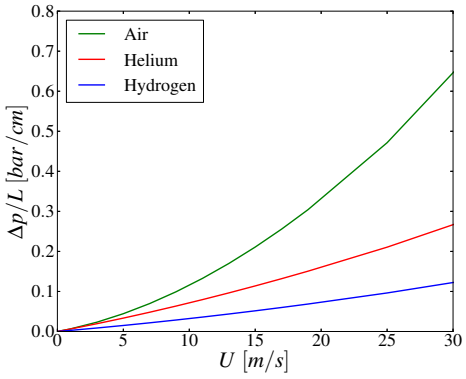

Figure 6.10: Pressure drop per unit of length $[bar/m]$ as a function of fluid velocity $[m/s]$

regenerator, helium an intermediate behavior, while air leads to the worst solid-fluid exchange. This is explained by the high thermal conductivity of hydrogen and helium, which result more important than the negative effect represented by high cinematic viscosities: in fact, for the same Nu number, the best heat transfer coefficient is given by the fluid with the highest conductivity while, on the other hand, high cinematic viscosities imply low velocities and low Re, reducing consequently the heat transfer (and the value of Nu). With regards to the pressure drop diagram illustrated in Fig. 6.10, it can be noticed that hydrogen is still the most performing fluid among the considered ones, while air leads to the highest pressure drop in the regenerator. This is explained by the low cinematic viscosity of the hydrogen compared to the other two fluids, which results in reduced friction forces through the

porous matrix; in addition, a high fluid density contributes to rise the pressure drop, and explains why air results disadvantaged in comparison with helium, despite having similar cinematic viscosities.

With regards to the considered engine, the electrical resistance was modeled by means of a source term, which means that the different fluids used do not affected the power input of the simulation. The cold sink instead is influenced by the different properties of the fluids, since comprehend the lower part of the displacer (where sub-models are implemented) and the cold cylinder surface (where a boundary layer is solved). Nevertheless, the power removed in the cold sink and the cold temperatures are similar in the three cases, as shown in Table 6.13. This means that the cold exchanger is really effective and guarantees a good heat removal in all the three cases, even when the heat transfer is disadvantaged (Air).
If friction effects are considered instead, the properties of the fluids reflect more consistently on the machine performances, and lead to the different working cycles of Fig. 6.8. In the hydrogen case it can be seen that the pressure differences between the hot cycle and the cold cycle is decreased during the regeneration phases (upper and lower part of the cycles) leading to lower regeneration works. The adoption of this fluid therefore, results in an higher power output and efficiency η_I ans an increased efficiency η_{II}, since less irreversibilities are produced.

6.5 Ideal analysis

In this section the operation of an ideal engine configuration will be modeled and simulated. The ideal hypothesis introduced will be then removed one by one in order to study the effects that each deviation from ideality imply on the hot and cold thermodynamic cycles. In Table 6.15 the power outputs of the various cases analyzed are shown.

Table 6.15: Power output of the different ideal cases studied.

Case	**Motion**	**Permeability**	**Heat exchangers**	$\mathbf{P_{out}}$ **[W]**
Base	Real	Real	Real	9.8
A	Ideal	Ideal	Ideal	43.7
B	Ideal	Real	Ideal	20.7
C	Ideal	Ideal	Real	21.5
D	Ideal	Real	Real	−10.5
E	Ideal 2	Real	Real	9.7
F	Real	Ideal	Ideal	25.6

Case A

In order to model the ideal case, at first the alternative piston/displacer motion was replaced with an ideal volume variation law; the comparison between the new ideal laws and the crank movement of the real device is shown in Fig. 6.11. The combination of the two ideal laws for the piston and the displacer allows to limit the variation of the global volume to the expansion and compression phases, while regeneration transformations are performed keeping the volume as a constant. Secondarily the permeability model of the regenerator matrix was disabled, removing all the pressure drops of the system, so that, instantaneously, the pressure is the same in both the hot and the cold space. Lastly, an ideal heat transfer was implemented in the working spaces, imposing to the fluid a constant temperature of 700 K and 315 K respectively in the hot space and in the cold space. The working cycles obtained with these assumptions are shown in Fig. 6.12; in this case, since no pressure differences occur in the engine, the global cycle obtained by means of the average pressure of the spaces truly represents the thermodynamic cycle of the engine, and it is visible how its shape results close to the theoretical one. Due to the ideal movement the transformations are clearly discernible in every cycle and can be observed: 1-2) isothermal compression, 2-3) isochoric regeneration (fluid flows from the cold space to the hot space), 3-4) isothermal expansion, 4-1) isochoric regeneration (fluid flows from the hot space to the cold space). From the ideal diagrams is possible to observe that the ideal permeability leads to a null regeneration work; in fact, the regenerative transformations of the hot cycle and the cold cycle are equal and mirrored, and the sum of their relative works is therefore zero. A further observation is that in the ideal movement the displacer moves till the lower dead point of the power piston, so that the expansion takes place entirely in the hot space; therefore, unlike what happens in the real motion, in this case the maximum and minimum volumes of the two cycles are the same.

Case B

Fig. 6.13 shows the effects related to the introduction of the real permeability of the regenerator matrix. In this case a pressure difference is established between the two working spaces so that the regeneration phases involve a negative work for the system. During these transformations, since the air can not flow freely from one space to the other, the movement of the displacer causes a slight compression of the space from which the air is removed, and a depression in the space where the air is flowing into. This effect is visible observing that point 1 in the hot cycle and point 3 in the cold cycle are shifted upwards, increasing the negative work connected to the regenerative

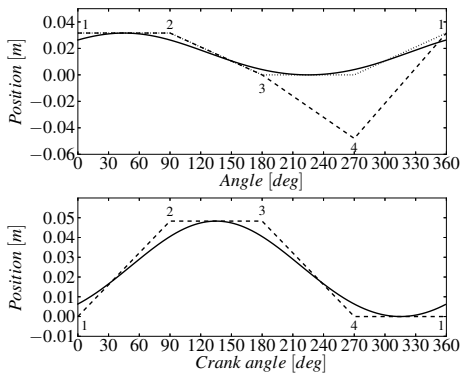

Figure 6.11: Motion laws adopted for the power piston (bottom) and the displacer (top) - real law (continous line), ideal law Case A (dashed line), ideal law 2 Case E (dotted line).

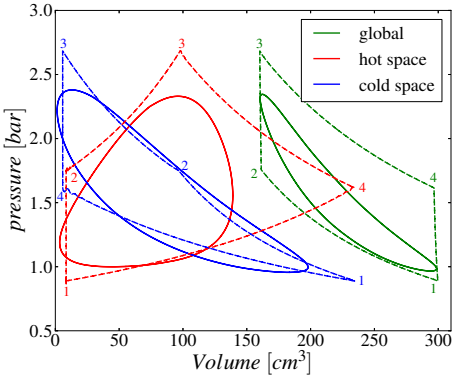

Figure 6.12: Case A - Comparison between the base case (continuous line) and ideal case A (dashed line)

transformations 4-1) of the hot cycle and 3-4) of the cold cycle, while points 2 in the hot cycle and 4 in the cold cycle are lowered, diminishing the positive contributes of transformation 2-3) of the hot space and 4-1) of the cold space. This unbalance of the regenerative transformations of the two spaces, caused by the pressure drop due to the real permeability of the regenerator, is equal to the work spent to displace the air during these transformations. It can be observed that the regeneration at the lower pressures involves a more pronounced deviation from the ideal transformations than the other displacement; this is due to, in the prescribed ideal motion, it was decided to impose the same duration to the four transformations, so that, since this displacement has a longer stroke, its consequent higher velocity leads to higher pressure drops. A last observation related to the ideal law introduced is that the velocities of piston and displacer are constant, involving a constant pressure drop during the regenerations. As a result of the the introduction of this non-ideality the loss of work estimated with respect to the ideal case is of 53 %.

Case C

This case concerns the application of the real heat exchangers (electrical resistance and water cooling system) to the ideal case; the thermodynamic cycles associated are shown in Fig. 6.14. The major effect of this non-ideality is the considerable increase of the cold cycle area in comparison with the hot, due to the rise of the compression transformation 1-2); this is accountable to

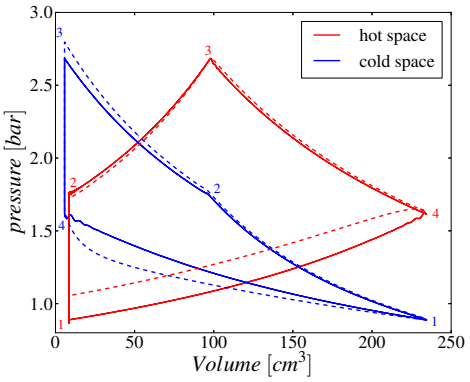

Figure 6.13: Effect of real permeability: Case B (dashed line), ideal case A (continuous line)

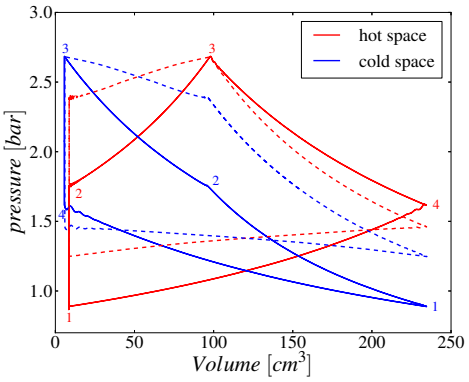

Figure 6.14: Effect of real heat exchangers: Case C (dashed line), ideal case A (continuous line)

the real cold exchanger which is not effective enough to maintain a constant temperature in the cold space. Therefore the air temperature during the compression phase increases considerably requiring the introduction of a work higher than in the ideal case. Furthermore, as a consequence of the higher temperatures in the engine it can be noticed that the mean pressure of the cycle increase. To a less extent, a negative effect can be observed also for the expansion phase 2-3) of the hot cycle: here the electrical resistance does not introduce the amount of power necessary to have an isothermal expansion and the expansion work results slightly decreased. The effect of the non-ideality is less significant in this case because the electrical resistance is simulated by means of a constant source term and, therefore, the simulated heat transfer is more similar to an ideal case rather than to a real case. The reduction of the work output related to the introduction of the real heat exchangers is estimated of 51 %.

Case D

In this case is studied the combined effect of the adoption of a real permeability in the regenerator and real heat exchangers; it can be noticed that the resulting cycle, shown in Fig. 6.15, presents simultaneously the characteristics observed in case B and case C. In particular, as observed before, the real cold exchanger is not effective enough to maintain low temperatures during the compression phase, resulting in increased pressures at the end of the compression and in an higher work required by this transformation. Even the expansion phase is disadvantaged, since the electrical resistance do not provide sufficient power to prevent the decreasing of the temperatures.

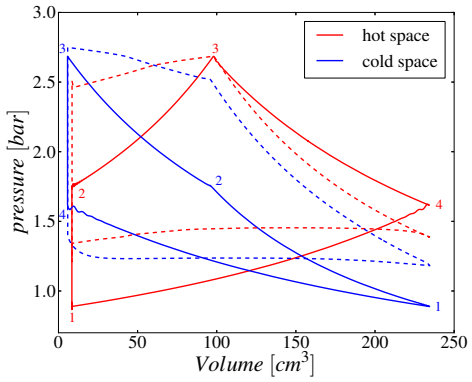

Figure 6.15: Effect of simultaneous real permeability and real heat exchangers: Case D (dashed line), ideal case A (continuous line)

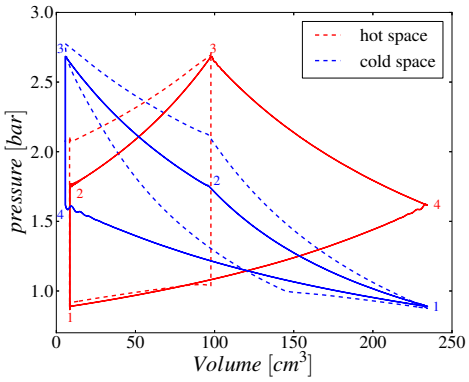

Figure 6.16: Effect the ideal law of motion 2: Case E (dashed line), ideal case A (continuous line)

The real permeability on the other hand, establishes a pressure difference between the working spaces, so that the regenerations imply a negative work for the system. It can be noticed how the combination of the two non-ideal hypothesis leads to a very disadvantaged regeneration at the lower pressures 1-4), where the pressure drop is higher. In this configuration the negative effects on the cycle caused by the non-idealities are so important that the cold cycle area is larger than the hot cycle area so that, globally, the total work is negative. This result is important because implies that, in presence of non-idealities of the other components of the engine, the introduction of an ideal motion law can lead to worse performances of the engine rather than improve the power output. In fact in the base case, even if the real components models were adopted, the power output was positive.

Case E

Starting from the observation done at the end of the previous paragraph, it is interesting to analyze which aspect of the real motion makes it more performing than the ideal volume variation, if real components are considered. It can be observed that, in case D, the regeneration at low pressures 4-1) represents a significant loss for the system, especially because of its long stroke. An important difference between the ideal and the real movements in fact, is that in the first the displacer can reach the lower dead point of the cold piston while, in the practical technical solution, the stroke of the displacer is limited to the upper part of the cylinder. Therefore it was implemented a second ideal law of motion, shown in Fig. 6.11, which limits the displacer

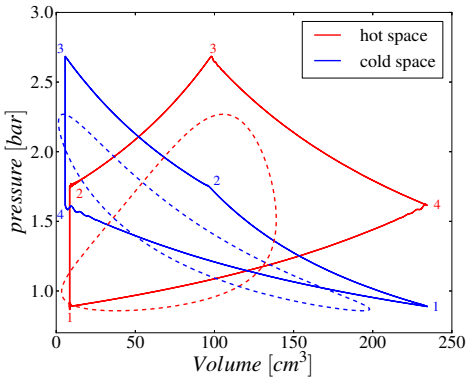

Figure 6.17: Effect of the real motion: Case F (dashed line), ideal case A (continuous line)

stroke as happens in the real movement; the results of this case are presented in Fig. 6.16. It can be noticed that that major positive aspect of the new motion is to considerably reduce the regeneration work of 1-4), since in this case the displacer moves slower than in the other regeneration and a minor pressure drop is produced. Furthermore, the second ideal low implies that the expansion transformation is done totally in the cold space, because the displacer is stopped at the end of the regeneration at its lower dead point, and does not move downwards along with the cold piston. This represents a loss for the cycle, because the air is expanded at lower temperatures than in the hot space, and heat is removed during the expansion by the cooling system. On the other hand, the longer time spent by the air in the cold space causes a decrease of the lower temperatures (and pressures), so that the successive compression requires a lower work. As a matter of fact, the negative outcome represented by a colder expansion has a minor influence compared to the positive impacts of a minor regeneration and compression work, so that the power output of this configuration is globally positive and is close to the power obtained using the real motion.

Case F

In this last case, the effect of the introduction of a real movement in an ideal engine is analyzed. As is illustrated in Fig. 6.17, if an ideal permeability and ideal heat exchangers are considered, the adoption of a real movement strongly penalize the performances of the machine. This allows to conclude that the real motion, with respect to the ideal case, represents a loss for the system, since causes an overlapping of the different transformations reducing their effectiveness. In fact, while the compression is still occurring, the

regeneration starts heating part of the air and, during the expansion phase, the displacer moves upwards activating the regenerative cooling. In addition, as a consequence of the configuration of this engine, the real movement implies that the air expansion occurs in the cold space, further disadvantaging the cycle performances. The loss connected to the introduction of the real motion is of 41 %, value that is in agreement with similar studies reported in the literature [2].

Conclusions

In this work a CFD model for the simulation of a generic Beta-type Stirling engine has been developed on the basis of the finite volume open-source code OpenFOAM. Different sub-models have been implemented in order to take into account particular features of this machine, related to mesh motion, heat transfer, turbulence modeling and interaction with the porous media; a particular attention was given to the modeling of the regenerator, for which two approaches *single-region* and *multi-region* have been proposed. The model has been successfully validated on the case of a small 300*cc* Beta Stirling configuration, by means of comparison of both global quantities, such as the power and heat transferred to the cold sink in a cycle, and of local measurement of temperature in the machine.

Once validated, the *multi-region* model was applied to perform a parametric study on different machine parameters, such as mean cycle operating pressure, amount of heat introduced at the hot end, regenerator properties and working fluid. With regards to the regenerator characteristics, from the simulations results it can be concluded that the effective conductivity of the porous matrix is the regenerator property that mostly influence the engine performances; in particular a low conductivity should be pursued, in order to promote regenerator temperature stratification and increase its efficiency. The effective heat capacity of the porous matrix instead, seemed to have a negligible influence on the engine performances; nevertheless it was noticed that this property is subjected to a lower limit, under which the engine operation is rapidly penalized. This situation occurs when the heat capacity of the porous matrix is so low that has the same order of magnitude of the working fluid heat capacity; in this case the amount of heat which can be stored by the regenerator material results smaller than the amount of heat that the fluid would be able to transfer, so that the regenerator efficiency drops. In addition, with regards to the considered engine, regenerator heat capacity resulted to be the most important parameter influencing the thermal transient of the machine. The analysis on the working fluid led to the conclusion that, for wire porous matrices, hydrogen leads to better performances than helium and air. This behavior is accountable to the hydrogen

high thermal conductivity, which enhances the heat transfer with the regenerator, and to its low dynamic viscosity, which reduces the friction losses in the porous matrix. As last part of the work, the model was used to evaluate the effects resulting from the adoption of real components, such as a finite porosity of the regenerator, real heat exchangers, and a real law of motion, which as been compared to an ideal volume variation law. An interesting result is that, with regards to the studied engine, the application of the ideal movement for the piston and the displacer leads to worse operating performances than the real motion. This is due to the fact that the ideal motion, if adopted in conjunction to real components, leads to higher regenerator work and limits the heat transfer. As a consequence it can be concluded that, in a real device, the ideal movement can not represent the optimum law of variation of the volumes, but the other engine components (e.g. regenerator and heat exchangers) should be taken into account during the definition of the motion, in order to find the best compromise between their losses and their performances.

In conclusion it can be said that the results provided by the CFD model for the studied engine represented an important tool for the comprehension of the machine components operation and the internal physical phenomena. Moreover, the outcomes obtained by the parametric study are reasonable and show a satisfactory agreement with the behaviors expected on the basis of the existing theoretical models. It can be concluded therefore that CFD analysis can actually give a substantial contribution for the prediction of Stirling machine performances, and can be applied with success during the design phases and for the optimization of the engine geometry and components.

Future works and development

The present work has to be intended as a preliminary validation of the developed CFD model and involves many simplifications, also accountable to the simplicity of the considered engine. Future works should be focused on the simulation and the optimization of more complex real configurations, where more measurements and accurate informations are available. In particular a wider number of losses should be included in the model, such as radiative losses, conduction and convection losses towards the environment and seal losses. From a numerical point of view the development of ad-hoc mathematical methods for Stirling engines should be pursued, in order to enhance the accuracy of the simulations without compromising the computation velocity and stability. Lastly, efforts should be spent in the direction of developing methods to promote a faster convergence of the model to the cyclic steady state, so that it can be easily applied to very detailed computational grids.

Bibliography

[1] A.J. Organ. Thermodinamics and Gas Dynamics of the Stirling Cycle Machine. Cambridge, Cambridge University Press, 1992.

[2] I. Urieli and D.M. Berchowitz. Stirling Cycle Engine Analysis. Bristol, Adam Hilger Ltd, 1984.

[3] R. Gheith, F. Aloui, M. Tazerout, and S. Ben Nasrallah. Experimental investigations of a gamma stirling engine. Int. J. Energy Res., 2012.

[4] S.C. Costa, Harritz Barrutia, Jon Ander Esnaola, and Mustafa Tutar. Numerical study of the heat transfer in wound woven wire matrix of a stirling regenerator. Energy Conversion and Management, 79(0):255 – 264, 2014.

[5] S.C. Costa, Harritz Barrutia, Jon Ander Esnaola, and Mustafa Tutar. Numerical study of the pressure drop phenomena in wound woven wire matrix of a stirling regenerator. Energy Conversion and Management, 67(0):57 – 65, 2013.

[6] N.C.J. Chen and F.P. Griffin. A review of stirling engine mathematical models. Oak Ridge National Laboratory, August 1983.

[7] R.W. Dyson, S.D. Wilson, and R.C Tew. Review of computational stirling analysis methods. NASA/TM-2004-213300, October 2004.

[8] M.B. Ibrahim, Z. Zhang, Rong Wei, T.W. Simon, and D. Gedeon. A 2-d cfd model of oscillatory flow with jets impinging on a random wire regenerator matrix. In Energy Conversion Engineering Conference, 2002. IECEC '02. 2002 37th Intersociety, pages 511–517, July 2002.

[9] M. Ibrahim. 2-d cfd simulation of the heat transfer and fluid dynamics in an experimental model of the hot end of a stirling engine. In Energytech, 2012 IEEE, pages 1–11, May 2012.

[10] Z. Zhang and M. Ibrahim. Development of cfd model for stirling engine and its components. 2nd International Energy Conversion Engineering Conference, 2004.

[11] K. Mahkamov. Design improvements to a biomass stirling engine using mathematical analysis and 3d cfd modeling. J. Energy Resour. Technol., 128(3), September 2005.

[12] R.W. Dyson, S.M. Geng, R.C. Tew, and M. Adelino. Towards fully three-dimensional virtual stirling convertors for multi-physics analysis and optimization. Engineering application of computational fluid mechanics, 12(1), 2008.

[13] G. Walker. Stirling-Cycle machines. Oxford University Press, 1973.

[14] D. Gedeon and J.G. Wood. Oscillating-flow regenerator test rig: hardware and theory with derived correlations for screens and felts. NASA CR-198442, 1996.

[15] H. G. Weller, G. Tabor, H. Jasak, and C. Fureby. A Tensorial Approach to CFD using Object Orientated Techniques. Computers in Physics, Vol. 12(No. 6):620, 1998.

[16] OpenFOAM documentation. Available from: http://www.openfoam.org/docs/.

[17] B.H. Van Arsdell. Around the World by Stirling Engine. American Stirling Company, 2003.

[18] W.R. Martini. Stirling engine design manual. NASA-CR-158088, January 1983.

[19] G. Schmidt. Theorie der geschlossenen calorischen Maschine von Laubroy und Schwarzkopf in Berlin. 1871.

[20] T. Finkelstein. Regenerative thermal machines. University of California, Los Angeles, University extension, 1974.

[21] A. Schock. Nodal analysis of stirling devices. Fairchild Space and Electronics Company.

[22] M. A. Nawafleh N.Al-Kloub M. Tarawneh, F. Al-Ghathian. Numerical simulation and performance evaluation of stirling engine cycle. Jordan Journal of Mechanical and Industrial Engineering, 4(5), November 2010.

[23] W. Talaat M. Abdelnasser M. Leheta H. Abdelsattar, M. Gamal. Computational fluid dynamic-based analysis and optimization of stirling engines: an insightful survey. In nternational Conference on Energy Systems and Technologies (ICEST 2011), 11-14 March 2011.

[24] R.W. Dyson, S.D. Wilson, and R. Demko Tew. Fast whole-engine stirling analysis. NASA/TM-2004-213300, October 2005.

[25] R.W. Dyson, S.D. Wilson, and R. Demko Tew. Overview 2004 of nasa-stirling convertor cfd model development and regenerator research and development efforts. NASA/TM—2004-213404, November 2004.

[26] T.L. Bergman, A.S. Lavine, F. P. Incropera, and D.P. Dewitt. Fundamentals of heat and mass transfer. 2011.

[27] J. H. Ferziger and M. Perić. Computational methods for fluid dynamics. Springer, 1997.

[28] H. K. Versteeg and W. Malalasekera. An introduction to computational fluid dynamics. Longman Scientific & Technical, 1995.

[29] S. B. Pope. Turbulent Flows. Cambridge University Press, 2000.

[30] F. Menter and T. Esch. Elements of Industrial Heat Transfer Prediction. 16th Brazilian Congress of Mechanical Engineering (COBEM), 2001.

[31] A. Della Torre. Multi-scale cfd modeling of intake and exhaust systems for internal combustion engines. Doctoral Dissertation, 2013.

[32] R. Gheith, F. Aloui, and S. Ben Nasrallah. Experimental study of a beta stirling thermal machine type functioning in receiver and machine modes. Journal of Applied Fluid Mechanics, 2011.

[33] F. Formosa and G. Despesse. Flow and heat transfer characteristics of the stirling engine regenerator in an oscillation flow. Energy Conversion and Management, 51(10):1855 – 1863, 2010.

[34] Chen Li and G.P. Peterson. The effective thermal conductivity of wire screen. International Journal of Heat and Mass Transfer, 49(21–22):4095 – 4105, 2006.